Paleoseismic Investigation of the Meadow Bank Lineament in the Wabash Valley Seismic Zone

Final Technical Report USGS Grant G12AP20045
April 1, 2013 to January 31, 2014

Timothy Larson	**217-244-2775 (phone)**	**thlarson@illinois.edu**
Andrew Phillips	**217-333-2513 (phone)**	**aphillps@illinois.edu**
Scott Elrick	**217-333-3222 (phone)**	**elrick@illinois.edu**

Illinois State Geological Survey Division
Prairie Research Institute
University of Illinois Urbana-Champaign

615 E Peabody Drive
Champaign, Illinois 61820 **FAX: 217-244-7004**

Abstract

The Meadow Bank lineament (MBL) is a 10 km (~6 mi) long scarp in glacial sediments trending NNE along the west edge of the Wabash River Valley. The MBL closely parallels the trace of the Herald Phillipstown Fault Zone (HPFZ) which is located 1 km (0.6 mi) west of the MBL in Paleozoic bedrock. In many circumstances, the straightness of the MBL and its parallel orientation to the HPFZ would be considered *prima fascia* evidence for a tectonic origin for the MBL. Given the glacial origin of the sediments, the implied age of faulting would be within the last 20,000 years, and possibly younger. If this were the case, then the dimensions of the MBL (10 km [6 mi] long and 5 to 10 m [15-30 ft] high) would imply the epicentral area of a large magnitude (M6 to M7.5), relatively young earthquake. This event would have been similar in magnitude to the New Madrid earthquakes of 1811-1812 and, if confirmed, would have serious ramifications for earthquake hazard assessment in the Lower Wabash River Valley. However, our research leads to a different conclusion: the MBL is the result of erosion, not tectonics.

White County Coal Company's Pattiki Mine straddles the MBL. This mine extracted 30 million tons of coal between 1982 and 2002, fully exploiting the Herrin Coal beneath the study area. We examined the Final Map (2003) of the Pattiki mine. This map shows the mine workings, faults, and elevation of the mine floor with a contour interval of 3 m (10 ft). The mapping indicates that directly below the MBL, and in a band within a few hundred meters on either side of the MBL trend, there is no alteration to the mine plan, no offsets within the coal, and only gently sloping coal elevations consistent with the local structural pattern. The lack of offset in the coal beneath the MBL is conclusive evidence that the MBL was not caused by tectonic faulting.

We collected and analyzed new cores, geophysical data, and LiDAR data to investigate the composition and history of the MBL. We drilled a series of eight closely spaced shallow boreholes traversing the MBL. From the core collected in these boreholes we processed 16 OSL age-dates, 2 ^{14}C age dates, 8 porosity samples, 80 particle-size samples, 26 XRD samples, 38 Chittick analyses, and measured magnetic susceptibility at 0.5 ft (15 cm) intervals on each core. We acquired three earth resistivity profiles traversing the MBL to investigate the Quaternary sediments on either side of the lineament at three locations. One profile coincided with the drilling transect, the others were north and south of this main profile. The texture, mineralogy, geophysical character, and age results are all more consistent with sedimentological explanations rather than tectonic faulting of the valley fill. Furthermore, LiDAR elevation data reveals that the Meadow Bank is not unique. Although it is distinctively straight, long, and high, a family of similar landforms can be identified along the valley.

Instead, the Meadow Bank Lineament is most likely the result of large torrential flood events near the end of Late Wisconsin Episode glaciation. Outbursts of glacial meltwater pulsed large volumes of bedload-starved water down the Wabash Valley. This combination of high fluid volume and low river gradient resulted in erosion of aggraded banks, and releasing of slack-water lakes. Bedrock exposures along the edges of the valley limited the extent of the erosion and controlled the shape of the erosion scarps immediately downstream of the exposures. Soon after these outbursts, the major glacial drainage was diverted eastward through the St. Lawrence River, thus drastically reducing the volume of water in the Wabash System. The meanders of the now much smaller modern Wabash River have only cut into a very small part of the north end of the MBL, leaving the rest intact.

Table of Contents

Executive Summary 4

Introduction 8

Methods 9

Results of Investigations 12

Interpretation 18

Conclusions 23

Future research questions 23

References 24

Figures 28

Appendices 49

Executive Summary

The Meadow Bank lineament (MBL) is a 10 km (~6 mi) long scarp in glacial sediments trending NNE along the west edge of the Wabash River Valley. The MBL closely parallels the trace of the Herald Phillipstown Fault Zone (HPFZ) which is located 1 km (0.6 mi) west of the MBL in Paleozoic bedrock. In many circumstances, the straightness of the MBL and its parallel orientation to the HPFZ would be considered *prima fascia* evidence for a tectonic origin for the MBL. Given the glacial origin of the sediments, the implied age of faulting would be within the last 20,000 years, and possibly younger. If this were the case, then the dimensions of the MBL (10 km [6 mi] long and 5 to 10 m [15-30 ft] high) would imply the epicentral area of a large magnitude (M6 to M7.5), relatively young earthquake. This event would have been similar in magnitude to the New Madrid earthquakes of 1811-1812 and, if confirmed, would have serious ramifications for earthquake hazard assessment in the Lower Wabash River Valley. However, our research leads to a different conclusion: the MBL is the result of erosion, not tectonics.

The history of the Wabash Valley begins with Precambrian rifting or failed rifting at the cratonic margin during the break up of Rodinia. These structures were reactivated in late Paleozoic to Mesozoic time as the Wabash Valley Fault Zone, a system of high angle normal fault zones and grabens trending NE-SW away from the EW Cottage Grove fault on the south. The faults and minor positive flexures within the grabens provide constraints on the local and regional drainage patterns such as parallel ridges, stair-step tributaries, and angular bends in the Ohio River, which can also be traced as lineaments into the Lower Wabash Basin.

Modern mid-continental tectonic forces, possibly driven by isostatic adjustments following glaciation have reactivated the late Paleozoic faults. Moderate seismicity is ongoing in the Lower Wabash Valley. A 2008 magnitude 5.3 earthquake located 40 km (25 mi) NW of the MBL produced sympathetic vibrations along the HPFZ that was felt by miners in the White County Coal Company's Pattiki Mine. Although the MBL is north of the New Madrid Seismic Zone, the area is close enough to New Madrid to have been affected by the 1811-1812 earthquakes. Residents of the Lower Wabash River Valley reported that vibrations from the 1811-1812 earthquakes resulted in liquefaction which displaced sand onto the ground surface east of the MBL. Earlier liquefaction episodes, observed today as dikes and buried sills exposed in the banks of the Wabash River and tributaries, provide evidence for several significant earthquakes in the region dating back 4,000 to 6,000 years.

Widespread Pennsylvanian age coal swamps produced several commercially extractable coal beds within the Illinois Basin. Specifically, the Herrin (No. 6) Coal of Middle Pennsylvanian age is approximately 2 m (7 ft) thick at a depth of about 300 – 350 m (985-1150 ft) beneath the study area. The Pattiki Mine extracted 30 million tons of coal between 1982 and 2002, fully exploiting the Herrin Coal east of the Herald Phillipstown Fault Zone (HPFZ) in a room and pillar mining pattern. A new shaft was sunk west of the HPFZ and mining is continuing westward while using the same surface facilities. We examined the Final Map (2003) of the Pattiki mine. This map shows the mine workings, faults, and elevation of the mine floor with a contour interval of 3 m (10 ft). A tectonic fault capable of creating a 6 to 9 m (20-30 ft) displacement at the ground surface would presumably also create at least 6 m (30 ft) of displacement within bedrock. A displacement of as little as 1.5 m (5 ft; the nominal thickness of the coal seam) will result in altered mining patterns in room and pillar operations and will be evident on the mine map. The mapping indicates that directly below the MBL, and in a band within a few hundred meters on either side of the MBL trend, there is no alteration to the mine plan, no offsets within the

coal, and only gently sloping coal elevations consistent with the local structural pattern. By comparison, a small normal fault within the coal was encountered 600 m (1950 ft) to the west, close to the HPFZ near the mine entrance. This fault is clearly associated with the HPFZ. The lack of offset in the coal farther east, beneath the MBL, is conclusive evidence that the MBL was not caused by tectonic faulting.

Our proposal called for a program of shallow drilling with percussion methods complemented by drilling through bedrock with wireline methods and downhole logging. After analyzing the mine records, we realized that the deep wireline boring would (a) add no information to the surficial sampling, (b) require drilling to 90-150 m (300-500 ft) depths to encounter correlatable stratigraphic units, and (c) correlation would add little to our understanding from the coal mine mapping. However, the shallow drilling was necessary to investigate alternative origins for the MBL.

We collected and analyzed new geophysical data, cores, and LiDAR data to investigate the composition and history of the MBL. We drilled a series of closely spaced shallow boreholes traversing the MBL. The sandy glacial outwash sediments did not contain discrete sedimentary layers or marker beds that could be traced across the MBL to determine offset. Instead, we had to rely on more general stratigraphic properties and a suite of optically stimulated luminescence dates (OSL) to interpret the subsurface. The texture, mineralogy, and age results are all more consistent with sedimentological explanations rather than tectonic faulting of the valley fill. Within the suite of OSL ages, several appear to be out of sequence at intermediate depths. They are coherently older than ages above or below. This seemingly paradoxical condition could be consistent with remobilization of older sediment from the upper reaches of the Wabash, with only partial resetting of the optical signal during transport to the area of the MBL while entrained as bedload in the swollen, aggrading river, although additional analysis of the dates continues.

We acquired three earth resistivity profiles traversing the MBL to investigate the Quaternary sediments on either side of the lineament at three locations. One profile coincided with the drilling transect, the others were north and south of this main profile. All three profiles recorded similar resistivity patterns. The resistivity of the sediment west of the MBL is very high – 300 to over 1000 ohm-m, typical of dry sand and gravel, but decreases abruptly below the MBL to 100 to 200 ohm-m, more typical of saturated sand and gravel. Farther east, the central and northern profiles encountered low-resistivity sediments typical of organic-rich silts and clays of alluvial origin. The cause of the very high resistivity sediment has not been fully determined, but it is consistent with a fluctuating groundwater table or erosion of a larger mass of high-resistivity sand. The resistivity profiles also imaged the top of the bedrock surface. Consistent with the drilling data, the imaged bedrock surface dips gently to the east into the Wabash River Bedrock Valley.

LiDAR data collected in 2010 superseded 40-year old, 10-foot elevation contours and constitute the first functional digital topographic surface ever produced for the region. Close study of the digital elevation model indicates the presence of multiple terrace levels. West of the MBL, the highest terrace represents the surface of delta that merges up a tributary valley with the floor of a Wisconsin Episode slackwater lake.

Immediately east of the MBL is a narrow remnant of a second terrace formed in Wisconsin outwash sediments. It may represent the floor of the outburst flood that eroded the MBL. This terrace was also internally eroded by a small Holocene stream. A lower terrace of late-Wisconsinan-aged braided stream deposits that was partly modified by Holocene alluviation continues eastward from this stream to the village of Maunie along the banks of the modern Wabash River. In this reach of the valley, the modern

Wabash River floodplain and older Holocene meandering-phase terraces are restricted to the northernmost tip of the MBL and to the east part of the river valley.

Furthermore, LiDAR elevation data reveals that the Meadow Bank is not unique. Although it is distinctively straight, long, and high, a family of similar landforms can be identified along the valley. These each occur at a tributary confluence, and are terraced above the Wabash Valley fill. Specifically, terrace scarps are located at the mouth of the Embarras River, upstream of the mouth of Bon Pas Creek and at the mouth of the Saline River. Each formed downstream of a bedrock exposure. Preliminary investigations suggest that each of these features was formed at the end of the Wisconsin Episode, and possibly during the same event. Further investigation may reveal additional scarps.

We conclude that a tectonic origin of the MBL is not likely. Bedrock faulting was not encountered in the coal mine below the MBL. Sedimentary sequences and OSL dates from sediments spanning the MBL are not consistent with faulting. Three resistivity profiles across the MBL encountered very high resistivity sediments west of the MBL, but only moderately high resistivity sediments east of it. The observed scarp length and height are not consistent with the dimensions of observed earthquake rupture length and vertical displacements (Wells and Coppersmith, 1994). Earthquake scarps rarely attain 10 m (30 ft) of vertical surface displacement. Such large surface displacements are normally associated with rupture lengths on the order of 150 km (100 mi), not 10 km (6 mi). Conversely, earthquake surface ruptures that are 10 km (6 mi) long typically exhibit displacements on the order of 0.3 m (1 ft), not 10 m (30 ft).

Another possible earthquake-related cause of the MBL could be an earthquake induced landslide similar to those observed in the lower Mississippi River valley and tributary valleys following the 1811-1812 New Madrid earthquakes. Landslides, however, tend to have arcuate, not straight, alignments. The extreme length of the straight reach of the Meadow Bank scarp is well beyond the maximum straight reach observed in documented landslide settings. The shape and the low height to width ratio of the MBL both suggest that a landslide origin is unlikely. Furthermore, there are no continuous clay layers present beneath the MBL that could act as either a slip surface or as a confining layer to facilitate mass movement.

Instead, the Meadow Bank Lineament is most likely the result of large torrential flood events near the end of Late Wisconsin Episode glaciation. The Wabash River was a major conduit for glacial meltwater and sediment from the Huron and Erie Lobes of the Laurentide ice sheet from late Illinois Episode through the late Wisconsin Episode. North–northeasterly trending structural features in the underlying bedrock funneled large volumes of mostly sand-sized sediment into the main valley of the lower Wabash River. The rapidly aggrading river blocked the flow of tributary streams including the Little Wabash River to form slackwater lakes. Deltas building from the main Wabash River distributed fine sands back into the slackwater lakes. Subsequent outbursts of glacial meltwater pulsed large volumes of bedload-starved water down the Wabash Valley. This combination of high fluid volume and low river gradient resulted in erosion of these deltas, releasing the slack-water lakes. Bedrock exposures along the edges of the valley limited the extent of the erosion and controlled the shape of the erosion scarps immediately downstream of the exposures. Similar lakes formed in the dammed Embarras, Bon Pas, and Saline drainages. Likewise, similar high, long, straight to gently arcuate terrace scarps are also present at the mouths of these ancient lakes. Like the MBL, these scarps tended to form downstream of bedrock exposures. Northwesterly to westerly winds redistributed the sands into dunes on the eastward ends of the now dry lake basins. Soon after these outbursts, the major glacial drainage was diverted eastward through the St. Lawrence River, thus drastically reducing the volume of water in the Wabash System. The meanders of the now much smaller modern Wabash River have only cut into a very small part of the

north end of the MBL, leaving the rest intact. Similar features are present in the lower Ohio River Valley near Evansville as a result of similar late glacial flooding in the Ohio River drainage system.

All available evidence suggests that the MBL is the result of Late Wisconsin Episode fluvial processes and not recent tectonism, as Heigold and Larson (1994) previously concluded. Although unusually long and straight, the MBL is only one of several scarps which formed at the mouths of dammed tributaries when one or more Late Wisconsin Episode glacial outbursts eroded through thick glacial outwash. Furthermore, the glacial outwash and the slackwater lake sediments appear to mimic the linear fault and fracture patterns of the Paleozoic rocks below them. Both drilling and seismic refraction suggest a small bedrock valley exists parallel to the HPFZ beneath the MBL. The MBL is clearly parallel to the HPFZ, but so are several other ridges or stream reaches in the area, whereas other features are aligned at near right angles to these. Taken together, these features suggest a regional pattern of structural control on recent geomorphic activity, not simply a single reactivated fault.

Introduction

The Meadow Bank Lineament (MBL) is a remarkably straight 5 to 10 m (15-30 ft) high escarpment along the lower Wabash River Valley in east-central White County, Illinois (Fig. 1). This location coincides with the southern part of the Wabash Valley Seismic Zone (WVSZ) which has produced multiple moderate earthquakes (Fig. 2), several exceeding M 5.0 within the past 175 years (Herrmann et al., 2008). Instrumentally recorded earthquakes originate at mid-crustal depths averaging 15 km (9 mi; Herrmann et al., 2008). One is clearly associated with a previously mapped fault (Kim 2003). Paleoseismic studies indicate that the WVSZ experienced at least seven earthquakes with magnitudes likely greater than M 6.0 within the Holocene (Obermeier, 1998). Recent research has identified Quaternary displacement on faults in the northern Mississippi Embayment (McBride et al., 2008) and the lower WVSZ, (Woolery 2005). Berry (1908) reporting an interview with an eye witness of the 1811-1812 New Madrid earthquakes (Fuller, 1912) described a large area of liquefaction and a 2-mile (3-km) long fissure ("crack") running west-east across the Wabash River flood plain just east of the MBL. Heigold and Larson (1994) used constant-space resistivity profiles to search for the reported fissure. They did not find the fissure, but did find evidence of liquefaction. Hough et al. (2005) visited the area and conducted a single p-wave reflection profile with ambiguous results. Based on the information provided by Berry (1908) and their preliminary seismic data, Hough et al. (2005) proposed the existence of an active east-west cross fault in the area.

The MBL is parallel to, but about 1.5 km (1 mi) east of, the Herald-Phillipstown Fault Zone (HPFZ) one of the major fault zones within the Wabash Valley Fault System (Bristol and Treworgy, 1979, Nelson, 1995). The HPFZ defines the west side of a graben with the east side defined by the Maunie Fault zone (Fig.3). Both fault zones consist of high-angle normal faults striking slightly east of north. Displacement of strata within the graben is approximately 50 to 100 m (160-330 ft) down (Fig. 3), and generally dips northward. Displacement is asymmetrical, with significantly greater downward displacement on the west resulting in a minor anticlinal form within the graben (Bristol and Treworgy, 1979) and locally strongly westward apparent dip. Nelson (1995) indicated that development of the WVFZ is thought to have initiated when deep crustal Cambrian rift faults were reactivated during compressional Ancestral Rocky Mountain (ARM) orogenesis, which caused folding and faulting of strata. Subsequent Mesozoic extension resulted in normal faulting and graben development. In many cases throughout the WVFZ, compressional reverse faults, formed during ARM orogenesis, were reactivated as normal faults.

Subsurface geologic data of coal seam structure and faults in the White County Coal company's Pattiki Mine within the field area were recently released to the public. The Pattiki mine extracted 2 m (7 ft) of Herrin coal at a depth of approximately 300 – 350 m (985-1150 ft). While the mine was operating, coal extraction efforts in the underground mine encountered multiple minor faults, all part of the HPFZ. These faults are too far west to be associated with the Meadow Bank.

In previous investigations, Heigold and Larson (1994) used continuous seismic refraction, VES electrical soundings and limited test borings to investigate the nature of the Meadow Bank Lineament. Electrical properties of the shallow sediments were found to be strikingly different east and west of the MBL, consistent with the interpretation that the sediments west of the MBL were deposited in Glacial Lake Carmi. However, neither geophysical method was able to resolve displacements within the Quaternary or Pennsylvanian sediments. Closely spaced boreholes on either side of the MBL indicated that the bedrock surface was lower east of the MBL, but shallow limestone markers within the Pennsylvanian bedrock did not show a similar pattern of displacement. The geophysical tools available to Heigold and

Larson (1994) had insufficient resolution to adequately test for displacements in the Quaternary and shallow bedrock sediments. Their finding of a lack of offset was not conclusive.

The close parallel orientation of the MBL and the HPFZ, the location of the MBL within the WVSZ, historical reports of liquefaction in the area, raise important questions: Is this surficial feature genetically related to the HPFZ or some parallel, but unknown fault? Is it a seismically induced landslide? Or is this a recent erosional feature? If this surficial feature has a tectonic origin genetically related to the HPFZ, it could pose a future threat to the area. In this case, it is directly relevant to the earthquake hazard reduction program and warrants more investigation.

Methods

Coring

A borehole transect across the MBL along County Road 1175 N was prepared to characterize the age and lateral continuity of sediments, look for marker beds or stratigraphic horizons that could indicate fault-related vertical offsets within the sediment package, and ground truth the earth electrical resistivity profile data. A total of 8 cores (33023-33031) spaced 50-200 m (160-650 ft) apart were obtained by percussion methods in June and July 2013 (Fig. 4). The ISGS Power Probe uses Geoprobe tooling, and acquires samples in 4.7 cm (0.15 ft) ID clear plastic liners in 1.5 m (5 ft) increments. Three cores, 33023-33025, penetrated the sediment to bedrock. Core 33026 reached the limit of our tooling at 30 m, although we suspect that bedrock occurred shortly below that based on archival data and the new geophysical data. Samples for optically stimulated luminescence (OSL) analysis were obtained by using opaque liners at preselected intervals. The liners were rendered opaque by spray painting them in advance with black paint (both alkyd enamel and automotive epoxy paints were used), or covering them with aluminum foil tape. Both methods worked to a limited extent because the coverings could be scratched by the injection of fine to medium sand between the liner and the barrel. Field descriptions were limited to samples that were retained in the core catcher. Core locations were determined by handheld GPS with an approximate horizontal accuracy of 1-5 m, and were crossed checked against how they plotted on aerial photography. Borehole elevations were determined by inspection from a 1.3 m (4.3 ft) pixel DEM with 0.08 m (0.26 ft) vertical accuracy.

The proposal called for mud rotary coring into bedrock in addition to percussion coring. However, we determined that mud rotary would not be helpful. The Quaternary package is entirely sand and fine gravel, which would be poorly sampled by the mud rotary method although the hole could be logged geophysically. More importantly, the bedrock coring would need to penetrate tens of meters in order to encounter a correlatable limestone. The Pattiki coal mine data (below) were deemed sufficient to characterize this deep geology, so the mud rotary coring was abandoned as redundant.

Thirty (30) cm (~1 ft) long intervals of the opaque runs were cut from the core for OSL analysis before further study. The remaining core liners were then split, photographed, and described. Macroscopic descriptions included color, texture, fabric, contacts, pedologic features, and inclusions. In addition, suites of samples were obtained for additional testing in ISGS laboratories. Particle-size distributions were determined using a Mastersizer 3000 Particle Sizer laser diffractometer. Some clayey to loamy textured sediment was also characterized for sand-silt-clay distributions by hydrometer. Mineralogy of a suite of sand samples was determined by bulk x-ray diffraction after first micronizing the sample. Calcite-dolomite contents were determined by the Chittick method (Dreimanis 1962). Finally, ages were obtained through OSL (n=16) and radiocarbon (n=2) methods.

Porosity and Water Content

Water content is a parameter in OSL age calculations. For samples above the water table, sediment samples were taken immediately upon core retrieval and retained in 4 oz. metal cans that were then sealed with electrical tape. The samples were weighed before and after drying in a 90°C oven for 24 h. The gravimetric moisture content was then determined as m_{wet}-m_{dry}/m_{dry}*100, where m = mass.

For samples below the water table, porosity was estimated from texture and summary tables developed by McWhorter and Sunada (1977) and assumed to be equivalent to saturated water content. As a cross reference, porosity was determined quantitatively on a selection of samples. For those samples, a measured volume of sand (~30 cm^3 [0.0011 ft^3]) subsampled from the core was poured into a TEMCO helium porosimeter. After evacuating the air from the sample chamber, helium at a known pressure and contained in a set volume was allowed to expand into the chamber. The volume of the sand particles was then calculated with Boyle's law using the known volumes of the sample and helium chambers, and the observed pressure drop. The porosity, determined as the inverse of this volume, was then assumed to be equal to the saturated water content.

Dating

Sediment ages were determined by OSL using the single aliquot regenerative dose protocol (Murray and Wintle 2000; Wintle and Murray 2006) and by radiocarbon dating of plant fossils and wood fragments in ISGS Geochronology Laboratories. For OSL determinations, 30 cm (~1 ft) sections were cut from selected core intervals that had been obtained with opaque liners. Each sample was opened and processed in an amber-light lab. From each subsampled interval, ~ 110-130 grams of sample were weighed then dried overnight in a 90°C oven. A gravimetric moisture content of the sample was then determined from the weight difference. This measurement can be compared to the gravimetric moisture contents estimated from bulk core samples and porosity measurements as described above. Differences could be caused by drainage or equilibration of the core between acquisition and subsampling. Organic material was removed from the dry samples by baking in a 450°C furnace for at least 4 hours. The baked samples were crushed and ground to fine powders for U, Th, and K content measurement by gamma spectrometry.

Samples of 250 µm to 150 µm size fraction from the middle of each sampled interval were segregated by wet sieving. Each segregated sample was treated with a 2M HCl and bleach solution for two days to remove carbonates and organics. Quartz and feldspar grains were separated from heavy minerals in a centrifuge using a 2.70 g ml-3 lithium metatungstate liquid. The separated quartz and feldspar grains were treated with 48% HF for two hours followed by DI water, 2M HCL, and DI water rinses. Finally, naturally dried quartz grains that had been etched to smaller than 150 µm by the acid treatments were sieved out and discarded. The remaining sample was used for equivalent dose analysis.

The equivalent dose (D_e) of purified quartz grains was obtained from the interpolation of sensitivity-corrected natural OSL signals from a sensitivity-corrected regenerative dose-response curve (Fig. 5), after rejection of unacceptable aliquots. Preheat temperature from 240 to 260°C for 10s and cut-heat temperature from 200 to 220°C were used depending on individual dose recovery, preheat plateau, and thermal transfer tests (Fig. 6). The dose recovery test (Fig. 6A) showed that the quartz could be reset and equivalent doses determined precisely within the range of the instrumentation. Preheating is performed in the OSL procedure to force the release of unstable electrons. Preheat plateau tests (Fig. 6B) showed that the optimal preheat temperatures were 200-260°C. Thermal transfer tests (Fig. 6C) showed that equivalent dose determinations were stable over preheat temperatures from 240-300 °C,

i.e., that the preheat temperature was low enough to not also move the stable electrons between crystal traps. All D_e were measured on odd positions of a carousel in a RISØ TL/OSL-DA-20 reader with a 90Sr/90Y built-in source, blue LEDs centered at 470 nm, a Hoya U-340 filter, and an EMI 9635 QA Photomultiplier tube. The D_e analysis used software by Duller (2007), which includes Monte Carlo approaches as well as other criteria for accepting or rejecting individual aliquots. The criteria for rejection included recycling ratios between 0.9 and 1.1, an indicator of the quality of quartz grains; IRSL/OSL ratios between 0.9 and 1.1, an indicator of contamination by feldspar, and OSL signal saturation. Weighted means of accepted D_e were taken for central age model calculations (Fig. 7).

Dose rates were determined on pulverized and baked samples weighing approximately 100 g, which were tightly held in Marinelli beakers using a low background ORTEC GEM-40190P Gamma Spectrometer. Test samples were packed to a fixed thickness using a lab-made plunger that perfectly fits the internal volume of the Marinelli beakers. The beakers were further sealed with several layers of plastic paraffin film for 3-4 weeks to achieve equilibrium of radon gas before measuring.

Organic material (soil, seeds, and shell fragments) suitable for radiocarbon dating was found in two sedimentary units. The material was submitted to the ISGS Chronology Laboratory where the samples were prepared and the carbon was pyrolized (Wang et al., 2003). The pyrolized sample was sent to the Livermore CAMS Center for testing by Accelerated Mass Spectroscopy (AMS).

Magnetic Susceptibility

Volumetric magnetic susceptibility (MS) was measured at systematic intervals in each core. MS variability in Quaternary sediment is caused by variations in magnetic mineral contents, which can be caused by sediment provenance, concentration of heavy minerals by sorting, reductive dissolution in waterlogged soils catalyzed by iron reducing bacteria in the presence of organic matter (Grimley and Arruda 2007), or by neoformation of ultrafine magnetite in moderate to well-drained soil A horizons. MS was measured on a flattened surface of the core at 15 cm (~0.5 ft) depth increments with a Bartington MS2 meter and MS2F probe. The volume SI units (Système International d'Unités) are dimensionless. Replicate measurements were taken at each increment to ensure instrumental stability, and multiple measurements were taken over ~2 cm (0.07 ft) radius to assess possible abnormal influence of heterogeneous lithologies.

Electrical earth resistivity

We acquired three earth resistivity profiles traversing the Meadow Bank Lineament in June 2013. These profiles were designed to investigate the Quaternary sediments on either side of the lineament in three distinct geomorphic locations (Fig. 4). One profile crosses the lineament in the center of the feature and continues east across the eastern apron into the bottomlands of the Wabash River. This is the location of the focused drilling transect. A second profile, on the north end of the feature crosses both the main scarp and the offshoot scarp. The third profile, on the south end of the feature crosses at a point where the lineament was eroded and steepened by meanders of a small stream.

The dipole-dipole electrode configuration with a 5-m nominal electrode separation on 400-m long lines extended at 100-m increments was used to create resistivity pseudosections to depths of 60 m. GPS locations were obtained every 100 m (330 ft) along the profiles, and topography was calculated from LiDAR-based DEMs. Loke's finite difference algorithm (Loke and Barker, 1996) was used to invert the pseudosections to resistivity models.

Results of Investigations

The subsurface across the MBL was investigated with new geophysical surveys, a borehole transect, geomorphic mapping using high resolution topographic data, and study of subsurface coal mine maps. Although various geophysical and sedimentological features were distinguished, none of them show vertical offsets that could indicate a tectonic origin for the MBL. Rather, the data are consistent with a terrace scarp formed by erosion during one or more late Wisconsin Episode flood events.

Description

A cross section was constructed with data from archived 2 mud rotary borings with gamma logs, 8 percussion probe borings obtained for this study with nominally continuous sampling including 3 that reached bedrock, and the EER profile (Fig. 8). The new cores were described for macroscopic features including texture, color, contacts, pedologic features, and inclusions. Suites of samples were obtained for particle size (laser diffraction and hydrometer), mineralogy (x-ray diffraction, micronized bulk pack), porosity, and calcite-dolomite contents (Chittick). Finally, ages were determined by OSL (n=16) and radiocarbon (n=2) methods.

The 850 m (2790 ft) long core transect crossed the MBL at nearly a right angle and crossed the high (Glacial Lake Carmi) terrace, middle terrace including the colluvial slope, and the low terrace. Borings were taken along the south road shoulder and into a farm field, along the same line as the central resistivity survey. Also included in our analysis are two borings that were acquired adjacent to our transect line by Heigold and Larson (1994). The borings penetrated 12-25 m (40-80 ft) of bedrock, were logged by natural gamma, but were not physically sampled. The core data allowed for the delineation of 3 zones of Quaternary sediment, comprised of 8 map units.

Map Units

The core were visually described and classified into lithostratigraphic units following previous investigations in the Wabash Valley (Bryk et al. 2012; Phillips 2012; Phillips et al. 2013) and nomenclature by Hansel and Johnson (1996). Individual core descriptions are in Table A1. The cross section stratigraphy is summarized as follows.

Hudson Episode (~12,000 years ago until today)

Qc [Cahokia Fm]. Alluvium, including fluvial and paludal facies. Gray brown (2.5Y5/2), brown (10YR3/2) to dark yellowish brown (10YR4/3) silty clay loam to clay loam; massive to weakly bedded; modern soil development, typically cumulic.

Qpy [Peyton Fm]. Colluvium, interbedded slopewash, eolian, and fluvial deposits. Dark brown to yellow brown (10YR3/6-5/6), silty clay loam, sandy clay loam, silt, and coarse sand, bedded to weakly laminated; modern soil development, typically cumulic.

Wisconsin Episode (~55,000 – 22,000 years ago)

Qh-pk [Parkland Member, Henry Formation]. Eolian dunes, may include minor intercalated loess, deposited from westerly winds. Light yellow brown to reddish brown

(5YR4/3) fine to medium sand, loamy, bedded; upper part includes modern soil development, illuvial clay-rich horizons; distinct lower contact, intercalates with loess on lee (east) side of dunes.

Qp [Peoria Silt]. Loess. Dark yellow brown (10YR4/4), brown (10YR4/3), to light brownish gray (2.5Y6/2) silty clay to silty clay loam, massive to laminated; modern soil development in upper part; distinct lower contact.

Qh(s) [Henry Formation (sandy facies)]. Outwash. Light brown to gray medium to coarse sand, with fine sand, laminated to thick bedded (<0.6 m (<2 ft)); calcareous (C-D horizon); mainly sedimentary lithic fragments, but also igneous and metamorphic lithologies; rare pebbles, gastropod fragments; C to D horizon (calcareous); gradual to distinct contact.

Qh(g) [Henry Formation (gravelly facies)]. Outwash. Light brown to gray very fine gravel to gravelly sand, with sandy zones; beds 0.3-0.6 (1-2 ft) thick; mainly sedimentary lithic fragments, but also igneous and metamorphic lithologies; C to D horizon (calcareous); lower contact distinct.

Illinois Episode (~300,000 to 150,000 years ago)

Qpl. Outwash [Pearl Formation]. Yellow brown to very light brown with pink hue very fine gravel to sandy gravel and granular medium sand; beds 0.15-0.6 m (0.5-2 ft) thick; root (upper C horizon) of paleosol indicated by v. weak to weak acid reaction (dolomitic) over strong reaction (calcareous); lower contact is bedrock.

Pennsylvanian (~330,000,000 – 268,000,000 years ago)

Pm(sh). Shale [Mattoon Formation]

Pm(co). Coal [Keensburg Coal, Mattoon Formation]

Pb(ls). Limestone [Millersville Limestone, Bond Formation]

Pb(ss). Sandstone [unnamed, Bond Formation]

Sedimentology

The bedrock surface steps from ~94 m (310 ft) asl below the high terrace, to 88 m (290 ft) asl below the low terrace, separated by a 5 m (16 ft) deep trough. This trough cannot be traced yet in the subsurface because lateral borehole control is limited, but is a target in ongoing mapping studies. The trough cannot be seen at the 1:500,000 scale of the bedrock topography map by Herzog et al. (1994). The deep borings (32588 and 32589) penetrate the Millersville Limestone, which spans the MBL. The difference in elevation of the Millersville Limestone between the borings is in accordance with regional dip. The bedrock encountered in cores 33023-5 was shale.

Immediately above bedrock occur 3-17 m (10-55 ft) of poorly sorted fine and very fine gravel to medium sand. Within the trough is an overall fining upwards sequence of interbedded very fine gravel, granular sand, fine gravelly coarse sand, and medium sand with single-grain thick gravel contacts, mapped as the

Pearl Formation (Qpl). Massive to weakly graded beds are 0.15-0.6 m (0.5-2 ft) thick. The abundance of metamorphic and igneous lithic fragments increases with depth. The upper 2 m (7 ft) are lightly oxidized to light brown and are mostly leached of carbonate as evident by a very weak (dolomitic) reaction to hydrochloric acid. The reaction increases with depth to vigorous in the lowermost meter.

Overlying Qpl and extending onto the bedrock over the rest of the section is interbedded light brown coarse to fine sand with fine gravel beds, mapped as a gravelly facies of the Henry Formation (Qh(g); (Fig. 8). The massive to graded beds are 0.15-0.6 m (0.5-2 ft) thick. The contact between Qh(g) and Qpl is sharp and the eastern end is depicted as unconformable on the east side of the trough.

The Qh(g) is abruptly overlain by broadly uniform, moderately well sorted medium to coarse sand with little gravel (Fig. 8), mapped as the sandy facies of the Henry Formation (Qh(s). The contact between the Qh(g) and Qh(s) is easily recognized in the core, but whether it is conformable or erosional cannot be determined. It undulates with ~1.5 m (5 ft) of relief. Within Qh(s), several bedding horizons recognized by slight color changes or slightly gravelly zones can be correlated along horizontal planes between cores across the western portion of the section, but they are generally discontinuous. The overall fining upward sequence within the sandy units is evident in the grain-size curves, which have consistent unimodal and moderately well-sorted distributions. The sand, in turn, is overlain by any of 4 fine-grained surficial units ranging from silty clay (Qc), to silty (Qp), to loamy (Qpy), and sandy (Qh-pk) sediments. The grain-size distributions are more skewed to bimodal than the underlying sandy units (Fig. 9). The contact between the sand and the surficial units is abrupt and interpreted to be largely erosive in nature. The surficial units are interpreted to have both cross-cutting and intercalating relationships with each other.

The modern soil is developed into the upper 0.3-3.7 m (1-12) ft of the succession. Soils on the Carmi Terrace and the colluvial slope of the MBL are well drained, but they are poorly drained on the middle and lower terraces. Cumulic soils occur on the colluvial slope and in the alluvium of the low terrace.

Porosity

Porosity was determined on a limited number of samples from the sandy units to test the assumptions of saturated water content in the OSL analysis (Table A2). Porosity ranged from 20-30% in well sorted fine sand to moderately sorted coarse sand, but there is not a consistent relationship to the measured grain-size distributions (Table A3, Fig. 9). The values fall within established ranges for unconsolidated sand (e.g. McWorter and Sunada 1977).

Mineralogy

Mineralogy was characterized by x-ray diffraction (XRD) (Table A4) and calcite/dolomite determinations by Chittick (Dreimanis, 1962; Table A5). The XRD determinations were intended to qualitatively inform interpretation of the gamma, resistivity, and MS response curves. The mineralogy was dominated by quartz, with isolated zones of elevated plagioclase and minor potassium feldspar concentrations. These concentrations occurred non-systematically in non-weathered (Qh(s), Qh(g)) and, surprisingly, in weathered (Qh-pk, Qc) units. Thus they cannot be used as indicators of provenance or for stratigraphic discrimination.

Carbonate content has been used to discriminate provenance and to characterize weathering profiles (Dreimanis 1962; Johnson 1971). The 4 longest borings, 33023-33026, were assayed for carbonate content below the surficial weathering profile, in which carbonate was determined to be 0 by reaction

to HCl. The longest boring, 33026, was sampled at ~2 m (7 ft) intervals or finer. The other borings were sampled on a coarser interval.

Total carbonate (TC) ranged from 1.2-19.1%, with a threshold of ~10% between “high” and “low” TC (Table A5). TC broadly increased with depth between ~120 m (~390 ft) asl and ~104 m (~340 ft) asl, then decreased to a minimum at 88 m (290 ft) asl. Within the Qpl, TC increased with depth from 1.0-3.7 m (3.3-12.1 ft), and the upper 3 m (9 ft) of Qpl was distinguished by very low calcite contents, consistent with a weak weathering profile. A threshold between high and low TC defines a gently eastward-dipping horizon in the lower half of Qh(g). Below the horizon, calcite was much lower than dolomite. Above this horizon, TC was generally above 10%, although isolated samples exhibited low TC and variability appears random. As well, calcite was higher than dolomite in much of Qh(s), but calcite was lower than dolomite in the middle of the unit in a < 20 m (67 ft) thick lens that pinches out eastward.

Natural Gamma and Magnetic Susceptibility

Included in the study section are two test holes (B1 and B2) from Heigold and Larson (1994). The holes were logged with natural gamma tools to provide continuous characterization of the Quaternary sediments. The natural gamma logs show distinct Quaternary and Pennsylvanian successions (Fig.10). Clear although small inflections can be correlated between the two. The gamma logs show moderately high count rates within the surficial fine-grained units, ranging from ~50-110 cps, before gradually decreasing to 30-40 cps within the sand. Short (~1 m) slightly higher count rate intervals occur at the Qh(s)/Qh(g) contact. In the lower 7 m (23 ft) of B1, the count rate decreases and correlates to the gravelly Qpl in boring 33026. There is a sharp increase of count rate at the bedrock surface, below which natural gamma is consistently greater than 110 cps.

Magnetic Susceptibility was measured at discrete points (Table A6), but is depicted as continuous curves in Figure 11. Variability between adjacent measurements was high; raw values were smoothed with a 5 point boxcar. MS is influenced by the presence of magnetite and magnetite-bearing minerals, grain size, and, for these volumetric measurements, the mass (size of the core) around the probe tip. MS is enhanced in the upper horizons of well-drained soils formed in warm and intermittently moist conditions by the in situ formation of ultrafine magnetite (Grimley et al. 2003). By contrast MS is decreased in poorly drained (anaerobic) soils, or strongly developed and intensely reduced inacidic soils (Grimley and Vepraskas 2000). Although the natural gamma and MS signals reflect different lithologic properties, both measurements can be sensitive to stratigraphic variability. The natural gamma and MS signals are both shown on Fig. 11, where the absolute values of the various signals is unimportant, but the relative shape and inflection points in the curves indicate differences.

Both high and low MS anomalies were measured in the upper few meters of each core, likely reflecting both varying grain size and soil development across the landscape. There is a distinct excursion in each curve at the base of the surficial unit (Fig. 11). Meter-scale anomalies at a 2-5 m (7-16 ft) depth are possibly correlatable although they reflect some as yet undetermined lithologic property. Sharp positive excursions occur at the Qh(s)-Qh(g) contact in borings 33024-33026. Large anomalies within Qh(g) occur in both 33025 and 33026, below which MS is relatively low.

Electrical earth resistivity

Resistivity values were similar on all three traverses (Fig. 12). In general, the resistivity varies from about 10 ohm-m in the shallow wet lands on the east of the lines to at least 2000 ohm-m beneath the Carmi

Terrace west of the MBL. Most of the other Quaternary sediments have resistivity values of 100 to 250 ohm-m, typical of sand and gravel encountered in boreholes. Generally lower resistivity values of 60 to 80 ohm-m occur deeper in the resistivity sections and likely mark the top of the Pennsylvanian-aged bedrock. Both the northern and southern lines encountered buried pipes and electric power lines that produce noisy resistivity models at shallow depths.

The Central Line is in Section 34 T. 5 S. – R. 10 E, White County. It was acquired on County Road 1175 N starting from the intersection with County Road 1500 E (UTM: 403,718 E; 4,211,821 N) and continuing east for 1200 m. This resistivity profile coincides with the borehole transect and provided considerable data that contributed to construction of the lithologic cross section. The western part of the Central resistivity line crosses nearly 500 m (1650 ft) of a dune field before encountering the MBL. A zone of very high-resistivity sediment (300 to over 1000 ohm-m) lies beneath the dunes on the Carmi Terrace. The top of this zone is at a depth of about 3 m (10 ft). It is thicker beneath the center of the Carmi Terrace and is only about 10 m (33 ft) thick east of this terrace. The very high-resistivity zone ends abruptly beneath the MBL. East of the MBL, a high-resistivity zone (about 200 ohm-m) occurs from the ground surface to about 7 m (23 ft) deep. Farther east, a small, shallow low-resistivity zone (10 to 30 ohm-m) marks sediments of an ephemeral tributary to the Wabash River. A second shallow, low-resistivity zone (40 to less than 10 ohm-m) was encountered at the east end of the line. This low-resistivity zone is consistent with organic-rich silts and clays of alluvial origin. Beneath all of these shallow resistivity zones is a continuous layer of moderate to high resistivity (100 to 200 ohm-m) that correlates with sand and gravel. This layer extends beneath the high-resistivity zone on the west and beneath the shallow low-resistivity zones in the center and east. It extends up to the ground surface on the east, between the zones of low-resistivity. The bottom of this moderate-resistivity zone is at a depth of about 25 m (80 ft) on the west, but is about 30 m (100 ft) deep on the east. A variable, but generally low-resistivity zone lies beneath this high-resistivity layer. This lower layer correlates with the top of Pennsylvanian-aged clastic bedrock. A small zone of relatively high resistivity (200 to 300 ohm-m) within this lower zone is consistent with limestone within the bedrock.

The zone of very high resistivity beneath the dune field is unusual and distinctive. In the Central Line, the high-resistivity zone continues eastward past the MBL at the ground surface, but has a much lower resistivity of 200 ohm-m instead of 300 to over 1000 ohm-m. This resistivity pattern is consistent with either a fluctuating ground water table or with erosion, but is not consistent with faulting.

Ages

Sixteen ages were determined by OSL (Fig. 7, Table A7) and two by radiocarbon AMS methods (Table A8). The optical age determinations show evidence of some partial bleaching, common to fluvial samples (Fig. 7). However, analysis of the totality of the results suggests that they are acceptable. Laboratory tests of the dose recovery and dose rates were acceptable (Fig. 6) Ages were based on 18-24 D_e determinations each, and showed dispersions of 6-28% (Fig. 7). Optical ages typically have errors of 10%. The corresponding ages ranged from 47.25±0.83 ka to 14.79±1.07 ka.

The stratigraphic distribution of ages is shown in Fig. 8. To the extent possible and limited by core recovery, samples for dating were taken along elevation planes. Within each boring, the ages generally become younger upwards, from 38-33 ka to 22-10 ka. Although the dune sediment sampled in boring 33023 was not dated, the dunes can be correlated geomorphically to dunes on a bedrock high 9 km (5.6 mi) to the southeast, with OSL dates of 21.7-22.9 ka (Phillips et al. 2013). There are instances of stratigraphic reversals of the ages. In 33024, the reversal from 45.1±4.8 ka at 99.4 m (326 ft) asl to 42.6±3.6 ka at 103.0 (338) ft asl is within the error of the ages. By contrast, in 33026, the reversal from

30.7±2.9 at 100.3 m (329) ft asl to 44.6±3.3 ka at 103.9 m (341 ft) asl is larger than the error. Reversals of optical ages are not uncommon, especially in fluvial sediments, but the cause in this study is yet uncertain. Analysis of the ages is continuing, so we do not yet reject the aberrant samples.

Comparison of suites of optical ages between cores is more problematic. Although the cores on the west (33023) and east (33025) are internally consistent, the eastern side ages are systematically ~5 ka younger at correlative elevations. That difference could be explained by relatively recent sedimentation closer to the valley axis. More problematic, there is a zone of anomalously old ages at the center of the section, below the MBL and middle terrace. The difference is larger than can be explained by the errors. However, there are so many of them (6/16), that they cannot be rejected as individual bad dates, especially considering that the laboratory results appear to be good. In fact, the zone includes ages with both our most confident (ISGS 244, 44.6±3.3 ka) and least confident (ISGS 246, 39.5±3.9 ka) determinations (Fig. 7).

At the contact between Qc and Qh(s), as shown in boring 33025, several organic layers were encountered with radiocarbon-datable material. At 2.1 m depth in map unit Qc, there was a 1 cm (0.03 ft) thick, organic, dark gray, silty clay loam bed at the base of a laminated sequence of silty clay and very fine sand alluvium. The bulk AMS date (ISGS A2843) was 9,470 ± 30 radiocarbon years before present (rcybp), which calibrates to 10,670-10.751 ka (Table A8). At 2.5 m (8.2 ft) depth in map unit Qh(s), seeds, ostracodes, gastropod fragments, and woody fibers were found in a 0.15 m thick bed of dark gray laminated silty fine sand and sandy clay loam alluvium. The seeds (Narja sp.) were dated to 14,230±45 rcybp (ISGS A2846), which calibrates to 17,231-17,436 ka (Table A8;). Between those two samples, at 2.3 m (7.5 ft) depth, an optical age was determined on fine sand as 14.79±1.07 ka. The accuracy of that age is thus strongly supported by the adjacent AMS dates.

Structure map of the Herrin Coal from Pattiki Mine

White County Coal Company's Pattiki mine extracted coal from beneath the MBL, and further to the east, from 1982 to 2002. The mining method was room and pillar. The mined out area resulting from this activity was a systematic network of intersecting entries 6 m (20 ft) across, interspersed with regularly spaced pillars 80 to 100 feet apart. The mine extracted 1.4-1.5 m (4.5-5 ft) of the Herrin coal at a depth of 290-305 m (950-1000 ft).

In accordance with MSHA regulations, the Pattiki mine produced a map that shows the mine workings, faults, and elevation of the mine floor with a contour interval of 3 m (10 ft; White County Coal Co., 2003; Fig. 13). Coal elevation maps are typically created by contouring in-mine survey points collected every few hundred feet or less, depending on mine plan, with test drilling providing elevation control outside of the mined areas. Fortuitously, the mining directly underneath the MBL is a dense network of rooms and pillars, many with room spacings of 30 m (100 ft) or less, thus providing a high degree of confidence in the elevation map.

The mapping provided by the company indicates that directly below the MBL, and in a band within a few hundred feet along the MBL trend, there is no alteration to the mine plan, no offsets within the coal, and gently sloping coal elevations. By comparison, 600 m (2000 ft) to the west, and closer to the HPFZ near the mine entrance, a small normal fault within the coal occurs. This fault ranges from a few cm to 3.7 m (12 ft) of displacement over a distance of approximately 1200 m (4000 ft), parallel to the HPFZ. The mine plan is altered by this fault.

Interpretation

Bedrock Structure

Structure maps of the Herrin Coal beneath the MBL and vicinity (Fig. 13) indicates that directly below the MBL, there is no evidence of faulting (White County Coal Co., 2003). A tectonic fault capable of creating a 6-9 m (20-30 ft) displacement at the surface would presumably need at least 6 m (20 ft) of displacement within bedrock. A displacement of as little as 1.5 m (5 ft) can alter mining patterns in room and pillar operations, as continuous miners need to mine 'up' or 'down' through either roof or floor rock to get back to mining coal. Fault perturbations of greater than 1.5 m (5 ft) in the coal seam can exhibit themselves as a continuous chain along the trend of displacement of extra-long entries across the fault, where machinery gets back into coal, or as a less dense network of excavation due to the company avoiding the unwanted extraction of noncommercial waste rock. The Pattiki mine map along the MBL shows no fault offsets or mine plan alterations.

To further constrain the inquiry, upon examining the mine map, it is tempting to associate the HPFZ, or an inferred fault trend of the HPFZ found near the mine entrance with the MBL. However, when the geometric relationship of the MBL, the in-mine fault, and the HPFZ are plotted in a cross section at a scale of 1 to 1 (Fig. 14), it is clear that any hypothetical tectonic feature involving bedrock offset would most likely have to originate within close map-view proximity to the MBL. It is not reasonable to propose an extreme low angle thrust within the current regional structural setting.

In summary, due to the extremely fortuitous situation of having a modern coal mine directly below the feature in question, we can rule out bedrock offset for the origin of the MBL.

Landslides

Another possible earthquake-related cause of the MBL could be an earthquake-induced landslide or lateral spread similar to those observed in the lower Mississippi River valley following the 1811-1812 New Madrid earthquakes (Fuller, 1912; Jibson and Keefer, 1988, 1993; Doyle and Rogers, 2005). Documented seismically-induced landslides occurred along the Chickasaw Bluffs of Kentucky and Tennessee as well as on Crowley's Ridge in Missouri and Arkansas. However, the mapped region of 1811-1812 landslides does not extend north of Cairo IL. Other landslides are documented along the lower Ohio River near Olmsted (Killey, et al. 1985), but landslides from any cause (except direct undercutting of river banks) are unknown in the Lower Wabash Valley (Killey et al., 1985; Bryk et al. 2012; Phillips, 2012; Phillips et al. 2013; this report). Landslides have distinct morphology (Jibson and Keefer, 1993) with arcuate head scarps, hummocky slide areas, depressions from pull apart areas and ridges along the toe. Although the overall dimensions may vary from very large to very small, the ratio of the width of the displacement to the height of fall tends to be on the order of 5 or 10 to one (Fig. 15). By contrast, the MBL is remarkably straight, not arcuate, and with a width to height ratio of 70 to one. Examination of LiDAR reveals a smooth, not hummocky topography downslope from the MBL scarp. Ephemeral streams are present at the base of the scarp, similar to what one would expect from a pull-apart graben. But these streams are equally explained by internal drainage on stepped terraces.

Typically, landslides fail along a clay layer or other weak zone at depth. In western Kentucky and Tennessee, for instance, this surface is usually a clay layer within the Jackson Formation (Jibson and Keefer, 1993). Lateral spreads occur when sand layers confined by overlying alluvial clay liquefy in response to the earthquake vibrations. The unsupported clay splits into blocks which float downslope on the liquefied sand (Doyle and Rogers, 2005). Drilling at the MBL revealed thick sandy outwash overlying

gravel above bedrock. There are no continuous clay layers that could act as slip surfaces and there is no alluvial clay cap that could confine the sand if it were to liquefy.

Other Lineaments

The MBL is an unusually long, straight feature expressed in soft sediments. It is developed within a region in which similar linear and rectilinear features are common (Fig. 16). We have not thoroughly examined the nature of the linear patterns expressed in the region, but point out some of them for possible future investigations. The Ohio River is characterized by long, straight, orthogonal northwest or southwest reaches. The azimuth of these reaches are remarkably parallel to each other. Bends in the river occur at regular intervals and at some locations repeat the same alignments on subsequent bends. Several of these major alignments can be traced to aligned tributaries, bluffs, and other features in the landscape including bends and reaches along the Wabash River and its tributaries. The northern reach of the Lower Wabash (from Vincennes to Grayville) appears to follow one of these lineaments. Downstream of Grayville, the river channel follows instead the line of the New Harmony Fault Zone. In this context, the MBL is sub-parallel to one of the main regional lineaments. Its length is within the same magnitude of several of the large bends on the Ohio River.

On a larger scale, several parallel and orthogonal lineaments to the MBL are evident in the immediate area around the MBL (Fig. 17). These lineaments, typically bluff lines, stream alignments, and meander margins extend for several miles on either side of the MBL. Some of the parallel lineaments are the same length as the MBL, suggesting that the MBL is not unusual in this area. We did not fully investigate these lineaments, but note that their presence suggests an underlying structural control on the drainage patterns in the region and that the MBL appears to be associated with this rectilinear pattern. Even though we conclude that the MBL was not the result of neotectonic activity, this does not preclude some neotectonic movement in the area.

Subsurface Geology

Tectonic movement can be identified in sedimentary sequences by vertical offset of correlative layers. That is made easier by the discovery of marker beds or distinctive contacts. In this study, the deeper sedimentary package is largely sand. Although several horizons could be correlated between cores, no marker beds were found. Instead, stratigraphic units, material properties, and ages were used as proxy. The surficial map units are characterized by cross-cutting and intercalating relationships. By contrast, the subsurface map units are sub-horizontal and continuous. The gently dipping, undulating contact between Qh(s) and Qh(g), in particular, is supported by gamma and MS (Figs. 10-11), texture (Fig. 9), and mineralogy (Tables A4, A5). This is consistent with erosion and sedimentation, not with tectonic offset.

Because of the weak lithologic distinctions, further consideration of the uncertainty in the luminescence ages is important. Despite significant uncertainties, we find the ages acceptable because:

- The results for shine down, thermal transfer, radioisotope activity, and dispersion are within acceptable limits.
- The age range (the valley fill in our study rich mostly occurred during advance of the Wisconsin Episode ice sheet) fits our expectations.
- Most of the age results are stratigraphically correct.
- The tight nesting of one sample between two radiocarbon dates (ISGS 2843, ISGS 2846) supports the accuracy of that optical date.

- Correspondence of the age at the top of Qh(s) and correlated age of the overlying dunes Qh-pk is consistent with their interpreted genesis.

The SAR method requires use of a Central Age Model to estimate ages from the equivalent dose. The SAR method is an improvement over older multiple aliquot methods because it allows recognition of the existence of partial bleaching. Single grain methods in which ~1000 grains are individually analyzed for each date are sometimes used for fluvial deposits because they potentially allow clearer recognition and more detailed analysis of partial bleaching (which tends to result in "old" ages), and also permit use of minimum age models (Duller 2008; Rittenour 2008). Use of minimum age models in this data set would make some but not necessarily all of the ages younger than we determined. However, single grain analyses make the luminescence characteristics and individual histories of each grain rather than the bulk of the sediment important, which are possible additional sources of error (T. Rittenour, pers. com., 2014).

One challenge in our data set is a zone of anomalously old ages in the central part of the section (Fig. 8). The old ages are possibly caused by laboratory error. However, our laboratory methods have been rigorously tested, and the laboratory characteristics of each age are acceptable. As mentioned, partial bleaching can make ages appear to be too old. Although instances of partial bleaching can be seen in our data set by skewed D_e histograms and high overdispersion, the anomalously old zone includes both ages with both the highest and lowest overdispersion in the data set (Fig. 7). Furthermore, the partial bleaching is not as extensive as has been found in some other fluvial systems (Murray et al. 1995; Thrasher, 2009). A plausible sedimentological explanation involves remobilization and partial bleaching of a nearby deposit of Illinois Episode-aged sediment (Qpl), although that begs the question of why the old ages do not span across the entire data set. Another possibility is changing provenance. Wabash Valley sediment was sourced from two different glacial lobes, the Lake Michigan and Huron-Erie Lobes, which deposited materials derived from largely sedimentary rocks in the Lake Michigan basin and largely metamorphic rocks in the Canadian Shield, respectively. OSL dates on quartz have been shown to be systematically affected by quartz provenance.

By contrast with fluvial deposits, eolian dune deposits are typically well-bleached, so OSL-SAR results are more reliable. The correlated age of the dunes on the Carmi terrace (Qh-pk; 21.7-29.1 ka) is identical to the immediately underlying date on Qh(s), further supporting confidence in that date.

Work is ongoing to affirm or improve our dating analysis. Replicates of two samples (ISGS 235; ISGS 250) were sent to an external lab for replicate SAR as well as single grain determinations. That lab will also date two additional samples (33029, 7.8 m (26 ft) depth; 33030, 5.3 m (17 ft) depth), and we are dating samples from borings 33025 (17 m; 56 ft) and 33026 (18 m; 59 ft) to fill out our data set.

Nonetheless, the totality of the dating results is consistent with the other sedimentological indicators: the valley is filled with largely flat-lying to gently eastward-dipping deposits with no abrupt vertical offsets.

History

The Wabash and tributary bedrock valleys were likely eroded in the early Quaternary period, similar to other bedrock valleys in southern Illinois (e.g. Grimley and Phillips 2011). The confluence of the Little Wabash with the Wabash bedrock valley occurs directly below the MBL. The Pre-Illinois Episode glaciation reached only a few kilometers south of the later Wisconsin Episode glaciation, about 70 km

(40 mi) north of the MBL, but the valley was a meltwater outlet (MacClintock 1929). In addition, the pre-Illinois Episode ice reached into the headwaters of the Little Wabash and some of its tributaries. However, since no pre-Illinois Episode sediment has been yet described in the Lower Wabash Valley, it was either buried or completely removed by erosion.

During the Illinois Episode glaciation, ice reached to approximately 5 km (3 mi) south of the MBL and 11 km (7 mi) south of the focused study section (CR 1175 N) (Phillips and Gemperline 2013). The ice margin was thus at this location for (presumably) thousands of years. Till with the Sangamon Geosol developed into the upper 1-2 m (3-6 ft) occurs above bedrock in uplands. We interpret slight oxidation and carbonate leaching of a sandy fine gravel unit from 91-88 m (300-290) ft asl in boring 33026 as the root (upper BC horizon) of the Sangamon Geosol. Thus, Illinois Episode outwash fills the depression in the bedrock immediately below the MBL, and probably originally filled the valley to an elevation of ~90-94 m (300-310 ft). Because the unit cannot be correlated eastward to boring 33025, we interpret that it was eroded out during the early Wisconsin Episode.

The Wisconsin Episode was marked by gradual filling of the valley with glacifluvial sand. Ice from the Huron-Erie and Lake Michigan Lobes first reached the watershed by about 39 ka. Both lobes provided meltwater and sediment to the Wabash Valley, although the relative importance of each lobe varied with time (Bleuer et al. 1982; Fraser and Bleuer 1988). The Lake Michigan Lobe reached its southernmost latitude of 39.33^{o}N by 23,290 ka (Hansel and Johnson 1996; Hansel et al. 1999; Curry and Petras 2011), where it remained for several thousand years. If our OSL ages are accurate, outwash reached the lower Wabash Valley soon thereafter and continued to aggrade until the glacial maximum. It is unclear why the sequence fines upward with a 2-10 m (7-33 ft) thick sandy gravel unit to a ~20 m (~66 m; before erosion) thick medium to coarse sand unit. Beds 0.5-1 m (1.6-3 ft) thick recognized only by cm-scale gravel layers at their bases indicate deposition from a braided fluvial system, typical of glaciofluvial environments.

The sediment aggraded rapidly enough in the WBV to block the LWBV and prograde up from the mouth as a fan or delta. The prograding sand and gravel caused slackwater lakes to develop in the Little Wabash and Skillet fork drainages. Well data indicate that the sand prograded at least 10 km (6 mi) up the LWBV (Fig.18). Although there was likely fluvial sediment contribution from the tributary watersheds, it was no doubt less than in the main valley. However, Wabash and Little Wabash/Skillet fork provenances are not distinguishable in the available data. Lacustrine clay and silt, derived largely from loessial parent material, intercalate with glaciofluvial gravel and sand up the tributary drainages (Fig. 18). Ultimately, the entire valley at the MBL cross section was filled with outwash to an elevation of 115-117 m (377-384 ft).

The barren plain provided an extensive source of material that could be transported by wind. Eolian dunes of fine sand up to 4-5 m high are apparent on the delta plain surface as well as in dune fields on west-facing bedrock uplands south of Carmi and along the eastern (Indiana) Wabash Valley wall (Fig. 18). The dunes on the Glacial Lake Carmi plain comprise amalgamated mound, barchan, barchan ridge, and incipient linear forms. They occur in isolation and in patches. Paleowind directions were ~SE, typical of paleowind directions across the Midwest. In addition, silt was deposited as loess in depressions on the delta surface and as blankets over eastern uplands.

Wisconsin Episode ice began to retreat from its terminal position by about 19.4 ka (Curry et al. 2014). The effects of ice retreat in the Wabash Valley are complicated by the fact that the Lake Michigan, Saginaw, and Huron-Erie Lobes had independent histories, retreating and temporarily readvancing over

their overall demise. Although meltwater discharge was in general much higher during deglaciation than at the glacial maximum, a few large flood events appear to dominate the sedimentologic and geomorphic record. Glacial lakes were impounded between moraines and retreating ice fronts. Lake volumes were discharged suddenly when the morainic dams failed. Curry et al. (2014) constrained the configuration and chronology of the lake outburst named the Kankakee Torrent which burst a dam that constrained Glacial Lake Chicago and flowed down the Illinois River at 19 ka. They proposed that prior to that event, Glacial Lake Chicago overflow discharged through the Tippecanoe Lowland into the Wabash Valley. Fraser and Bleuer (1988) explained cobble gravels with 2-5 m thick cross beds and scours up to 30 m deep by floodwaters emptying into the Wabash Valley at the Tippecanoe Fan. This event could have been overflow from the Kankakee Torrent.

The retreating Huron-Erie Lobe left several end moraines (Bleuer and Moore 1971). Glacial Lake Maumee formed behind the Fort Wayne Moraine. Glacial Lake Maumee is at least as old as 14.3±0.45 ka and drained catastrophically down the Wabash after 13.8±0.21 ka (Howard 2010). If those dates are correct and our OSL ages are sufficiently accurate, this flood left only erosive evidence in the lower Wabash Valley.

A wide fluvial strath with sandy levee deposits in an upland position near Keensburg is evidence of floodwaters overtopping the valley walls (Fig. 18). Based on geomorphic cross-cutting relationships, it appears to have been the last large event because there are no dunes within the strath but there are dunes outside of it. The strath plain occurs at 120-122 m (395-400 ft) asl. Recent hydraulic modeling by FEMA (2007) predicts a 6 m (20 ft) difference in flood elevation between Keensburg and the MBL. Although hydraulic conditions of flooding in the modern meandering system and the ancient outwash system are very different, there is a coincidental 6 m (20 ft) difference in elevation between the Keensburg strath and the middle terrace at MBL. We thus correlate the two and assert that the Meadow Bank scarp was likely formed by that flood.

Fine-grained Holocene alluvial sediments are inset into the sandy outwash sediments in both the middle and lower terraces. Based on geomorphic evidence, these alluvial systems operated during the early Holocene, and possibly correlate with the highest and oldest meander sets. The alluvial deposits partly eroded and onlap onto clearly Pleistocene outwash terraces near Maunie and elsewhere. A small mostly abandoned meandering stream – more of a swale today but partly exploited as a drainage ditch – can be discerned on the low terrace. It is this stream that appears to have been responsible for scalloping the MBL downstream of Epworth. Although the stream is quite small and appears much smaller than the scallops, the meander wavelength is about the same as the scallop wavelength, and, because the sedimentary fill is sandy with relatively low shear strength, small amounts of erosion at the base of the scarp could result in larger mass wasting. Colluvial sediments on the upper part of the middle terrace interfinger with the alluvial sediment, and could have been derived from the cascading of dunes over the edge of the scarped Meadow Bank as well as by run-of-the-mill slope processes over time.

Similar scarps at other tributary confluences

If our hypothesis for a sedimentological rather than a neotectonic origin for the MBL is correct, this straight channel configuration should be evident not only at the MBL, which is at the mouth of the Little Wabash Valley, but at the mouths of other tributaries in the lower Wabash River basin similarly affected by the meltwater outbursts. The largest tributary streams on the Illinois side of the Wabash River are the Embarras River, Bonpas Creek, Little Wabash River, and Saline Creek. Slackwater lakes formed in each of these tributaries as a result of aggradation of the main channel of the Wabash River during the late Wisconsin Episode. Figure 19 shows the current configuration of the confluence of each of these

tributaries with the Wabash River. The maps are shown at the same scale. Long, arcuate scarps occur at each location. The scarps are downstream of bedrock high points in the channel. Above the scarps the slack water terraces are preserved. Dunes are typical on these upper terraces. Several of the scarps have been partly modified by subsequent erosion by the Wabash River. Although the Meadow Bank has the longest straight reach, all of the scarps have straight reaches that exceed 3 km (2 mi).

Conclusions

The MBL is a long, straight scarp located within a known seismic zone. It is sub-parallel to a mapped fault zone. Yet, detailed structure mapping of the Herrin Coal bed within the Pattikki Mine indicates that there is no fault in the coal below the MBL. We consider this to be definitive proof that the MBL did not have a tectonic origin. Supporting this conclusion are the observations that the MBL does not have the characteristic shape of known fault scarps within the Central U.S. Also, parallel lineaments are common in this region, suggesting structural control of the drainage which may not necessarily be the result of recent tectonism.

Instead, we conclude that the MBL is the result of erosional processes. The distinctive scarp was formed when late glacial floods, constricted by bedrock valley walls, lowered the valley fill and scoured the tributary deposits. The scarp was preserved when the Wabash drainage was captured by the St Lawrence River system and flow conditions within the Wabash system decreased substantially. This erosional hypothesis predicts that similar scarps should be present at the mouths of other tributary streams along the Wabash Valley. Indeed, this is the case. Evidence of similar scarps can be found at the mouth of the Embarras River, Bonpas Creek, and the Saline River.

Future research questions

Regional lineaments
We did not fully analyze the lineament patterns evident in the Lower Wabash and Ohio River Systems. Careful measurements on multiple scales might reveal the origin and age of these lineaments. Some of them may indeed be the result of modern tectonism, but some, such as the MBL, are not.

Apparent anomalous ages within outwash
OSL dating suggested a region of anomalous, almost chaotic ages. Is this common within the Wabash River System? Many more OSL dates are needed to put our samples into proper context.

Apparent shallow depth of torrent
The dunes on top of the Glacial Lake Carmi terrace are correlated to be ~22 ka old. Their pristine appearance means that no floods ever topped that level. The outwash terraces constrain the base of the floodwaters, so flood depths must be <~4 m. This depth seems shallow for the lake outburst floods described by others (e.g. Bleuer and Moore, 1971; Bleuer et al., 1982; Fraser and Bleuer, 1988).

Numerical or flume model of torrent

Our research has provided data that could be used to constrain a numerical or physical model of the torrential late glacial floods within the Wabash System. What ranges of velocity, discharge, and load could produce these features? What is the role of bedrock outliers in controlling the erosion?

Acknowledgments

Rebecca Alberts provided careful and diligent laboratory and field support in all aspects of the project. Mike DeLucia helped especially with the resistivity studies. The ISGS Drill Team of Bob Bryant and Rich Padilla was stalwart in achieving good recovery in sand at depths well beyond those recommended for the equipment. The White County Coal Company Pattiki Mine staff were extremely helpful in providing access to their data, and accommodated our every request. Special thanks go to the landowners and farmers who allowed us to work on their properties.

References

Berry, Daniel, 1908, The Illinois earthquake of 1811 and 1812, Transactions of the Illinois State Historical Society for the year 1907, p 74-78.

Bleuer, N.K., Melhorn, W., and Fraser, G.S., 1982, Geomorphology and glacial history of the Great Bend area of the Wabash Valley, Indiana: Geological Society of America North-Central Section 16th Annual Meeting Field Trip Guidebook, 63 p.

Bleuer, N.K. and M.C. Moore, 1971, Glacial Stratigraphy of the Fort Wayne Areas and the draining of Glacial Lake Maumee. Proceedings of the Indiana Academy of Science 81: 195-209.

Bristol, H. M., and J. D. Treworgy, 1979. The Wabash Valley Fault System in Southeastern Illinois: Circular 509, Illinois State Geological Survey, 19 p.

Bryk, A., Phillips, A.C., Prokocki, E.W., and Best, J.L., 2012, Surficial geology of Wabash Island quadrangle, Gallatin County, Illinois. University of Illinois, USGS-EDMAP contract report, 2 sheets, 1:24,000.

Curry, B.B., and J. Petras, 2011, Chronological framework for the deglaciation of the Lake Michigan Lobe of the Laurentide Ice Sheet from ice-walled lake deposits. Journal of Quaternary Science 26: 402-410.

Doyle, B. C., and J. D. Rogers, 2005. Seismically induced lateral spread features in the western New Madrid Seismic Zone: Environmental and Engineering Geoscience, XI (3) 251-258.

Dreimanis, A., 1962, Quantitative gasometric determination of calcite and dolomite by using Chittick apparatus. Journal of Sedimentary Petrology 32(3): 520-529.

Duller, G.A.T., 2007, Assessing the error on equivalent dose estimates derived from single aliquot regenerative dose measurements. Ancient, TL 25: 15-24.

Duller G.A.T., 2008, Single grain optical dating of Quaternary sediments: why aliquots size matters in luminescence dating. Boreas 37: 589-612.Herrmann, R. B., M. Withers, and H. Benz (2008). The Aril 18, 2008 Illinois earthquake: An ANSS monitoring success. Seismological Research Letters 79, 830-843.

FEMA, 2007, Digital Flood Insurance Map Database [Wabash and White Counties]. Illinois State Water Survey for Federal Emergency Management Agency, accessible at www.illinoisfloodmaps.org.

Fraser, G.S. and Bleuer, N.K., 1988, Sedimentological consequences of two floods of extreme magnitude in the late Wisconsinan Wabash Valley. Geological Society of America, Special Paper 229, p. 111-125

Fuller, M. L., 1912, the New Madrid earthquake: U.S. Geological Survey Bulletin 494, 119 p.

Grimley D.A., and Arruda, N.K., 2007. Observations of magnetite dissolution in poorly drained soils, Soil Science 172: p. 968-982

Grimley, D.A., L.R. Follmer, R.E. Hughes, and P.A. Solheid, 2003, Modern, Sangamon, and Yarmouth soil development in loess of unglaciated southwestern Illinois. Quaternary Science Reviews 22: 225-244.

Grimley, D.A., and A.C. Phillips, 2011, Surficial Geology of St. Clair County, Illinois. Illinois County Geologic Map ICGM St. Clair-SG, Illinois State Geological Survey, Champaign, http://www.isgs.illinois.edu/?q=maps/county-maps/st-clair-surficial-geology.

Grimley, D.A., Vepraskas, M.J., 2000. Magnetic susceptibility for use in delineating hydric soils. Soil Science Society of America Journal 64, 2174–2180

Hansel, A.K., and Johnson, W.H., 1996, Wedron and Mason Groups: Lithostratigraphic Reclassification of the Deposits of the Wisconsin Episode, Lake Michigan Lobe Area: Illinois State Geological Survey Bulletin 104, 1 16 p.

Hansel, A.K., R. C. Berg, A.C. Phillips, and V.G. Gutowski, 1999, Glacial sediments, landforms, paleosols, and 20,000-year-old forest bed in east-central Illinois. Illinois State Geological Survey, Guidebook 26, 31 p.

Heigold, P.C., and T. H. Larson, 1994. Geophysical investigations of possible recent ground deformation and neotectonism in White County, Illinois, ISGS Open file Series 1994-5, 24 pages.

Holbrook, J., and Schumm, S.A., 1999, Geomorphic and sedimentary response of rivers to tectonic deformation: a brief review and critique of a tool for recognizing subtle epeirogenic deformation in modern and ancient settings: Tectonophysics, v. 305, p. 287-306.

Hough, S. E., R. Bilham, K. Mueller, W. Stephenson, R. Williams, and J. Odum, 2005, Wagon loads of sand blows in White County, Illinois, Seismological Research Letters, 76(3), 373-386.

Howard, J.L., 2010, Late Pleistocene glaciolacustrine sedimentation and paleogeography of southeastern Michigan, USA. Sedimentary Geology 223: 126-142.

Jibson, R. W., and D. K. Keefer, 1988. Landslides triggered by earthquakes in the Central Mississippi Valley, Tennessee and Kentucky: USGS Professional paper 1336-C, 24 p.

Jibson, R. W., and D. K. Keefer, 1993. Analysis of the seismic origin of landslides: examples from the New Madrid seismic zone: Geological Society of America Bulletin, 105, 521-536.

Killey, M. M., J. K. Hines, and P. b. DuMontelle, 1985. Landslide inventory of Illinois: Illinois State Geological Survey Circular 534, 27 p.

Kim, W.-Y., 2003, The 18 June 2002 Caborn, Indiana, Earthquake: Reactivation of Ancient Rift in the Wabash Valley Seismic Zone?: Bulletin of the Seismological Society of America, v. 93, p. 2201-2211.

Loke, M. H., and R. D. Barker, 1996. Rapid least-squares inversion of apparent resistivity pseudosections using a quasi-Newton method. Geophysical Prospecting 44: 131-152.

MacClintock, P., 1929, Recent Discoveries of pre-Illinoian Drift in southern Illinois. Report of Investigations 19, Illinois State Geological Survey, Urbana, p. 27-57.

Marshak, S., C. Abert, and T. Larson, 2014, Fault and fold traces of Missouri, Illinois, Indiana, and Kentucky, Map 11 *in* Marshak, S., T. Larson, and C. Abert, Surface and Subsurface Geological and Geophysical Maps of the Illinois Basin/Ozark Dome Region: Illinois State Geological Survey, Illinois Map 20-11 *(in preparation).*

McWhorter, D. B., and D. K. Sunada, 1977. Ground-water hydrology and hydraulics. Water Resources Publications. 290 p.

Murray, A.S. and Wintle, A.G., 2000, Luminescence dating of quartz using an improved single-aliquot regenerative-dose protocol. Radiation Measurements 32: 57-73.

Murray, A.S., Olley, J.M., and Caitcheon, G.G., 1995, Measurement of equivalent doses in quartz from contemporary water-lain sediments using optically stimulated luminescence. Quaternary Science Reviews 14:365-371.

Nelson, W.J., 1995, Structural Features in Illinois. Bulletin 100, Illinois State Geological Survey, 144 p.

Obermeier, S.F., 1998, Liquefaction evidence for strong earthquakes of Holocene and latest Pleistocene ages in the states of Indiana and Illinois, USA: Engineering Geology, v. 50, p. 227-254.

Phillips, A.C., Gemperline, J.M., Larson, T.H., and Caron, O., 2013, Surficial geology of Emma quadrangle, Gallatin and White counties, Illinois, and Posey County, Indiana. Illinois State Geological Survey, USGS-STATEMAP contract report, 2 sheets, 1:24,000.

Phillips, A.C., 2012, Surficial Geology of Grayville Quadrangle, Edwards, Wabash, and White Counties, Illinois: Illinois State Geological Survey, USGS-STATEMAP contract report, 2 sheets, 1:24,000.

Thrasher, I.M, Mauz, B., Chiverrell, R.C., and Lang, A., 2009, Luminescence dating of glaciofluvial deposits: A review. Earth Science Reviews 97: 133-146.

Wang, H., Hackley, K.C., Panno, S.V., Coleman, D.D., Liu, J. C-L., and Brown, J., 2003, Pyrolysis combustion 14C dating of soil organic matter: Quaternary Research 60: 348-355.

Wells, D. L. and K. J. Coppersmith, 1994. New empirical relationships among magnitude, rupture length, rupture width, rupture area, and surface displacement. Bulletin Seismological Society America, 84: 974-1002.

White County Coal Co., 2003. Pattiki Mine Final Map 2003. Available from Illinois Department Natural Resources Office of Mines and Minerals or from Illinois State Geological Survey Coal Section.

Wintle, A.G., Murray, A.S., 2006, A review of quartz optical stimulated luminescence characteristics and their relevance in single-aliquot regeneration dating protocols. Radiation Measurements 41: 369-391.

Woolery, E.W., 2005, Geophysical and Geological Evidence of Neotectonic Deformation along the Hovey Lake Fault, Lower Wabash Valley Fault System, Central United States: Bulletin of the Seismological Society of America, v. 95, p. 1193-1201.

Figures

Figure 1. Location of study area.

Figure 2. Seismicity

Figure 3. Structure contours

Figure 4 Core locations and resistivity lines

Figure 5. Luminescence analysis of a single aliquot

Figure 6. OSL Lab Analysis

Figure 7. Histograms and radial plots of OSL determinations

Figure 8. MBL cross section (includes OSL dates)

Figure 9. Particle-size distributions

Figure 10. Legacy gamma logs

Figure 11 Magnetic susceptibility

Figure 12. Resistivity profiles

Figure 13. Structure Herrin Coal

Figure 14. Cross section through the Pattiki Mine, 1:1 scale

Figure 15. Landslide comparison

Figure 16. Local Lineaments

Figure 17. Regional lineaments

Figure 18 Geomorphology map

Figure 19. Similar lineaments at other locations along the Wabash Valley

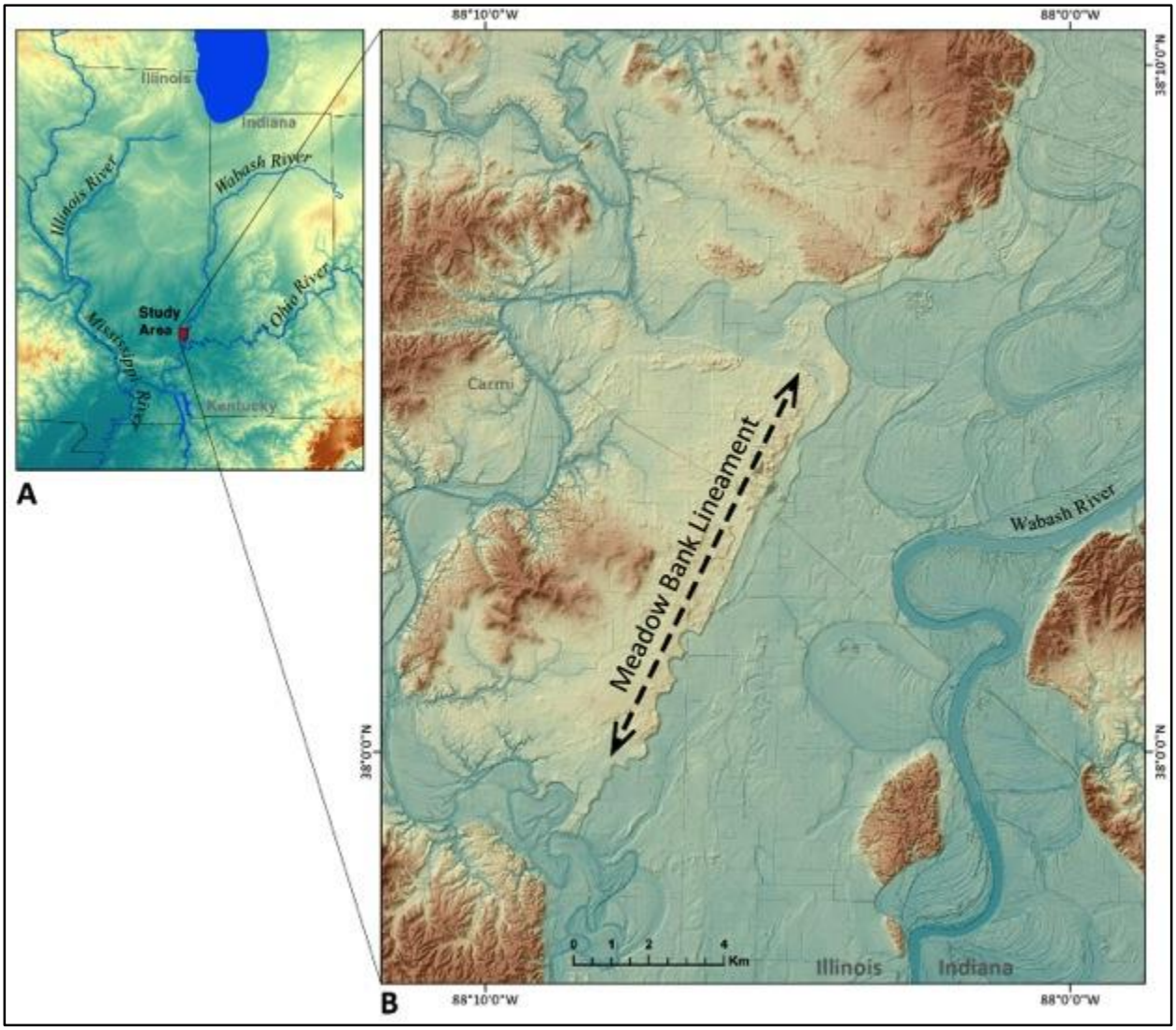

Figure 1. **A** Study area in southeast Illinois and southwest Indiana. **B** Meadow Bank Lineament along the west margin of the Wabash River valley.

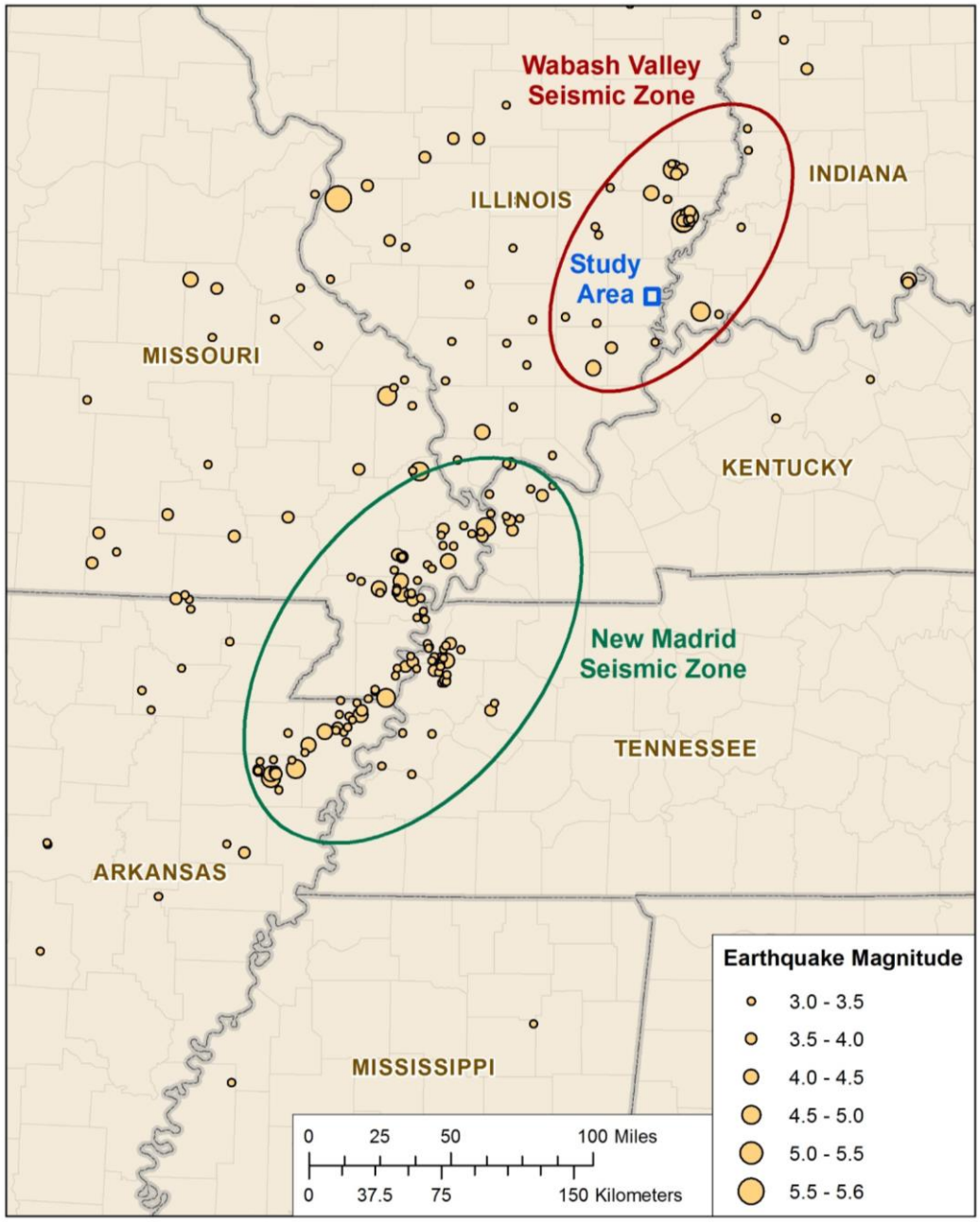

Figure. 2. Locations of earthquakes of M 3.0 or greater in Central US since 1973. Red ellipse outlines the Wabash Valley Seismic Zone. The green ellipse outlines the New Madrid Seismic Zone. Data from ANSS comprehensive catalog.

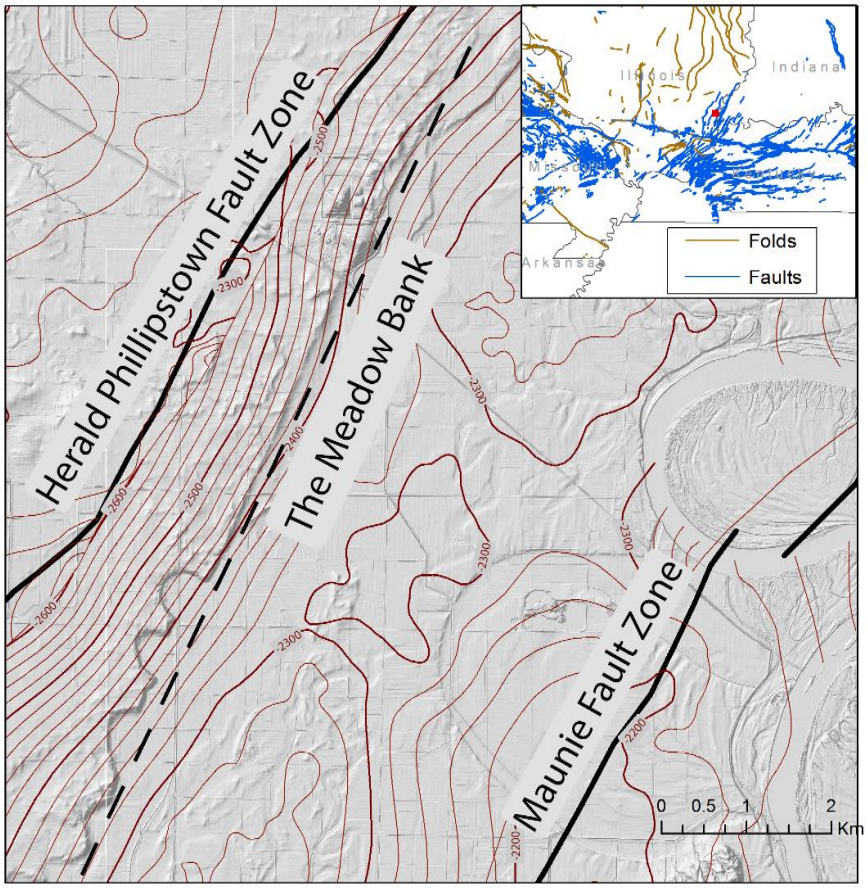

Figure 3. Structure contours on the base of the Beech Creek Limestone. Meadow Bank is ½ to 1 mile east of the Herald-Phillipstown Fault Zone. Strata beneath the Meadow Bank are locally dipping strongly to the west, toward the HPFZ. Inset: regional fault and fold axes (from Marshak, et al., 2014)

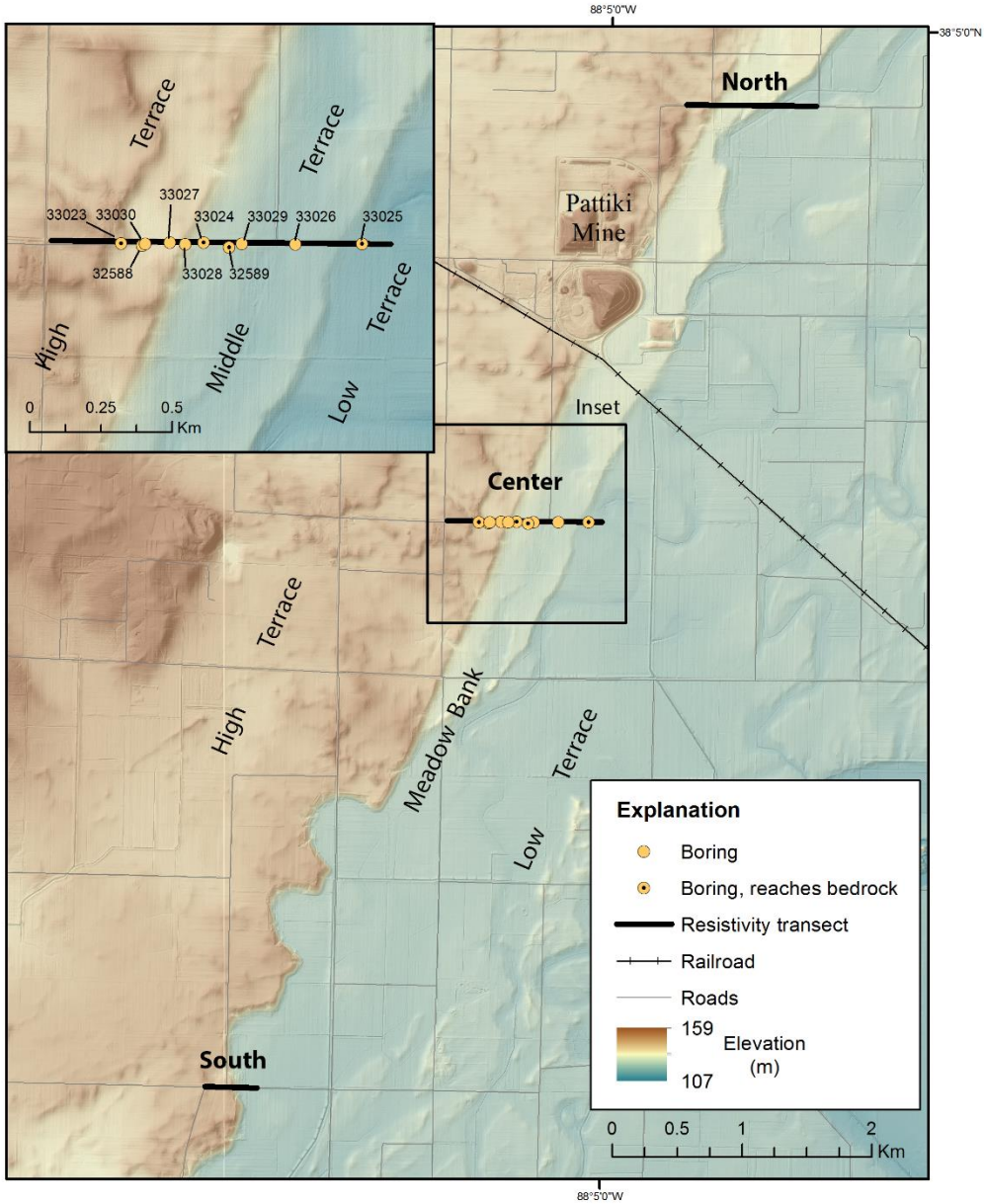

Figure 4. Location of borings and resistivity lines. The Center resistivity transect is co-located with the borings.

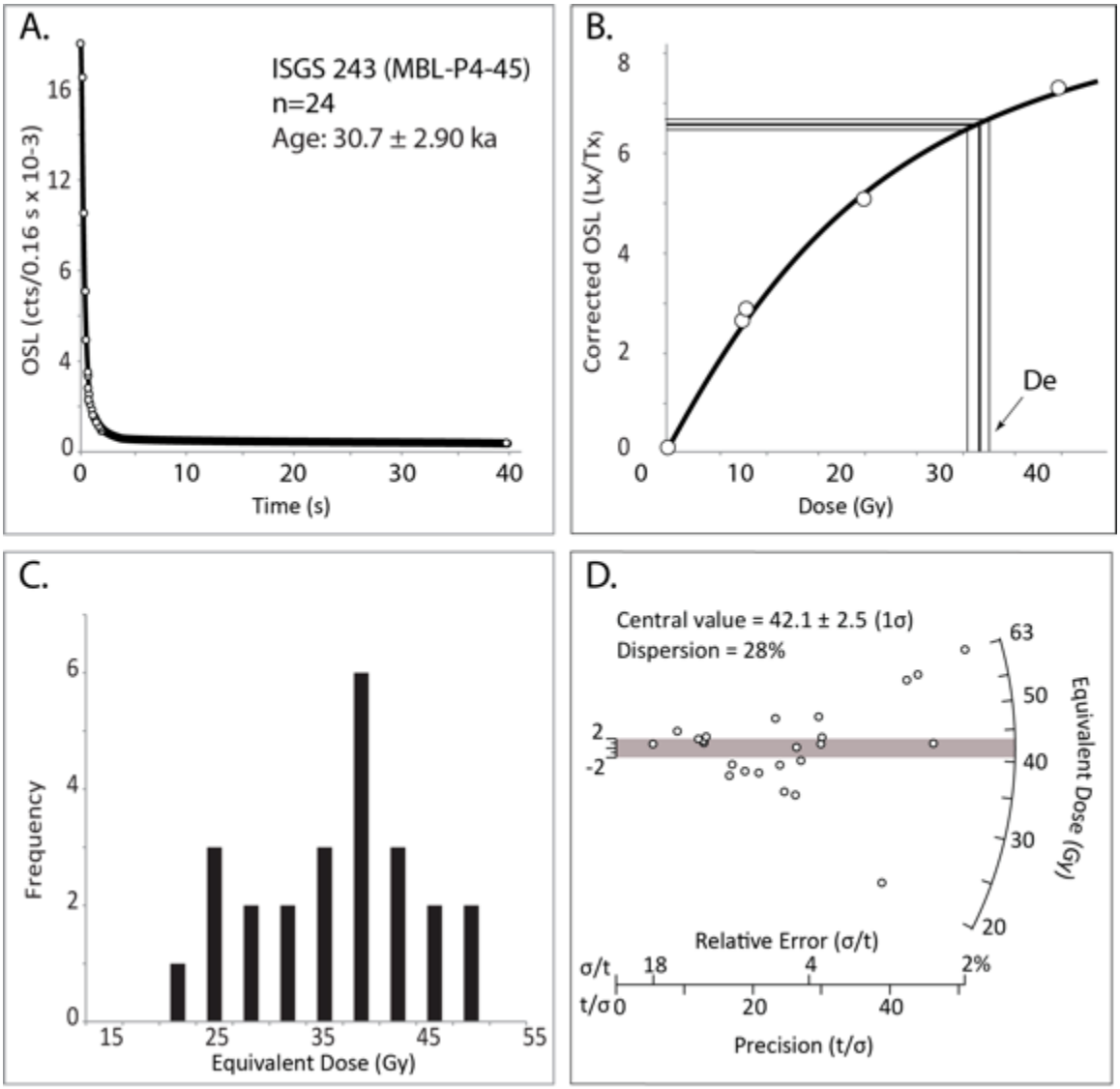

Figure 5. Luminescence analysis of a single aliquot. A. Shine down. Sample shows rapid response to illumination, i.e., is rapidly reset. B. Growth curve. Trapping of radiation increases exponentially with exposure, permitting clear identification of equivalent dose. C. Equivalent dose distribution. Analysis determined 24 acceptable aliquots. Broad distribution indicates partial bleaching exists. D. Radial plot. This example exhibits highest overdispersion of the data set. D_e of 42.1±2.5 Gy gives age of 30.7±2.9 ka.

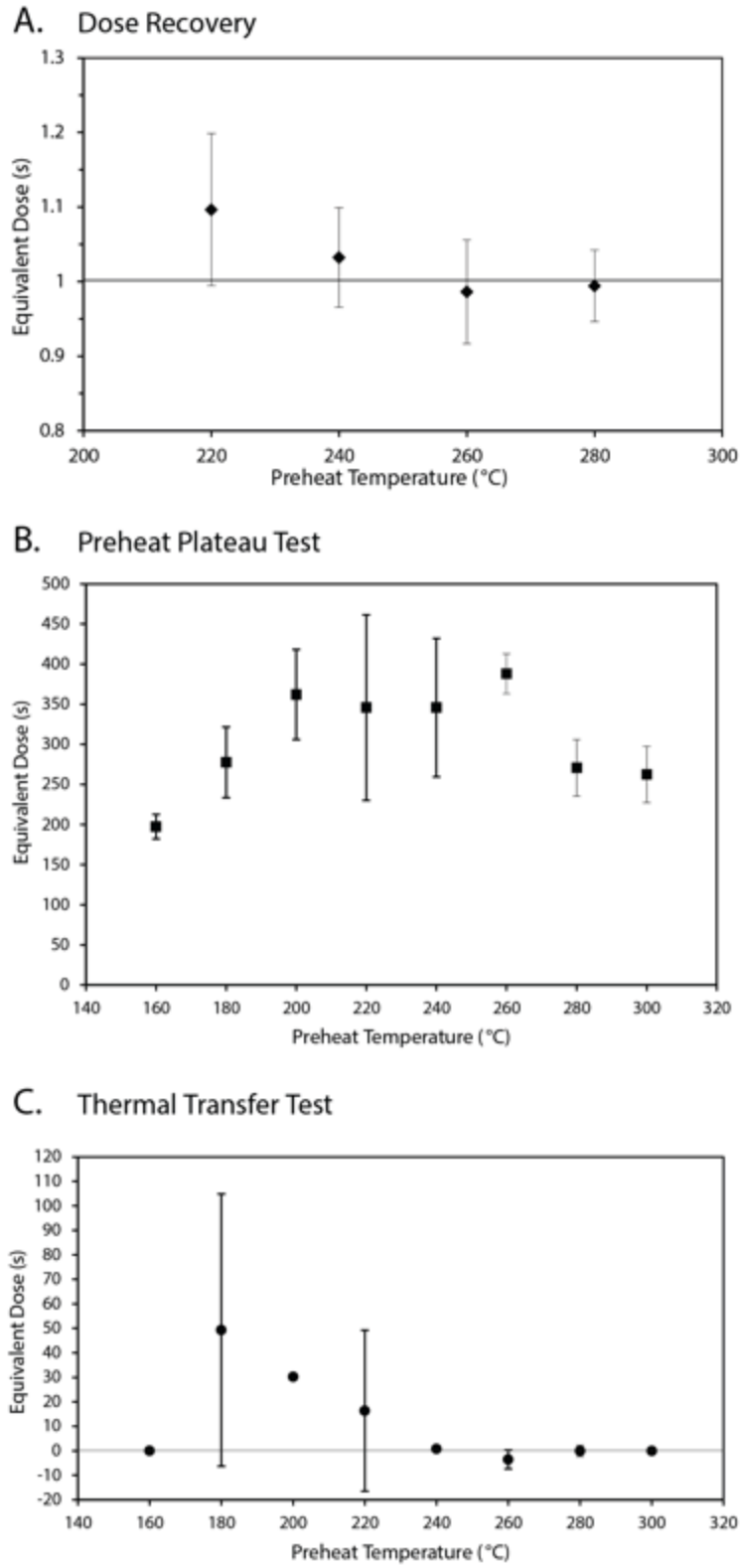

Figure 6. Laboratory analysis of OSL dates. Dose recovery test (A) on ISGS213. Preheat Plateau (B) and Thermal Transfer (C) tests on ISGS244. Equivalent dose in seconds can be converted to Grays by the time variable lab dose rate (0.134 Gy/s during test).

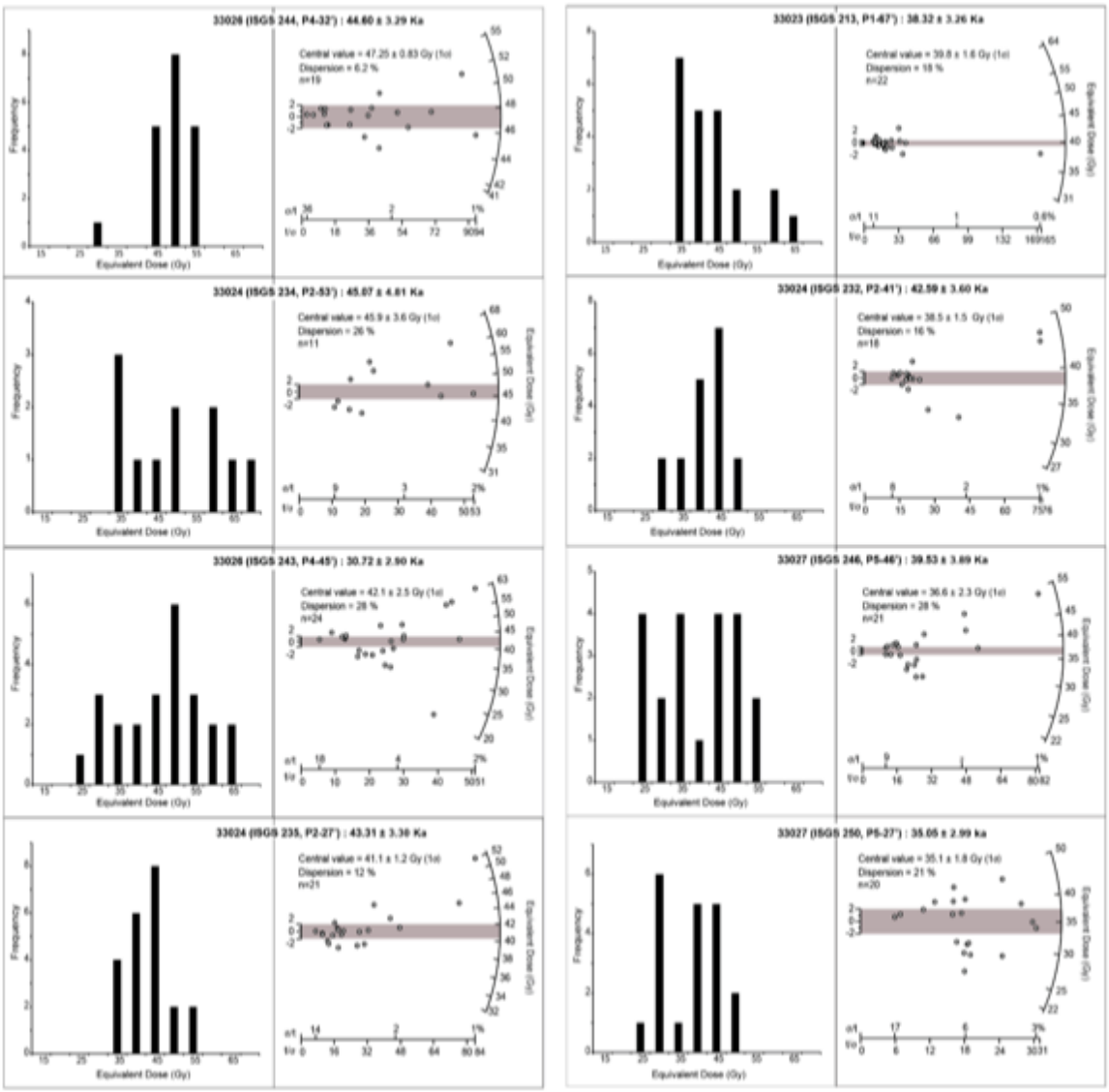

Figure 7A. Histograms and radial plots of OSL D_e determinations. Plots arranged by decreasing age 45 – 35 ka.

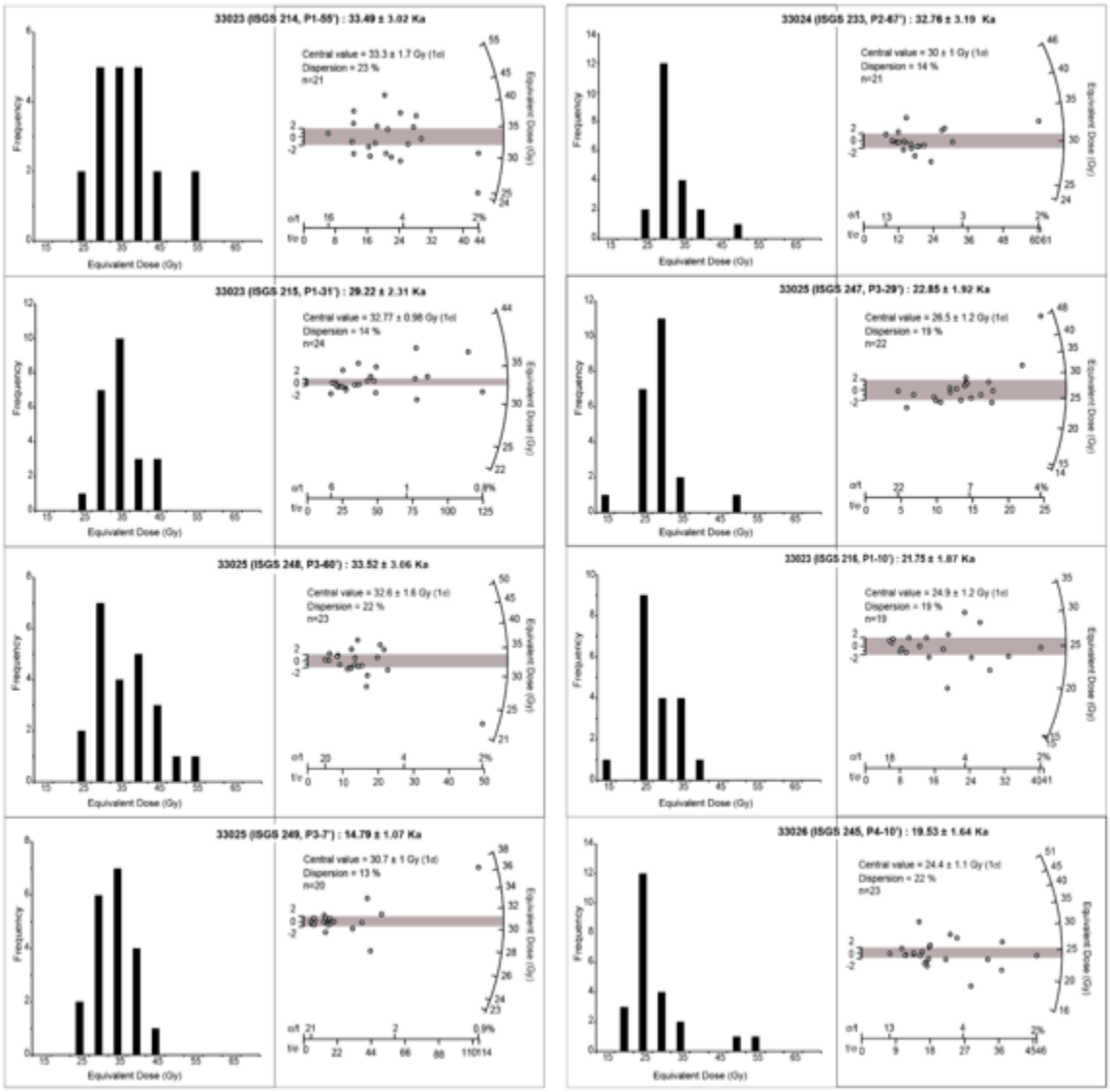

Figure 7B. Histograms and radial plots of OSL D_e determinations. Plots arranged by decreasing age 33 – 20 ka.

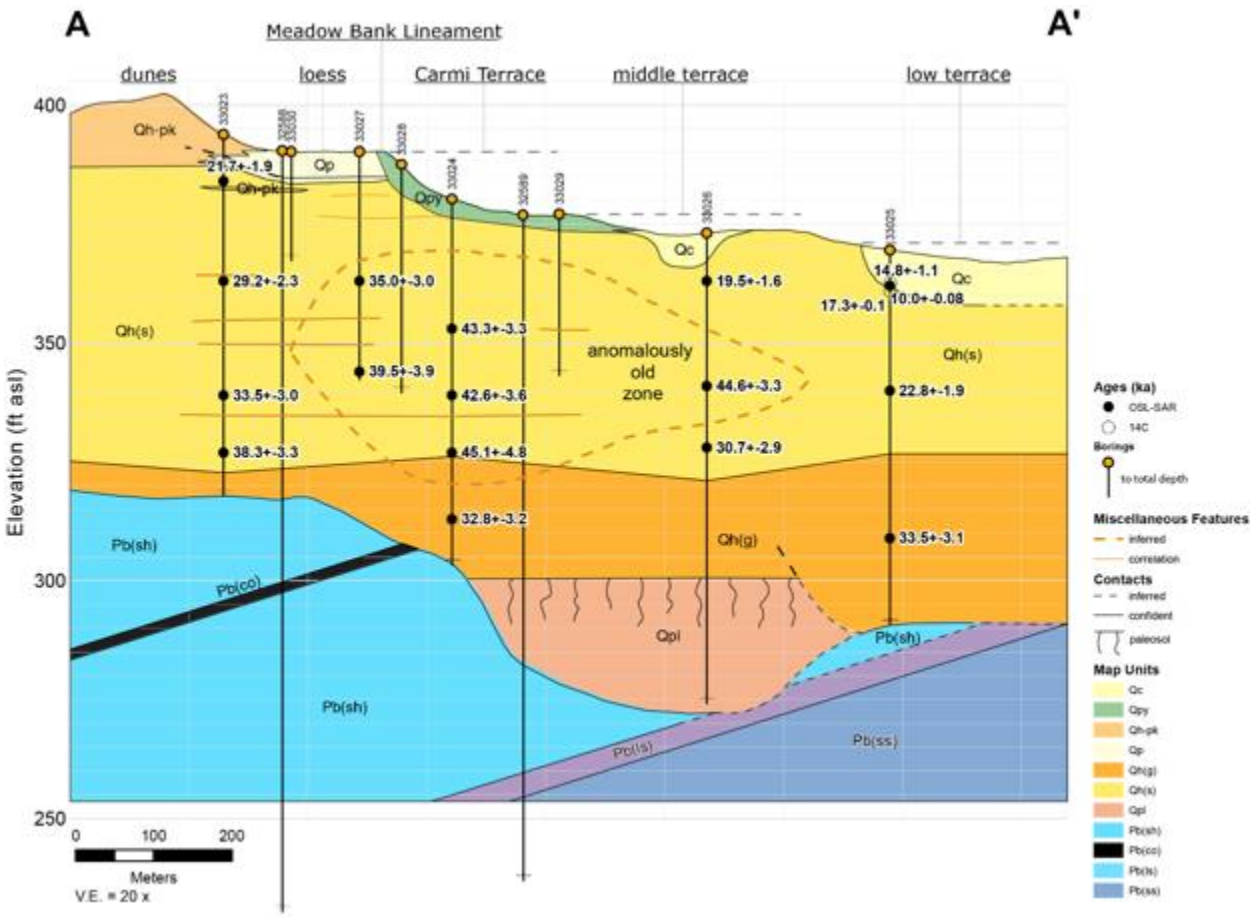

Figure 8. Section across the Meadow Bank Lineament from west (A) to east (A'). Stratigraphic borings are shown to their total depth. An eroded bedrock surface is infilled with outwash that once filled the entire section up to elevations of ~117 m (385 ft). An undulating horizontal contact between gravel-rich (Qh(g)) and sand-rich (Qh(s)) deposits does not support tectonic offset. Late-glacial erosion left stepped terraces that were subsequently modified by early Holocene alluviation. The Carmi Terrace is covered by a blanket of late-glacial eolian sand and loess. Colluvial sediment that covers the MBL includes components of slope, eolian, and alluvial sediment. The "anomalously old zone" differentiates dates determined by OSL-SAR that are out of vertical sequence and are somewhat older than expected. Lithologic features correlatable between cores are indicated by isolated lines.

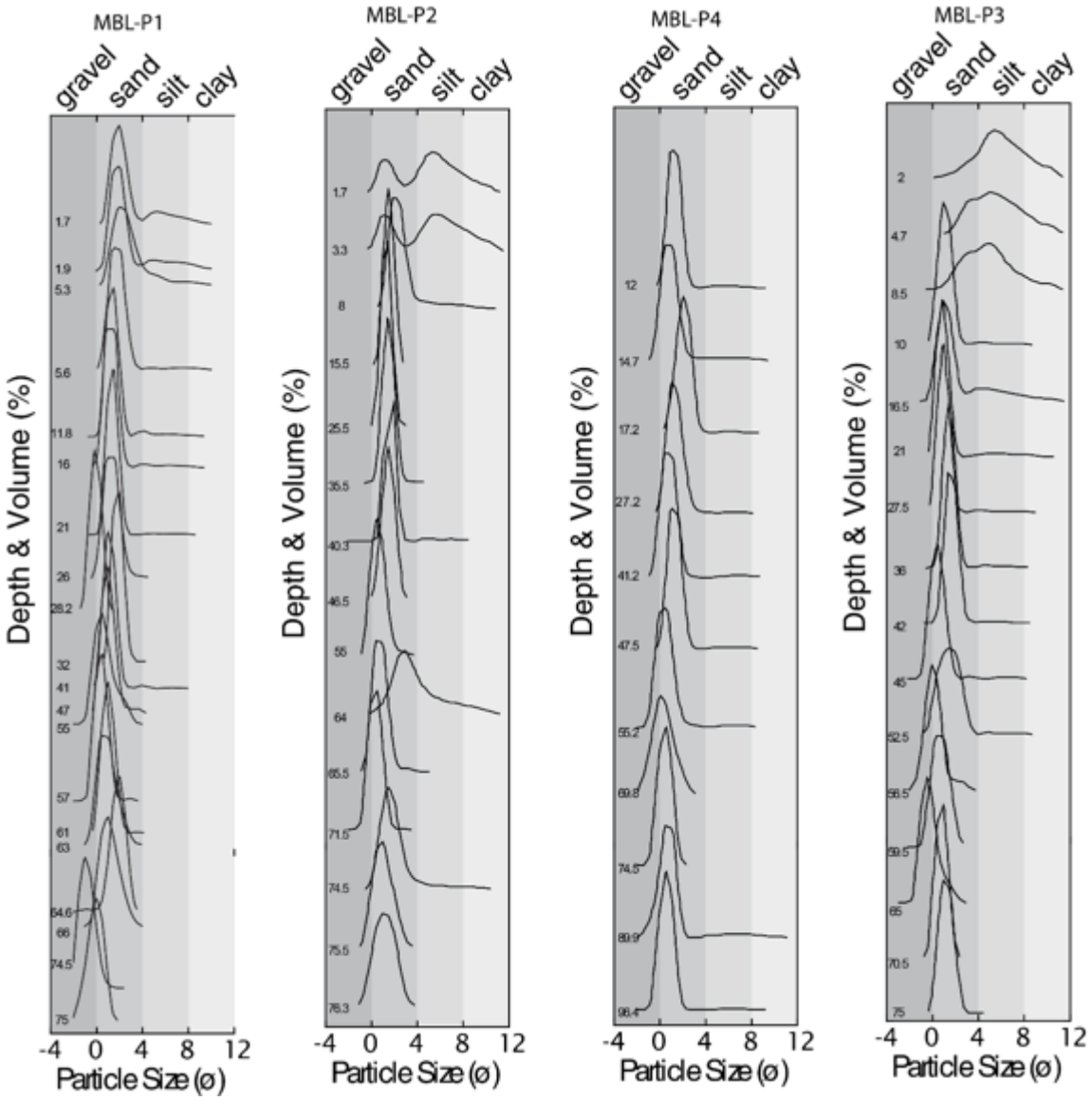

Figure 9. Particle-size distributions for four representative boreholes.

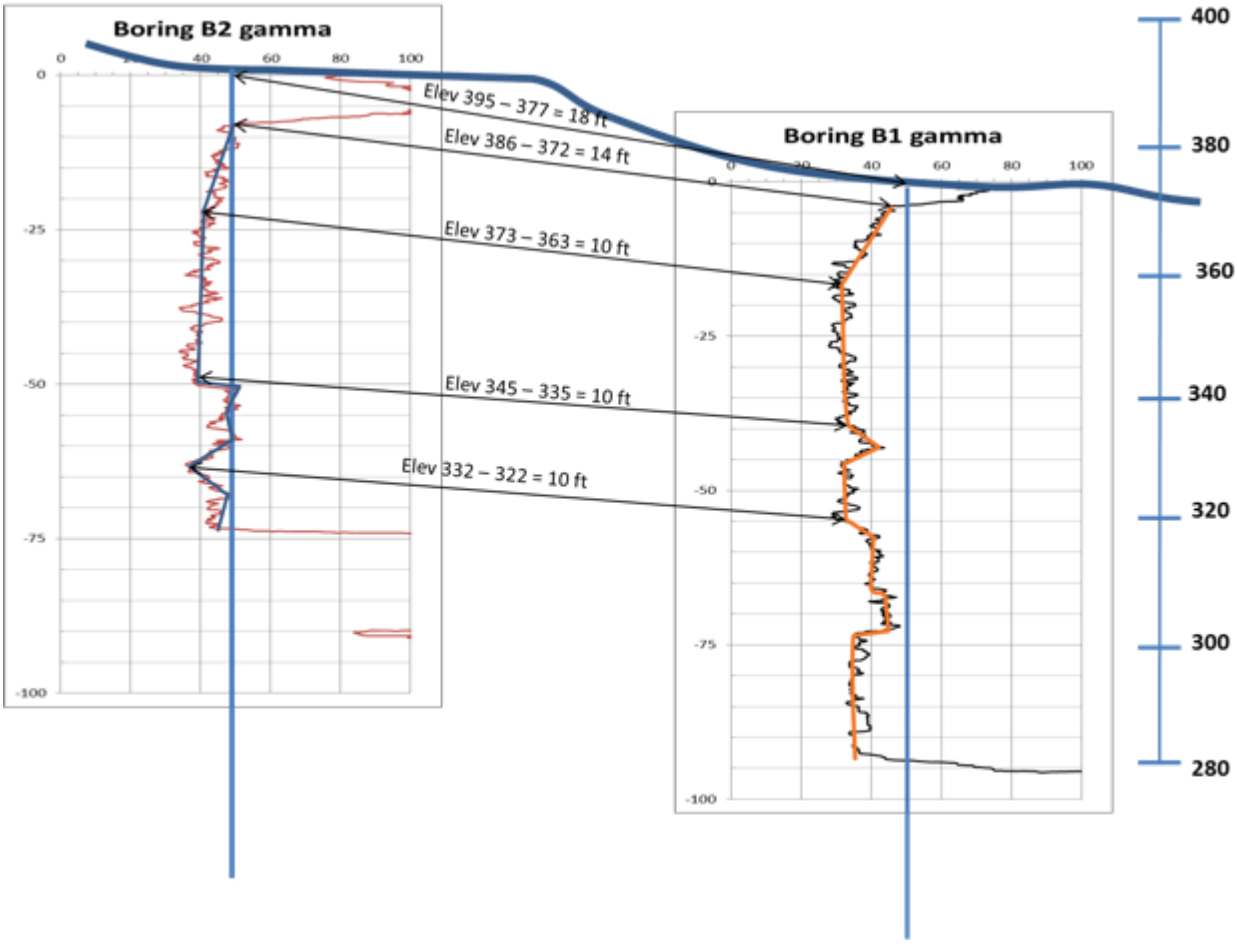

Figure 10. Gamma logs of the Quaternary sediments in boreholes B1 and B2 drilled in 1993 as part of a previous investigation (Larson and Heigold, 1994). Qualitative analysis comparing inflection points on the two logs demonstrates the similar nature of the sediments and the consistent 3 m (10 ft) offset between the two boreholes.

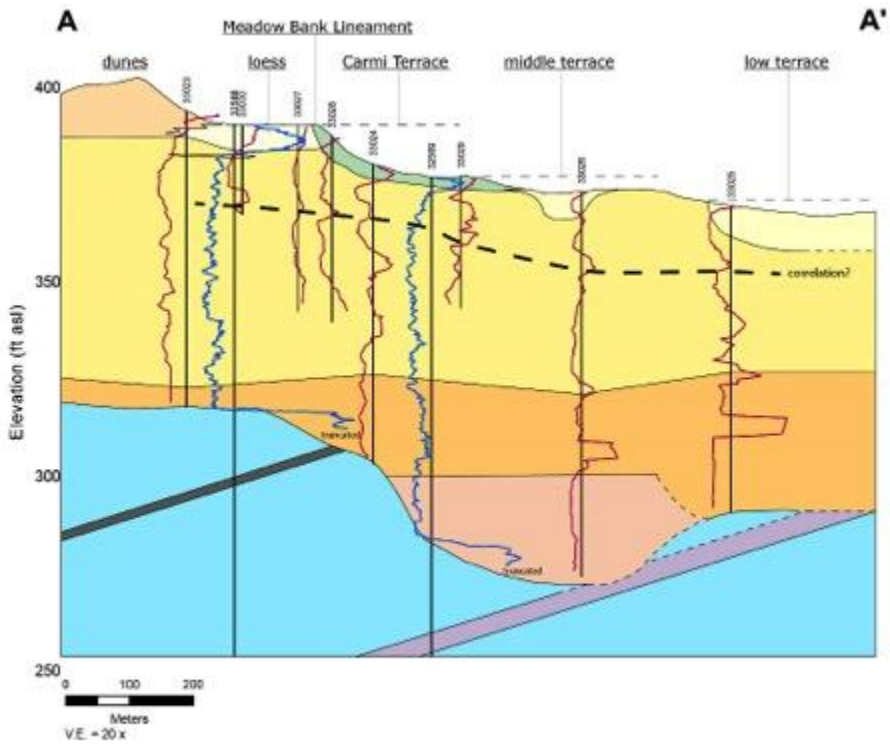

Figure 11. Magnetic susceptibility (red) and natural gamma (blue) from boreholes crossing the MBL.

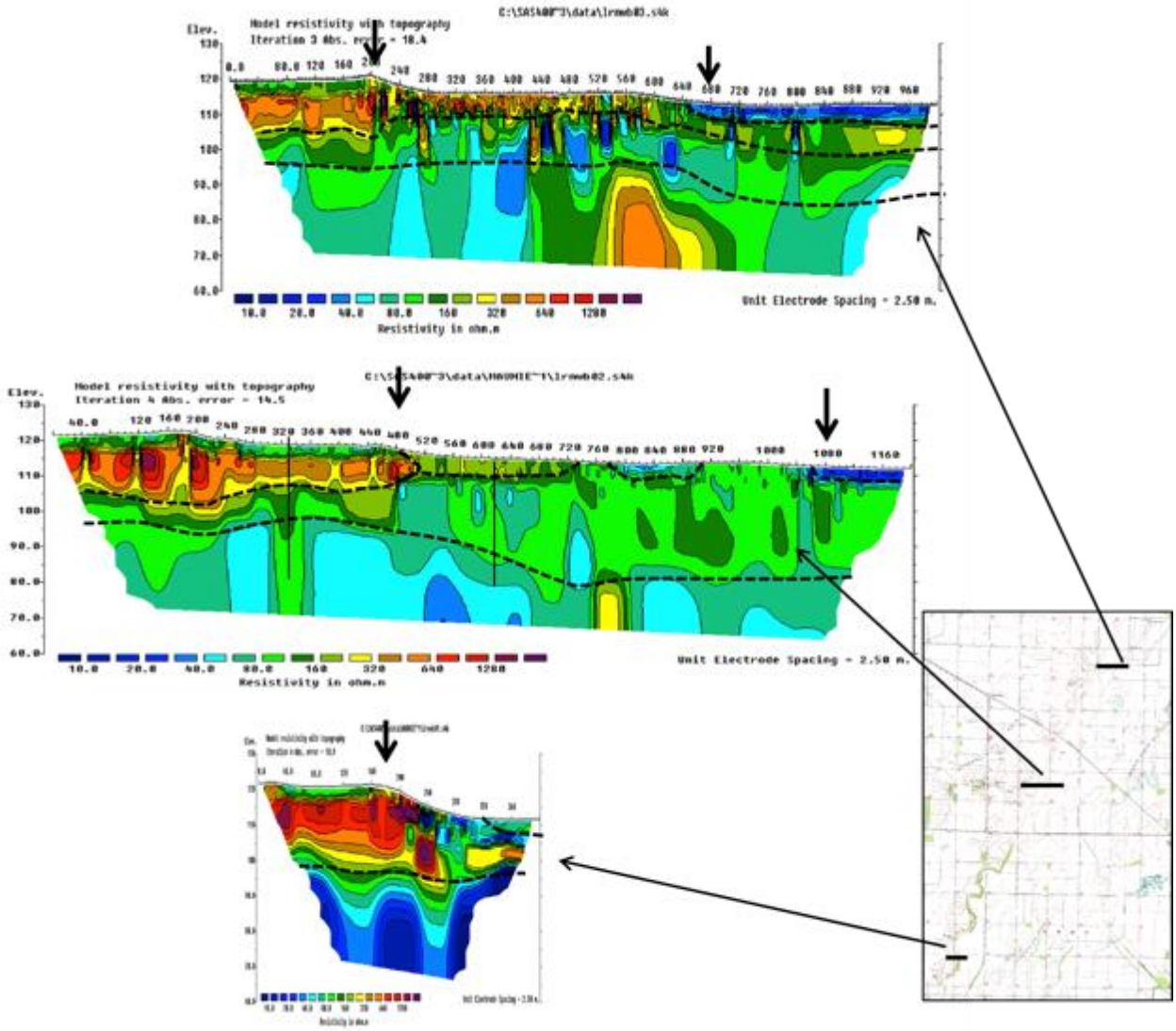

Figure 12. Resistivity profiles. North, Central, South lines from top to bottom.

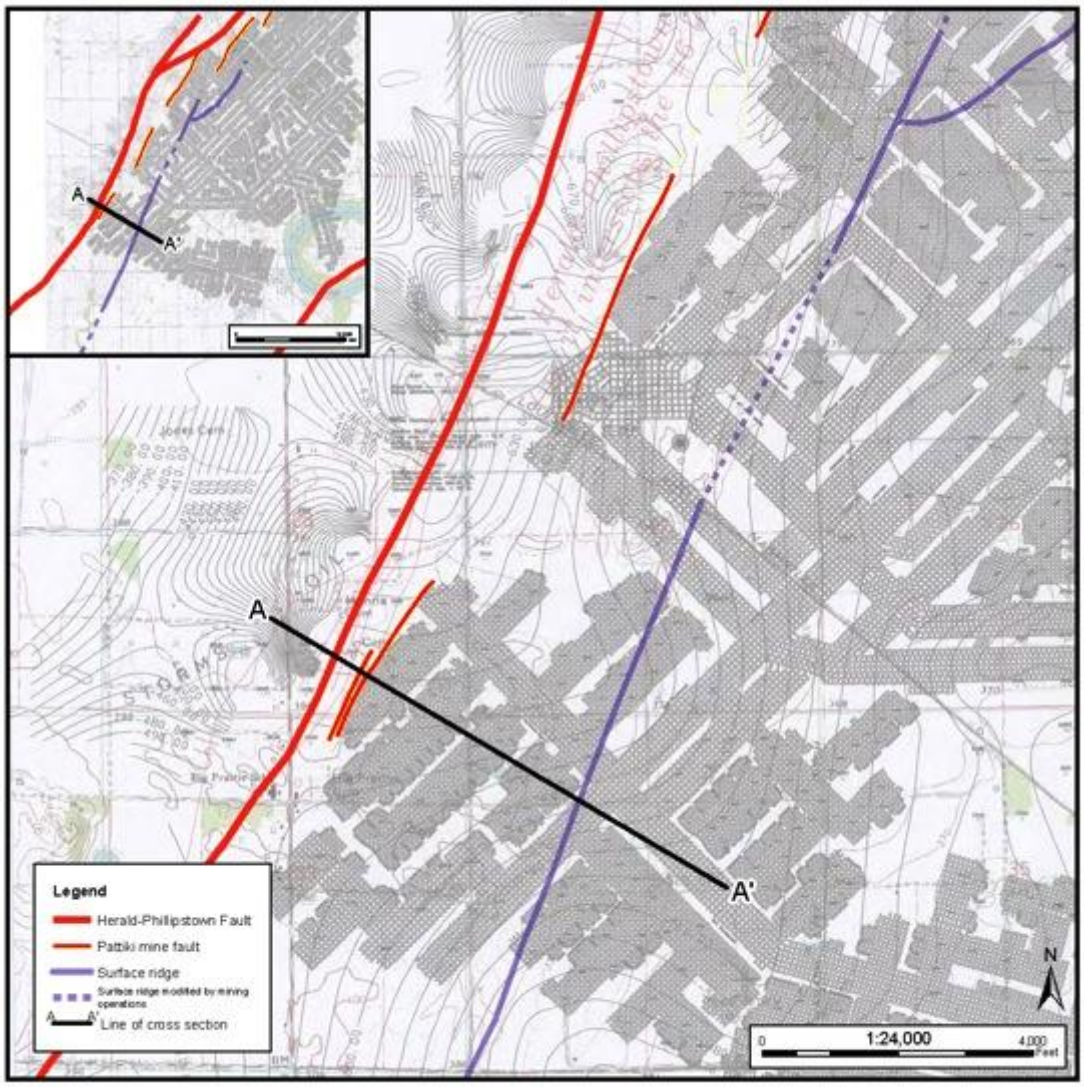

Figure 13. Structure map of the Herrin Coal based on a map of final mine-workings of the Pattiki Mine (White County Coal Co., 2003). Cross section along A A' shown in Figure 14.

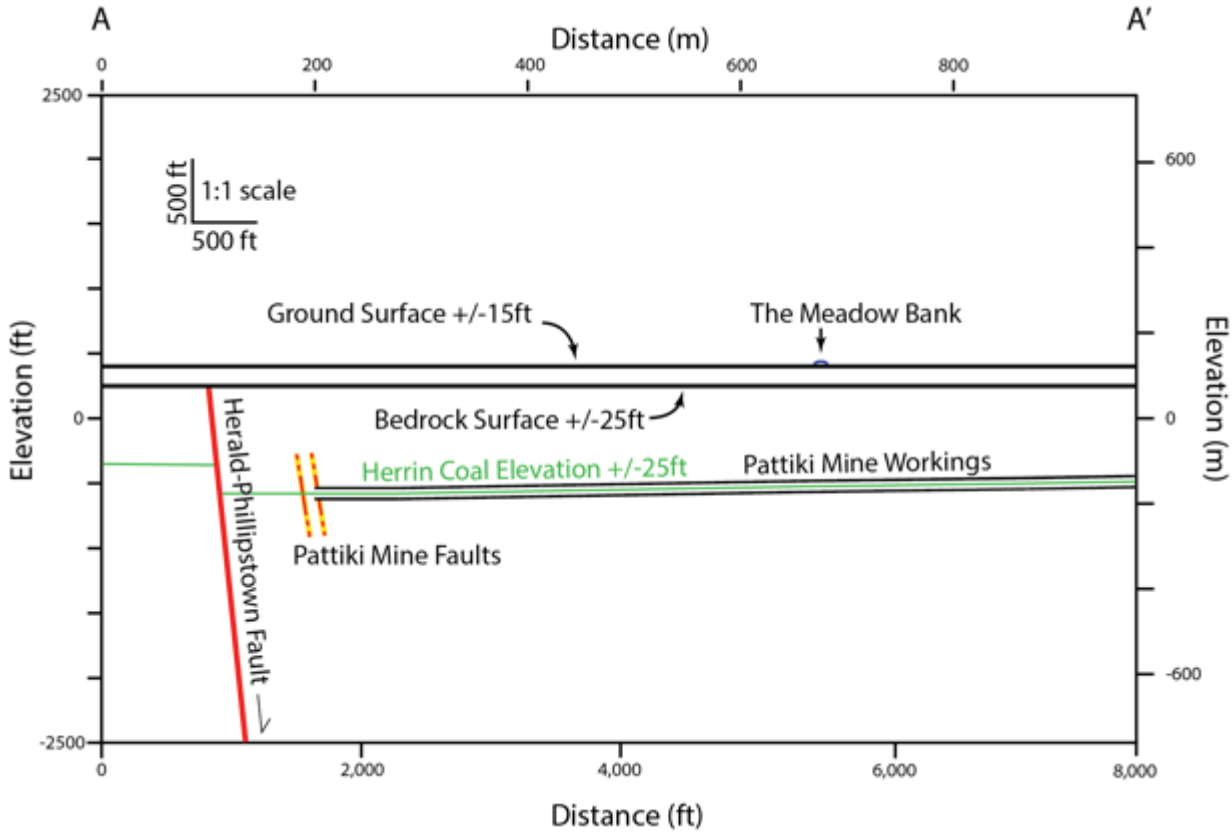

Figure 14. Cross section through the Pattiki Mine, 1:1 scale (data from White County Coal Co., 2003).

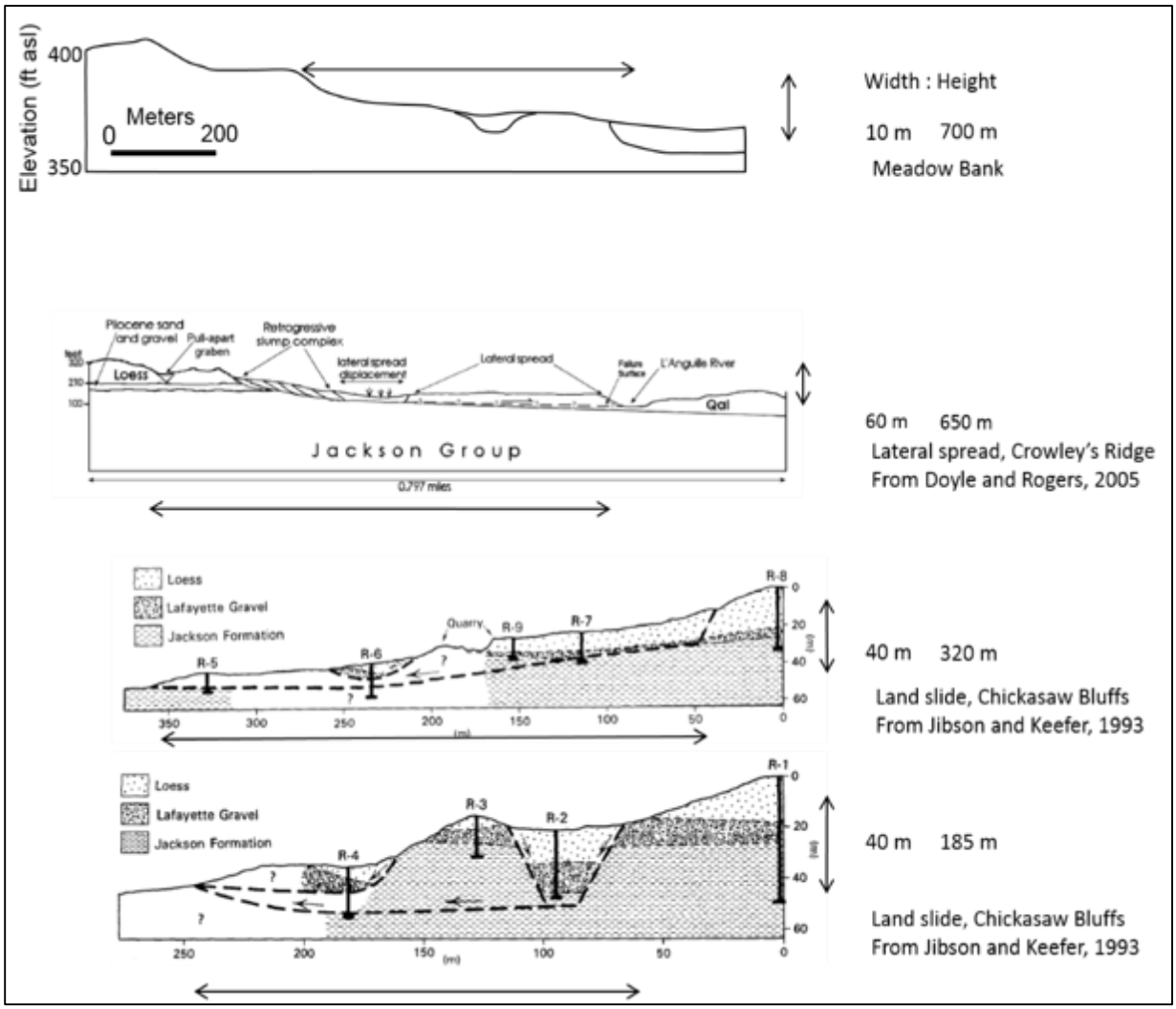

Figure 15. Comparison between profiles of the Meadow Bank Lineament (top) with three known seismically-induced mass movements. On the left are two landslides documented by Jibson and Keefer (1993) and on the right is a lateral spread documented by Doyle and Rogers (2005). All profiles are shown at approximately the scale. Arrows show the approximate length and height of the feature. The ratio of the length to height is much greater for the MBL than any of the mass movements. This suggests that the MBL is the result of some other process.

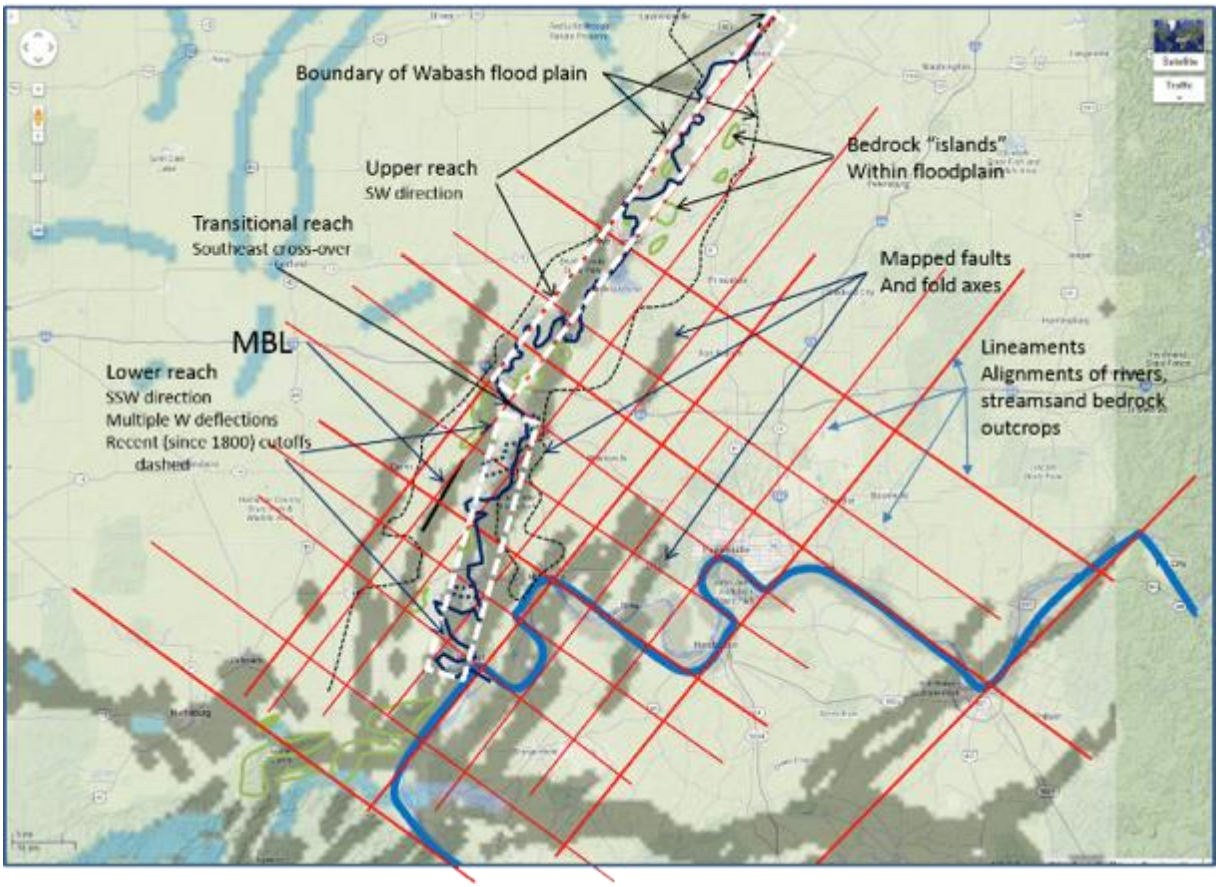

Figure 16. Regional lineaments drawn on a Google Map base.

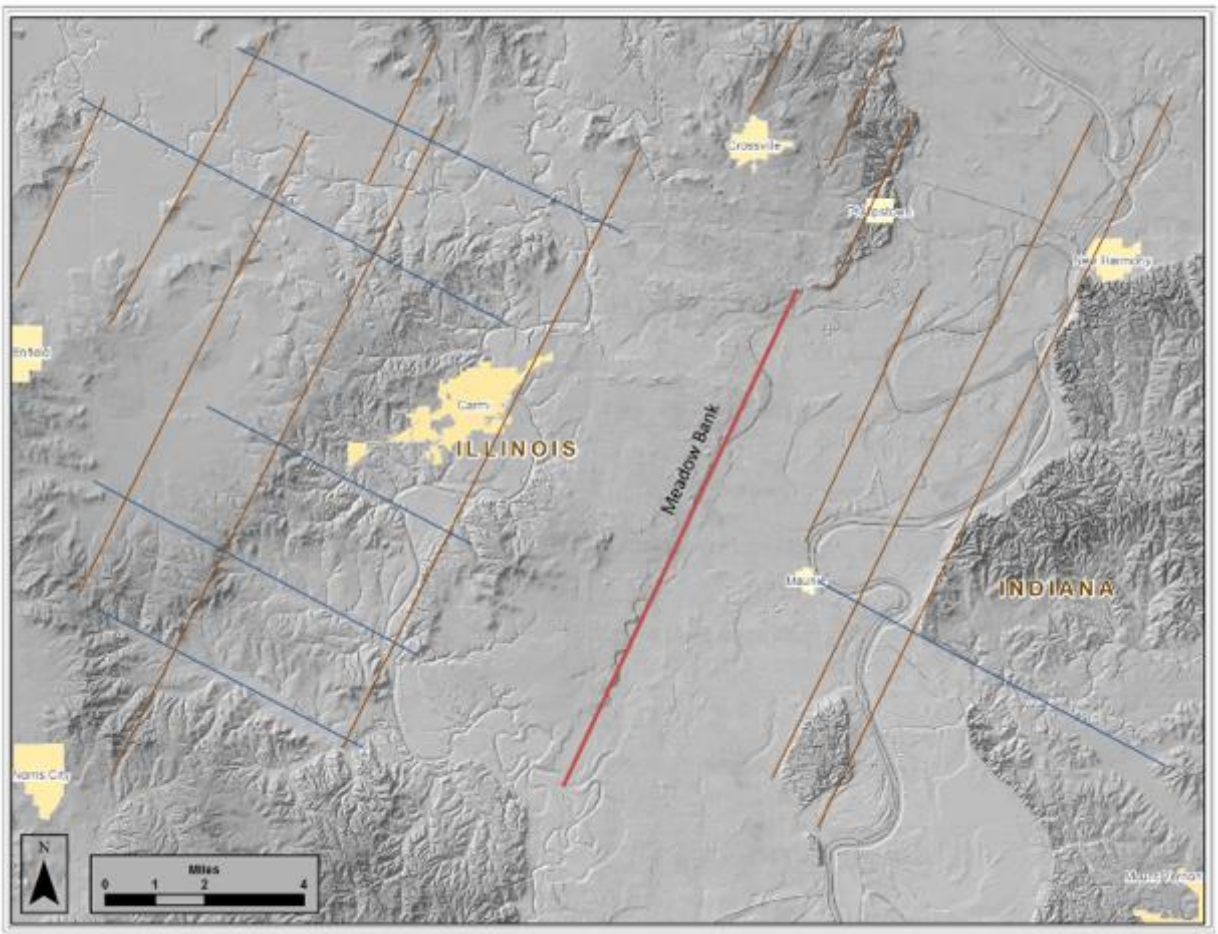

Figure 17. Local lineaments near the MBL drawn from the 30-m DEM of Illinois.

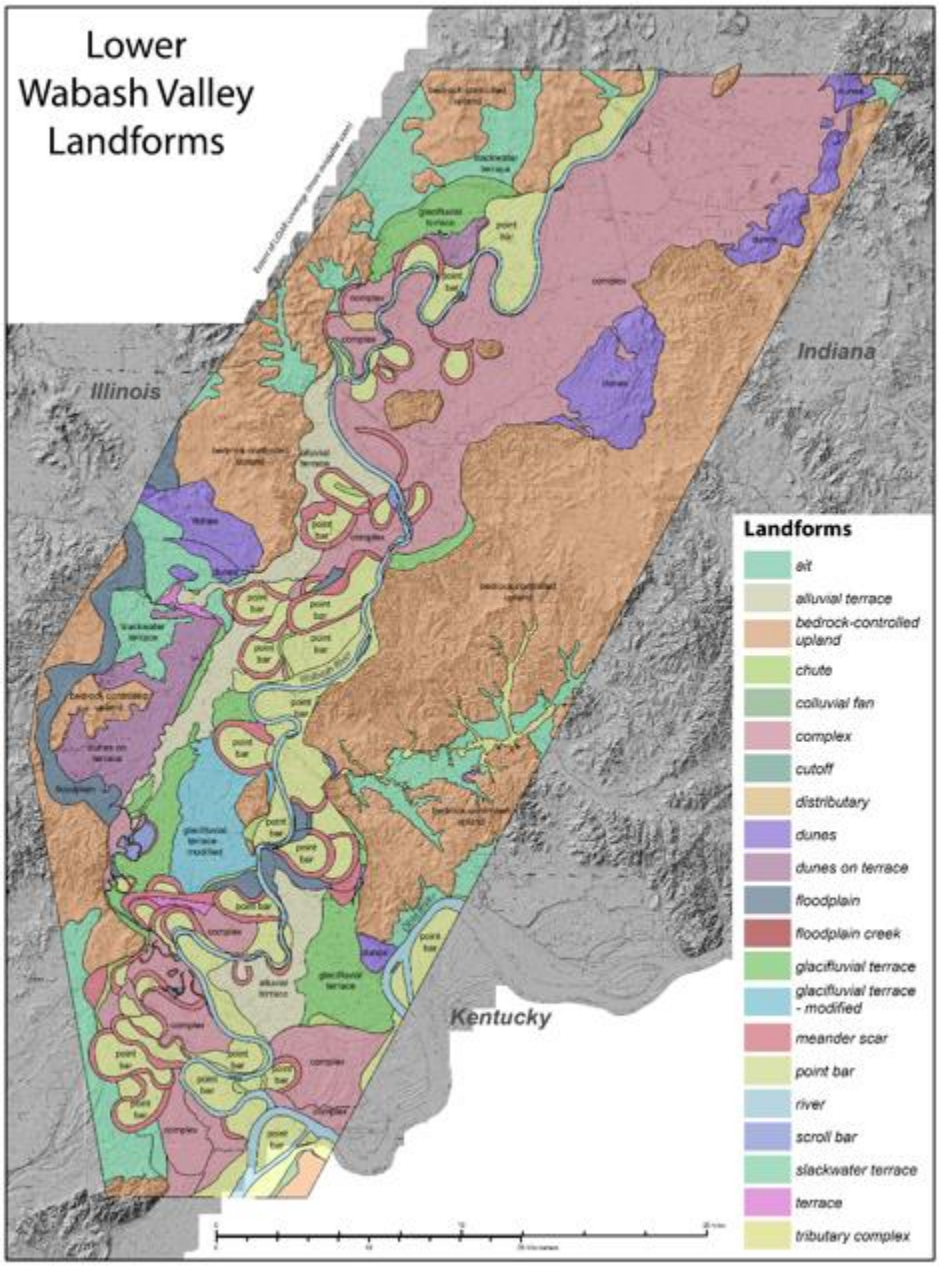

Figure 18. Geomorphic map of the lower Wabash Valley.

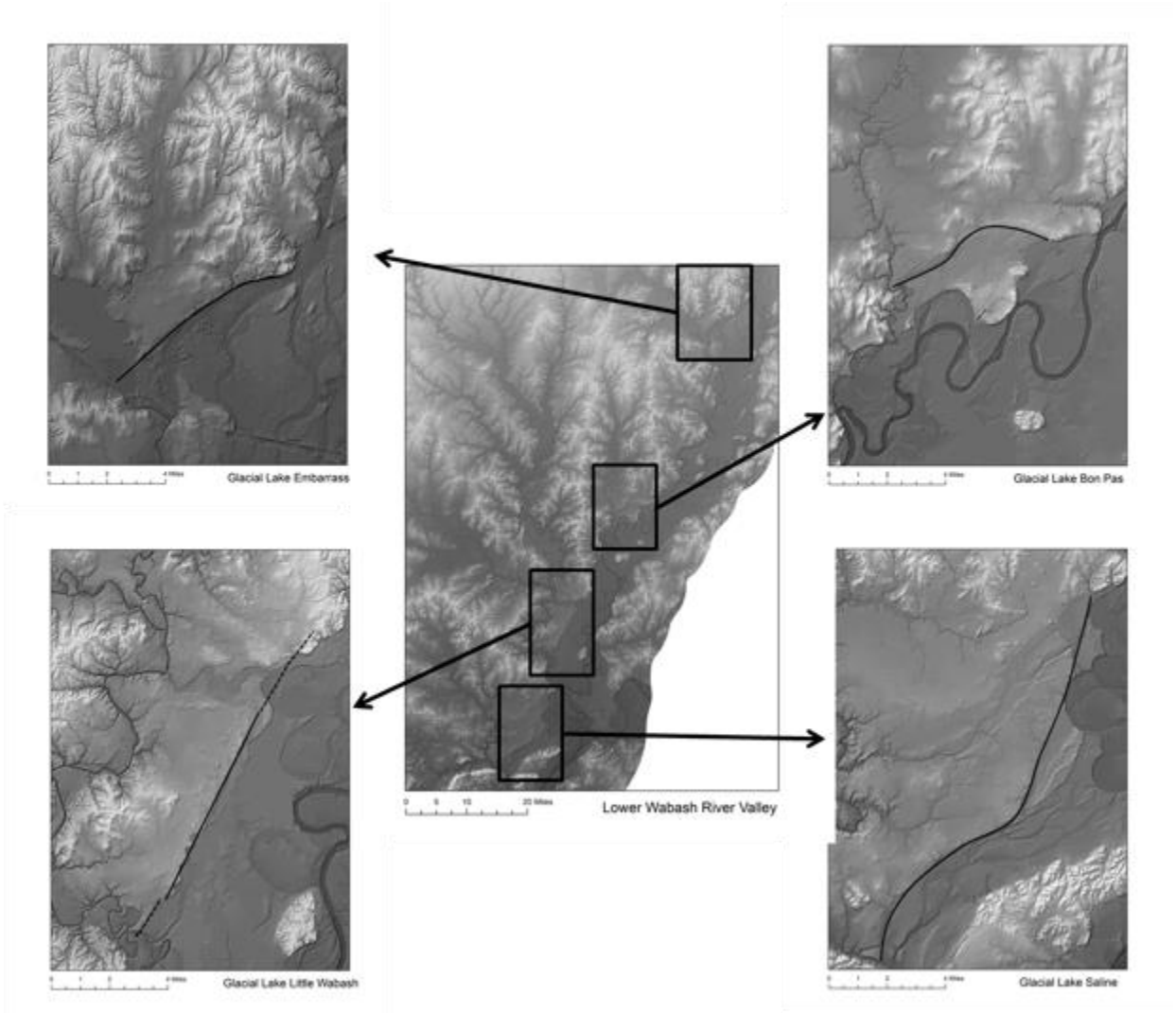

Figure 19. Digital elevation model of the lower Wabash River Valley with details of the confluence region of four tributary streams. Terrace scarps, including the MBL , are evident in each of the confluence regions.

Appendices

A1: Borehole descriptions

A2: Measured porosity

A3: Particle-size statistics

A4: X-Ray Diffraction micro-bulk sample results

A5: Results of Chittick analysis

A6: Magnetic susceptibility measurements

A7: Summary of OSL age dating

A8: 14C Age date summary

A1: Borehole descriptions

MBL-P1 API #121933032300 T5S R10E S34 1313S 853E NW 394 feet elev.
Longitude (NAD83): -88.094556 Latitude (NAD83): 38.048944

Top	Bottom	Description	Lithcode	Stratcode
0	0.6	Yellow brown pebbly loam; abrupt contact. [disturbed ground - road material]	pL	dg
0.6	0.9	Light brown fine sand, massive, to loamy sand with granules; fine roots (possibly grasses); distinct contact; leached. [subsoil, disturbed ground]	fS	dg
0.9	2.6	Reddish brown [5 YR 4/3] slightly loamy medium sand, massive, and dark yellowish brown [10 YR 3/6] medium sand, massive; interbedded with 0.1-0.15' thick beds, distinct contacts; leached; internally bioturbated (uniform texture); illuvial clay lamellae. [Colluvial and aeolian dune sedimentation]	mS	h-pk
2.6	4	No recovery	NR	h-pk
4	4.35	core spoil	mS	dg
4.35	4.75	reddish brown [5YR 4/3] slightly loamy fine sand, massive; leached; sharp contact. Similar to 0.9-2.6. Weak B horizon, paleosol.	fS	h-pk
4.75	6.2	Yellow brown- pale yellow brown fine sand, thinly and weakly bedded; leached; sharp contact. [dune sand]	fS	h-pk
6.2	6.45	Dark yellowish brown [10 YR 4/6] slightly gritty silty loam; weakly organic at base; leached; sharp contact; correlates to MBL-P8: 6.2-6.7 [Possible loess]	L	p
6.45	6.6	Light yellow brown medium-coarse sand, massive, with clay; leached; sharp contact w/ dolomitic silt bed; chemical contact. Bottom of surficial soil complex. [aeolian dune]	cS	h-pk
6.6	7.1	Light yellow brown coarse sand, massive; calcareous. [alluvium]	cS	h

7.1	9	No recovery	NR	h
9	9.1	core spoil	S	h
9.1	10	Light pale brown medium sand, massive, 0.5' beds; calcareous. [fluvial]	mS	h
10	11	Sample for OSL	OSL	h
11	11.4	Pale brown medium & fine sand, massive, thin (0.05') beds; calcareous; sharp contact. [alluvium]	m-fS	h
11.4	11.55	light yellow brown fine sandy loam to silty loam, laminated; calcareous; sharp contact; correlates to P8: 7.8-8. [eolian]	L	h
11.55	13	Light brown medium-fine sand, laminated (~3mm thick); [alluvium]	m-fS	h
13	14	No recovery	NR	h
14	18.2	light brown medium-coarse sand, massive	cS	h
18.2	19	No recovery	NR	h
19	19.05	Dark brown fine sand, laminated, with clay; slightly indurated; calcareous. Possible paleosol remnant (Piston muddy upon sampling).	fSo	h
19.05	23.1	Light brown medium-coarse sand, massive to horizontally bedded; weak graded beds ~1' thick; moderately well sorted.	c-mS	h
23.1	24	No recovery	NR	h
24	29.5	Light brown medium to coarse sand, massive; inclusions of laminated silt; arbitrary contact. (Photo incorrect: retook with 31' at top)	c-mS	h
29.5	37.4	Light brown fine-medium sand, massive to weakly bedded, slightly coarser and better sorted at bottom; 0.2' coarse sand bed, massive, at 36'; 30-31' sampled for OSL.	m-fS	h
37.4	39	No recovery	NR	h
39	42.8	Disturbed during coring; light brown medium sand.	mS(d)	h

42.8	44	No recovery	NR	h
44	46	Disturbed; light brown medium sand.	mS(d)	h
46	47.8	Light brown medium-coarse sand (horizontally bedded, graded); subangular dolomitic, rounded siltstone ≤ 10mm; overall graded upward.	c-mS	h
47.8	49	No recovery	NR	h
49	52.2	Disturbed; light brown coarse sand	cS	h
52.2	53.3	Light brown coarse/fine sand (horizontally bedded); beds 3-10 cm thick; few granules; single, subrounded quartzite pebble (1.5 cm).	c-fS	h
53.3	54	No recovery	NR	h
54	54.7	Disturbed. Sampled for OSL.	OSL	h
54.7	56.6	Very pale brown granular coarse sand, not clearly bedded or massive; poorly sorted; clear textural boundary, but color is gradational throughout.	cS	h
56.6	57.8	Gray and pale brown (bedded - oxidized zones) pebbly coarse sand (horizontally bedded); ~0.6' beds; rounded granite and broken sandstone lithologies and other sedimentary lithologies. Outwash. [Henry Formation]	pcS	h
57.8	59	NR		h
59	62.3	Gray medium sand, massive; few granules; rounded 1" metamorphosed pebble at 62'; sharp contact. Large coal pebble at 59', and igneous.	mS	h
62.3	64	Gray fine sand (horizontally bedded); thin beds defined by heavy mineral laminae; contact at bottom of core?	fS	h
64	64.05	Dark yellowish brown [10 YR 4/4] silty sand, massive; sharp contact; calcareous; quiescent water.	zS	h
64.05	66.7	Gray medium-coarse sand, massive, graded up to fine-medium sand.	c-mS	h
66.7	67.9	Sampled for OSL	OSL	h

67.9	69	No recovery	NR	h
69	71	Fine and medium sand, disturbed [69-76 correlates to 47-67 in MBL-P2 and 45-47 in MBL-P3]	m-fS	h
71	73	Very pebbly, very coarse sand to sandy fine gravel; disturbed	SG	h
73	73.7	Pebbly very coarse sand, up to 1.5" gravel	pcS	h
73.7	74	No recovery	NR	h
74	74.8	Gray very coarse sand; disturbed	vcS	h
78.4	75.2	Gray granular very coarse sand, poorly sorted; clear contact	vcS	h
75.2	76	Gray medium -fine gravel (graded); igneous and sedimentary lithologies, rounded.	m-fG	h
76	76.2	Gray shale in shoe.	SH	P

MBL –P2 API #121933032400 T5S R10E S34 1300S 1804E NW 380 feet elev.
Longitude (NAD83): -88.091254 Latitude (NAD83): 38.049000

Top	Bottom	Description	Lithcode	Stratcode
0	1.2	Dark yellowish brown [10 YR 4/4] sandy loam; worm burrows; road gravel in upper 0.1'; distinct boundary. AP horizon.	SL	dg/py
1.2	3.9	Dark yellowish brown [10 YR 3/4] sandy loam - sandy clay loam; granite pebble, weathered, well rounded; B horizon [cumulic olluvium]	SL	py
3.9	6.7	Brown [7.5 YR 4/4] loamy medium sand (4.1'); weak bedding with clayey zones; upper CB, cumulic. [colluvium and alluvium]	mS	py-h
6.7	11.8	Light gray to yellow brown fine sand; banded to bedded; bands/beds 0.1-1' thick; leached; distinct boundary with chemical boundary. Fine to medium sand at bottom. Gaps at: 3.5-4', 7.3-9'. Fluvial.	fS	h
11.8	45.6	Light yellow brown medium - coarse sand graded down to fine sand; bedding not obvious; few clay lens inclusions in disturbed portion; calcareous; gradual contact. Gaps at: 12.1-14', 17.7-19', 22.4-24', 42.6-44.0'. Post-glacial fluvial?	c-mS	h
45.6	54.1	Gray fine - medium sand (graded); 1.0' think beds; lenses of gravel, large-medium, well-rounded quartzite, granite, & other sedimentary lithologies; gradual contact. Gaps at: 27.6-29'. Transitional?	m-fS	h
54.1	74	Gray sandy fine gravel (massive) graded to medium-coarse sand, fine sand; beds 1-2' thick; chert, granite, quartzite, siltstone, and sandstone lithologies; sharp contact. Glacifluvial.	fG-mS	h
74	76.5	Gray pale brown sandy gravel grades to fine-medium sand, massive. Matrix is finer than above.	sG-fS	h
76.5	76.7	Light gray shale? Fine pebbles, rounded, are a curiosity: 2mm brown chert, metaquartz. Part of shale or injected? Rock.	SH	P

MBL-P3 API #121933032500 T5S R10E S34 1304S 1648W NE 369 feet elev.
Longitude (NAD83): -88.084893 Latitude (NAD83): 38.049025

Top	Bottom	Description	Lithcode	Stratcode
0	1.1	Dark grayish brown [10 YR 4/2] sandy clay loam; weakly mottled with burrows; sand bed; few Fe-Mn concentrations, 1mm; distinct contact. Farm road bed, dg/AP horizon.	SCL	dg
1.1	2.8	Dark brown [10 YR 3/2] silty clay loam; fine orange mottle; clay concentrated in skin and root pores; weak Fe-Mn concentrations (crumbly), ~1mm, common 3-4 mm Fe-Mn concentrations at base; clear boundary. Upper B-horizon, cumulic.	ZCL	c-c
2.8	5.3	Very dark gray [10 YR 3/1] with strong yellowish brown [10 YR 5/8] mottle grades down to brownish gray [2.5 Y 5/2] with strong brown [7.5 YR 5/8] pervasive mottle; silty clay-silty clay loam; differentiation in mottling increases with depth, clay skins in roots and cracks, Fe-Mn concentrations [2mm], leached; gradational contact; B horizon, cumulic	ZCL	c-c
5.3	5.6	brownish gray with strong brown mottle, clay loam, weakly bedded; leached; sharp contact; B horizon, cumulic; base of gradational unit, backswamp deposit.	CL	c-c
5.6	7	Grayish brown [2.5 Y 5/2] and very dark gray [10 YR 3/1] silty clay loam-silty clay with yellowish brown [10 YR 5/8] mottle, interlaminated with gray very fine sand- silt; leached. Dark layer, organic, at bottom [bulk 14C date 10.7 ka (calibrated), ISGS-A2843]. Alluvium.	ZCL	c-c
7	8	Sampled for OSL, includes chemical contact [14.8±1.07 ka, ISGS-249]	fS	h
8	8.5	Dark gray [2.5 Y 4/1] laminated silty fine sand- sandy clay loam; woody fibers and ostracodes (large); calcareous ; gradational contact. [seed dated at 17.3 ka (calibrated), ISGS-A2846] Alluvium.	fS-SCL	h
8.5	23.1	Brown sandy loam (horizontally laminated) grades down to yellow brown medium-coarse sand, thinly bedded, laminated pebbly granules to fine pebbles in zones;	SL	h

		subangular-subrounded chert, pink-white quartzite, granite, and sedimentary lithologies; clear boundary. Alluvium.		
23.1	24	No recovery	NR	h
24	42.8	Light yellow brown fine - medium sand; very weak thick bedding (probable coring distortion); sharp contact, correlates to MBL-P4: 52'. Alluvium.	m-fS	h
42.8	73.1	Pale brown granular very coarse sand - medium sand (graded); beds 0.5-2.0' thick; sub-angular - well-rounded coal, sandstone, limestone, layered metaquartz, pink granite pebbles up to 3cm, but typically 0.5-2mm; some beds of clean gravel; sharp contact with gravel bed. Outwash.	vc-mS	h
73.1	73.4	gray [7.5 YR 6/1] fine silt loam, laminated, with very fine sand, single bed; Ponded sediment; No fossil organics; sharp contact	ZL	h
73.4	79.3	gray sandy fine gravel - medium sand (graded); 1.5-2.0' thick beds, lower most bed is a massive granular gravel. Outwash. Correlates to lower unit in MBL-P2.	fSG	h
79.3	79.3	Refusal on hard rock: flared bit; no sample, possible limestone	I	P

MBL-P4 API #121933032600 T5S R10E S34 1311S 2417W NE 373 feet elev.
Longitude (NAD83): -88.087566 Latitude (NAD83): 38.048990

Top	Bottom	Description	Lithcode	Stratcode
0	0.7	Dark yellowish brown [10 YR 4/3] sandy loam; weakly organic; leached; clear boundary. Dg [farm lane], AP horizon.	SL	c-h
0.7	1	Brown [10 YR 4/3] sandy loam; depleted lenses; burrows; very weakly organic; leached; abrupt boundary. Weak E horizon.	SL	c-h
1	2.2	Dark yellowish brown [10 YR 4/4] sandy clay loam; few 1-3 mm Fe-Mn concentrations; burrows; leached; gradual boundary. BT horizon.	SCL	c-h
2.2	3.4	Dark yellowish brown [10 YR 4/6] sandy clay loam with mottles; clay and sand more segregated than above; common burrows; leached; sharp boundary. Loose sand in shoe. BT horizon.	SCL	c-h
3.4	4	No recovery	NR	c-h
4	5.6	Light gray [10 YR 7/2] sandy loam - weak sandy clay loam with weak yellowish brown [10 YR 5/6] mottles and strong dark brown [7.5 YR 3/4] mottling; leached; gradual boundary; CB horizon [alluvium]	SL	c-h
5.6	6.6	Brown [7.5 YR 4/3] weak medium loamy sand; bedded with gray interbeds; strong mottle; leached; abrupt boundary; upper C horizon	LS	c-h
6.6	7.4	Dark brown [10 YR 3/3] weak medium-coarse loamy sand; weak bedding, possibly with organic concentrations in clay beds; leached; chemical boundary.	LS	c-h
7.4	7.9	Brown medium sand; bedded; calcareous; C horizon	mS	c-h
7.9	9	No recovery	NR	c-h
9	52	Light brown medium-fine, coarse sand; generally 1-2' thick beds, with some smaller ~.5' beds; rare isolated gravel clasts and few < 0.1' granule beds; calcareous; graded contact. 10-11', 31-32', 45.2-46.2' sampled for OSL.	c-mS	h

52	63.7	Light brown coarse -fine sand with gravel beds; ≤ 2' thick beds; possible organic beds; moderately rounded, smooth dominantly sedimentary gravel lithologies, some pink granite, metaquartz, quartzite, and mafic meta-something; calcareous; contact missing. Glacifluvial.	c-fS, G	h
63.7	64	No recovery	NR	h
64	73	Light brown very fine gravel - gravel sand; horizontally bedded with 1-1.5' thick beds; well to poorly sorted; dominantly sedimentary gravel lithologies, but some granite or other igneous, chert, metaquartz, brecciated conglomerate; vigorously calcareous. Gravel bed in shoe.	fG-gS	h
73	74	No recovery	NR	h
74	80	Very light brown with a pink hue medium sand; horizontally bedded with thin gravel beds to single-grain thick; granules in lower foot; dominantly sedimentary lithologies and few meta- lithologies; very weak calcareous reaction; gradual contact. Root of paleosol - Farmdale or Sangamon? Small amount missing at 79'.	mS	h2 or pl
80	89	Yellow brown very fine gravel- granular coarse sand- moderately sorted gravel pebbly sand; weakly graded to massive bedding with 0.5-1.0' beds; sedimentary and weathered igneous lithologies; delayed (dolomitic?) calcareous reaction, stronger below 84'. Root of paleosol- Farmdale or Sangamon?	SG	h2 or pl
89	99	Light gray to brown gray granular medium sand to gravel sand; graded beds 0.5-2.0' thick; rounded sedimentary (conglomeratic) and igneous gravel/granule lithologies; very strong calcareous reaction. BOH - limit of tooling	SG	h2 or pl

MBL-P5 API #121933032700 T5S R10E S34 1300S 1416E NW 390 feet elev.
Longitude (NAD83): -88.092599 Latitude (NAD83): 38.048992

Top	Bottom	Description	Lithcode	Stratcode
0	0.3	Road spoil	D	dg
0.3	3	Brown [10 YR 4/3] (.7) - dark brown [10 YR 3/3] (2.2) sandy clay loam; fine roots and pores, burrows; few remaining organic roots; weak platy structure; leached; distinct color/textural boundary. More organic rich than below. Cumulic A horizon in loess.	SCL	p
3	5.3	Dark yellowish brown [10 YR 4/4] clay- sandy clay, brown [7.5 YR 4/4] silty clay; laminated; fine roots and burrows; clay concentrated in skins and crack; few ≤ 1mm Fe-Mn concentrations; leached; distinct textural boundary; No recovery 3.5-4.0'; modern BT horizon [loess]; Similar to 6.2-6.5 in MBL-P1;	ZC	p
5.3	6.3	Dark brown [7.5 YR 3/4] sandy clay loam; laminated (partly disturbed by coring); very few Fe-Mn concentrations, ≤ 1mm; possible burrows, 1 visible large root, 5cm, with 1mm clay skin; leached; distinct color/textural boundary; [Alluvium]. Interval to 7.2 correlates to MBL-P8: 5.4-6.7'; BC horizon.	SCL	e-h
6.3	7.2	Brown [7.5 YR 4/4] fine sandy clay; probably laminated, but disturbed by coring; ≥ 1mm roots/cracks with clay concentrations; leached; contact probably in sample collected for OSL/not recovered; CB horizon [alluvium]	SCL	e-h
7.2	8.2	sampled for OSL	LS	e-h
8.2	9	No recovery	NR	e-h
9	12	Light brown and dark brown medium sand, illuvial clay bands parallel to bedding ≤ 1cm - 0.6' thick; lignite layer at 10.8-11'; leached; CB horizon; contact not recovered [alluvium]. 9-16 correlates to bedded portions of MBL-P1 & MBL-P2.	mS	h
12	14	No recovery	NR	h
14	16	Yellow brown/dark brown coarse sand; Illuvial clay bands and sand beds < 1cm -0.2' thick; lignite fragments ~1mm	cS	h

		throughout; leached; gradual contact. Probably continuous with above, but graded. CB horizon [alluvium]		
16	26	Yellow brown coarse sand; no visible bedding or banding until 0.1' dark brown band at 22.0'; thin, 1-2 cm lignite bed at 25.0' overlying a 0.1' thick silty clay bed (0.3' section probably disturbed); 0.1' thick silty clay band, laminated, at 25.8' (both clays are yellowish brown [10 YR 5/4]; sampled for clay mineral analysis); leached; gradual color contact. 22.3-24.0' no recovery. [alluvium] similar appearance to above but no illuvial bands.	cS	h
26	33	Brown-dark brown coarse sand, completely disturbed (core casing cracked during coring); contains charcoal or coal fragments; leached; chemical boundary. 26.6-27.7 sampled for OSL; 27.7-29, no recovery. CB horizon [alluvium]	cS	h
33	33.8	Brown-dark brown coarse sand, disturbed by coring; calcareous; contact not recovered. C horizon.	cS	h
34	35	No recovery	NR	h
35	40.5	Gray-brown medium-fine sand; graded, coarsening upwards; clay laminations at 37.4'; calcareous; distinct (though slightly disturbed) grain size contact. 36.8-39, no recovery. Alluvium. Most similar to MBL-P1 34-45'.	m-fS	h
41	47.5	Gray brown coarse sand; no visible bedding or gradation; calcareous. 41.5-44, no recovery; 46-47 collected for OSL. Most similar to MBL-P1 45-54'. BOH	cS	h

MBL-P6 API #121933032800 T5S R10E S34 1317S 1593E NW 387 feet elev.
Longitude (NAD83): -88.091985 Latitude (NAD83): 38.048949

Top	Bottom	Description
0	0.3	Road Material
0.3	1.2	Dark yellowish brown [10 YR 3/4] silty clay loam with a strong brown [7.5 YR 4/6] mottle; roots up to 5cm; some skins in root pores up to 1cm; Fe/Mn concentrations up 1.5 cm diameter, are deeper in section; leached; distinct color & textural boundary. Plow zone.
1.2	1.65	Dark yellowish brown [10 YR 3/4] coarse sandy loam; poorly sorted; some roots ~1cm; leached; sharp color & textural contact. Plow zone.
1.65	2	Very dark brown coarse -very coarse sand; poorly sorted; loosely cemented; leached; distinct color contact. Original ground surface. A 2.
2	3	Strong brown coarse-very coarse sand; poorly sorted; cemented; leached; contact lost. Colluvium. B horizon.
3	4	No Recovery
4	4.1	Junk
4.1	4.5	Brown coarse sand; poorly sorted; weakly cemented; leached; contact missing. Colluvium. CB horizon.
4.5	5.5	Sampled for OSL
5.5	10.7	Orange brown fine sand; massive with few faint laminations; leached; sharp color/chemical contact. Alluvium. CB horizon.
10.7	21	Light brown fine-medium sand; graded, fining upward beds, bed ~1.5'-2.0', few lamine, silty band at 17.25-17.30'; calcareous; distinct grain size contact. 17.8-19 no recovery. Alluvium. C horizon.
21	42.9	Light brown coarse-medium coarse sand; massive; coal fragments at 31'; calcareous; grain size contact lost. 22.5-24.5, 26.6-29, 32.5-34, 37.5-39 no recovery. 25.6-26.6 sampled for OSL. Alluvium.
42.9	44	No recovery
44	48	light brown coarse sand; poorly sorted; coarser at bottom; calcareous. Distinct contact. 45.5-46.5 sampled for OSL.

48	48.3	Light brown pebbly medium to coarse sand; poorly sorted; metamorphic and sedimentary LF, sub-rounded. END.

MBL-P7 API #121933032900 T5S R10E S34 1310S 2246E NW 377 feet elev.
Longitude (NAD83): -88.089717 Latitude (NAD83): 38.048979

Top	Bottom	Description	Lithcode	Stratcode
0	0.4	Dark brown loam diamicton, sharp contact; [road spoil]	D	dg
0.4	1.1	Dark brown [10 YR 3/3] coarse sandy loam; leached; gradual color boundary.	SL	c-h
1.1	2.35	Brown [7.5 YR 4/4] sandy clay loam (1.4'); some Fe-Mn concentrations ~1mm; leached; gradual color/textural boundary. Upper B or Bt	SCL	c-h
2.35	3.5	Strong brown [7.5 YR 4/5] sandy loam (2.5'); leached; boundary not recovered.	SL	c-h
3.5	4	No recovery	NR	c-h
4	4.25	core spoil		I
4.25	6.1	dark yellowish brown [10 YR 4/6] coarse loamy sand-sand (4.4'); zones of strong brown [7.5 YR 4/6] mottling throughout; leached; sharp color boundary CB horizon [alluvium]	cS	c-h
6.1	6.5	Light gray [10 YR 7/1] weak sandy loam-loamy sand with a yellowish brown [10 YR 5/6] mottle; leached; distinct textural/color boundary. CB horizon [alluvium (bed)]	SL	c-h
6.5	7.4	Brown [7.5 YR 4/4] sandy loam; leached; contact lost. CB horizon [alluvium]	SL	c-h
7.4	9	No recovery	NR	c-h
9	10.1	Brown medium sand; thick laminations (clear, but disturbed by coring) of light gray and black (organics?); leached; color/ chemical and textural distinct contact; CB horizon [alluvium]	mS	c-h
10.1	11.4	Light brown fine sand bedded with .1'-1 cm beds of light olive brown [2.5 Y 5/4] "clay," light olive brown [2.5 Y 5/3] "silt/silty clay," olive brown [2.5 Y 4/4] "clay" (at bottom); calcareous; distinct textural contact. [alluvium]	fS	c-h

11.4	24.3	Light yellowish brown medium-coarse, laminated sand; clear <2mm black (organic?) laminations throughout and some sandy orange laminations (iron?) at 12'; thicker 5cm bed of black [2.5 Y 2.5/1] clay at 19.9'; yellowish brown [10 YR 5/6] laminated silty clay inclusions [possibly disturbed by coring] at 19.5' [sampled for clay mineral analysis], shell fragments of large (>5mm?) gastropod with ridged whorl, fine with finer silty sand than matrix; calcareous; sharp grain size contact. 16-17' sampled for OSL. No Recovery at: 13.2-19.0', 18.2-24'. [alluvium]	c-mS	h
24.3	29.4	Light yellowish brown coarse sand (massive) with clear brown/dark brown laminations at top near 24.6' only; calcareous; textural contact. No recovery 22.6-24'. [alluvium]	cS	h
29.4	33.6	Light yellowish brown very coarse sand; probably disturbed; calcareous. [alluvium] BOH	vcS	h

MBL-P8 API #121933303000 T5S R10E S34 1314S 1132E NW 390 feet elev.
Longitude (NAD83): -88.093589 Latitude (NAD83): 38.048947

Top	Bottom	Description	Lithcode	Stratcode
0	0.3	silt loam, organic; [road material]	D	dg
0.4	1	Dark brown [10 YR 3/3] sandy loam-loam; some Fe-Mn concentrations ≤ 1mm; leached; distinct textural/color boundary; AE horizon [loess]	L	p
1	1.7	Brown [10 YR 4/3] sandy clay loam-clay loam; few Fe-Mn concentrations ≤ 1mm (less than above); roots ≤ 1 cm with clay; leached; distinct color/textural boundary; AB horizon [loess]	CL	p
1.7	2.7	Dark yellowish brown [10 YR 4/4] silty clay - clay; Fe-Mn concentrations ≤ 5mm; leached; gradual color/textural boundary; upper B horizon [loess]	ZC	p
2.7	3.9	Light brownish gray [2.5 Y 6/2] clay - silty clay with a strong brown [7.5 YR 4/6] mottle; few Fe-Mn concentrations (much less than above) ≤ 4mm; leached; boundary lost; lower B horizon [loess]	ZC	p

3.9	4	No recovery	NR	p
4	4.3	Possibly junk	NR	p
4.3	4.7	Light brownish gray [2.5Y 6/2] sandy clay with a pervasive strong brown [7.5 YR 4/6] mottle; leached; abrupt color/textural boundary; BC horizon [eolian dune and colluvium, mixed]	SCL	h(pk)-py
4.7	5.4	Dark yellowish brown [10 YR 3/6] sandy clay loam; CB horizon [eolian dune]	SCL	h(pk)-py
5.4	6	Dark yellowish brown [10 YR 3/6] sandy clay loam; possible laminations, disrupted by coring; Fe-Mn concentrations ≤ 1 mm; leached; abrupt color/textural boundary; CB horizon [eolian dune and colluvium, mixed]	SCL	h(pk)-py
6	6.7	Yellowish brown [10 YR 5/6] silty clay loam; possible laminations disturbed by coring; clay in cracks < 2 cm; Fe-Mn concentrations ≤ 2 mm; leached; abrupt color/textural contact; correlates to MBL-P1: 6.2-6.45'; CB horizon [eolian]	ZCL	h(pk)-py
6.7	7.8	Dark brown coarse sand; thinly bedded with ≤ 2 cm thick beds; leached; organic in lower 0.2'; color/textural contact (in bag labeled 7.4').	cS	h(pk)-py
7.8	8	Yellowish brown [10 YR 5/6] silt; disturbed completely by coring; leached; contact not recovered; correlates to MBL-P1: 11.4-11.5'; upper C horizon [eolian dune and colluvium, mixed]	Z	h(pk)-py
8	9	No recovery	NR	h(pk)-py
9	10	Sample collected for OSL [fluvial]	cS	h
10	12.9	Light brown coarse sand; thinly & horizontally bedded with dark brown and very dark brown coarse sand beds 1mm - 3mm thick near the bottom; leached; contact lost.	cS	h
12.9	14	No recovery	NR	h

14	17.4	light brown fine sand; thinly bedded with dark brown fine sand < 1 cm thick and thin black laminations ≤ 1 mm; leached; chemical/color contact; upper C horizon [fluvial]	fS	h
17.4	19.5	No recovery	NR	
19.5	22.7	Light yellowish brown fine-medium sand; calcareous; C horizon [fluvial]. BOH	m-fS	h
	22.7	END		

Gamma log and driller's description of Test Boring H1 (referenced as B1 in this report) from Heigold and Larson, 1994.

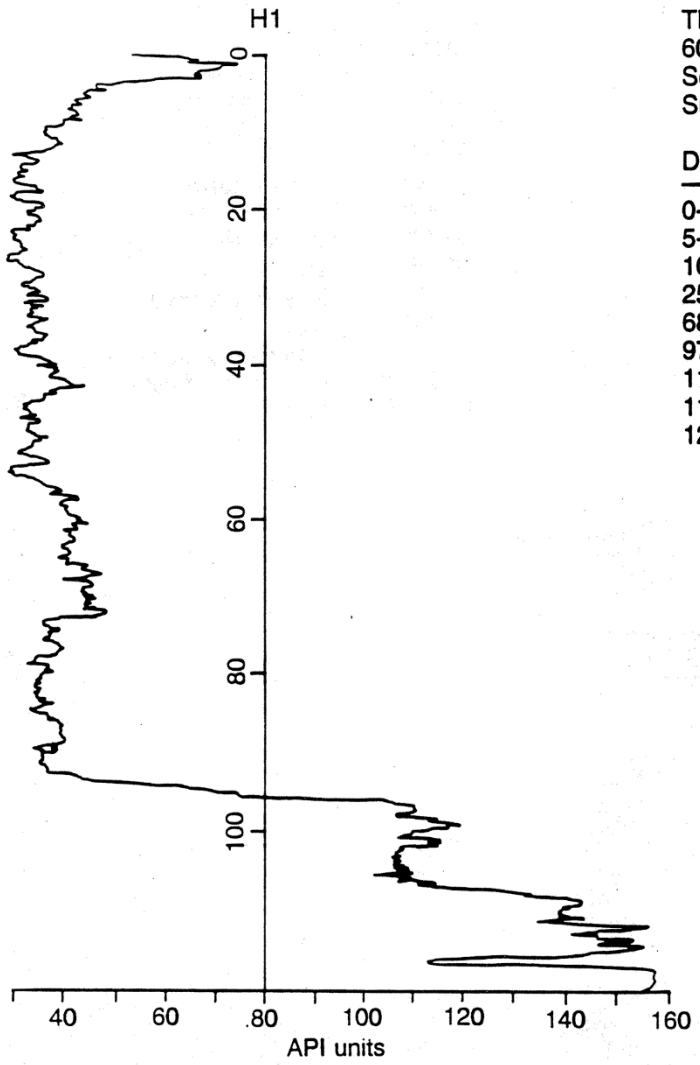

TEST BORING H1
600 ft W and 35 ft S NE cor SE NW
Sec. 34, T5S, R10E, White County, IL
Surface elevation 378.3 ft above msl

Depth (ft)	Material
0-5	Soil
5-10	Coarse sand, some gravel
10-25	Fine sand
25-6	Medium to coarse sand
68-97	Coarse sand and gravel
97-111	Gray clay
111-117	Gray Shale
117-122	Limestone with shale partings
122-140	Sandy shale

Gamma log and driller's description of Test Boring H2 (referenced as B2 in this report) from Heigold and Larson, 1994.

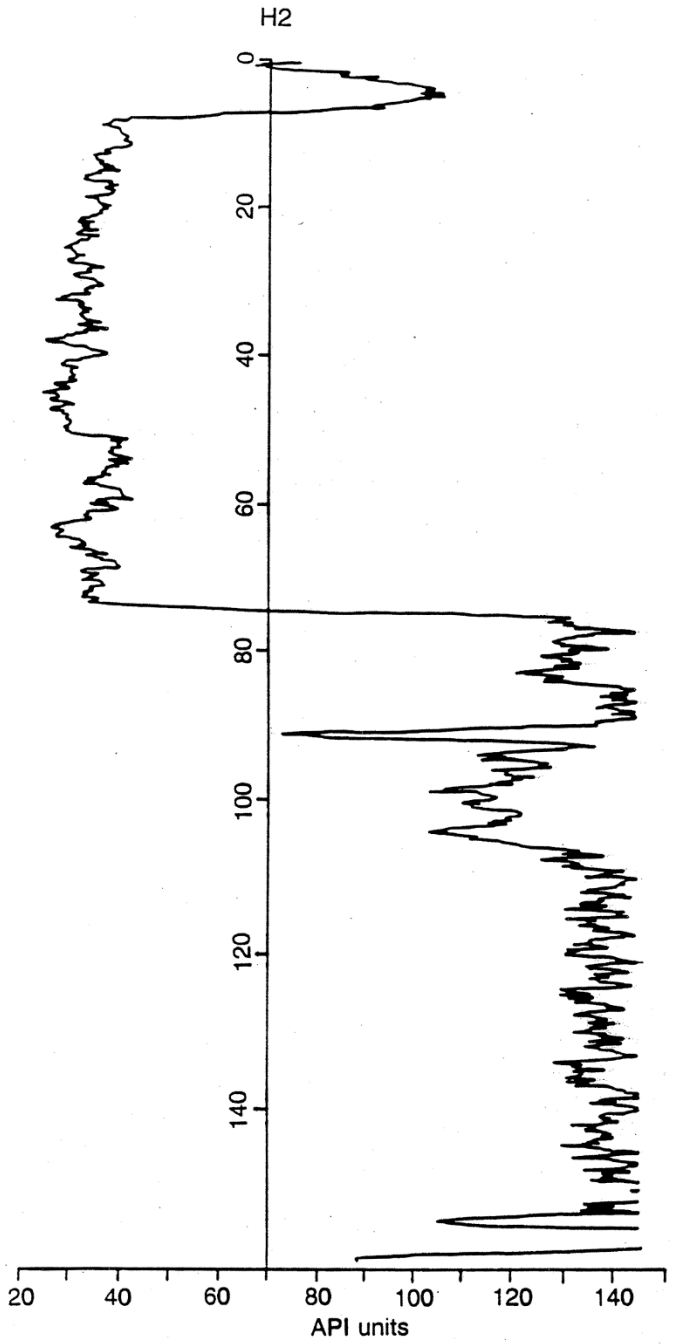

TEST BORING H2
50 ft S of NW cor SW NW
Sec. 34, T5S, R10E, White County, IL
Surface elevation 391.4 ft above msl

Depth (ft)	Material
0-9	Brown silty clay
9-25	Sand and gravel
25-27	Gravel
27-40	Coarse sand
40-50	Fine to medium sand
50-68	Coarse sand and gravel
68-75	Gravel
75-92	Gray sandy shale
92-93.5	Coal
93.5-148	Gray sandy shale
148-154	Shale with limestone partings
154-160	Gray shale

A2: Measured porosity

Core	Depth (ft)	Sample	Measured Volume (ml)	Set Volume (ml)	Porosity (%)	x (ϕ)	s(ϕ)	Descriptive Texture*
MBL-P1	16.5	A	21.54123764	30	28.19587452	1.6	0.7	moderately sorted medium sand
MBL-P1	32	B	20.72895242	30	30.90349193	2.1	0.5	well sorted fine sand
MBL-P1	47	C	21.52466821	30	28.25110598	1.3	0.6	moderately sorted medium sand
MBL-P2	26.5	D	21.56079391	30	28.13068697	1.6	0.4	well sorted medium sand
MBL-P2	52.6	E	22.38978694	30	25.36737686	0.9	0.6	moderately sorted coarse sand
MBL-P2	67	F	23.90634084	30	20.31219719	1	0.6	moderately sorted medium sand
MBL-P3	30	G	21.84211302	30	27.1929566	1.3	0.5	moderately sorted medium sand
MBL-P4	45	H	22.4533563	30	25.155479	1.5	0.6	moderately sorted medium sand

*Folk and Ward (1967)

A3: Particle-size statistics

API_Number	Core_ID	Depth (ft)	Mean (phi)	Sorting (phi)	Skewness (phi)	Kurtosis (phi)
121933032300	MBL-P1	1.7	3.280	2.022	0.625	1.643
121933032300	MBL-P1	1.9	3.128	2.032	0.651	2.022
121933032300	MBL-P1	5.3	3.184	1.754	0.450	1.533
121933032300	MBL-P1	5.6	2.084	0.721	0.107	1.064
121933032300	MBL-P1	11.8	1.695	0.805	0.307	1.771
121933032300	MBL-P1	16	1.567	0.728	0.222	1.467
121933032300	MBL-P1	21	1.658	0.507	0.052	0.983
121933032300	MBL-P1	26	1.610	0.707	0.110	1.037
121933032300	MBL-P1	28.2	1.381	0.515	0.040	0.938
121933032300	MBL-P1	32	2.095	0.469	0.024	0.946
121933032300	MBL-P1	41	1.450	0.541	0.078	0.981
121933032300	MBL-P1	47	1.284	0.607	0.104	1.012
121933032300	MBL-P1	55	0.973	0.911	0.224	1.061
121933032300	MBL-P1	57	0.663	0.569	0.035	0.955
121933032300	MBL-P1	61	1.287	0.560	0.049	0.946
121933032300	MBL-P1	63	1.216	0.804	0.145	0.971
121933032300	MBL-P1	64.6	2.156	0.641	-0.046	0.993
121933032300	MBL-P1	66	1.423	0.822	0.137	0.960
121933032300	MBL-P1	75	0.171	0.715	-0.082	0.969
121933032300	MBL-P1	75.4	-0.560	0.661	0.094	0.961
121933032400	MBL-P2	8	2.712	1.167	0.369	1.796
121933032400	MBL-P2	15.5	1.835	0.485	0.083	1.008

121933032400	MBL-P2	25.5	1.565	0.417	0.025	0.931
121933032400	MBL-P2	35.5	1.803	0.513	0.044	0.947
121933032400	MBL-P2	40.3	1.887	0.450	0.054	0.990
121933032400	MBL-P2	55	0.902	0.633	0.090	0.996
121933032400	MBL-P2	64	4.229	2.138	0.403	1.157
121933032400	MBL-P2	65.5	1.035	0.624	0.071	0.983
121933032400	MBL-P2	71.5	0.600	0.587	0.030	0.944
121933032400	MBL-P2	74.5	2.096	1.150	0.290	1.464
121933032400	MBL-P2	76.3	1.449	0.894	0.013	0.899
121933032500	MBL-P3	8.5	5.193	2.114	0.112	1.020
121933032500	MBL-P3	10	1.438	0.613	0.063	1.021
121933032500	MBL-P3	16.5	2.514	2.112	0.635	1.615
121933032500	MBL-P3	21	1.225	0.844	0.303	2.001
121933032500	MBL-P3	27.5	1.299	0.513	0.058	0.976
121933032500	MBL-P3	36	1.794	0.530	0.074	0.998
121933032500	MBL-P3	42	1.972	0.551	0.043	0.962
121933032500	MBL-P3	45	0.763	0.646	0.055	0.969
121933032500	MBL-P3	52.5	1.804	0.942	0.033	0.916
121933032500	MBL-P3	56.5	0.409	0.790	0.125	1.208
121933032500	MBL-P3	59.5	1.027	0.731	0.036	0.921
121933032500	MBL-P3	65	0.915	0.795	0.207	1.100
121933032500	MBL-P3	70.5	1.093	0.540	0.005	0.939
121933032500	MBL-P3	75	1.501	0.623	0.055	0.945
121933032600	MBL-P4	12	1.528	0.605	0.082	1.016
121933032600	MBL-P4	14.7	1.093	0.952	0.261	1.577
121933032600	MBL-P4	17.2	2.281	0.633	-0.025	0.973

121933032600	MBL-P4	27.2	1.504	0.668	0.112	0.991
121933032600	MBL-P4	41.2	0.980	0.662	0.035	0.964
121933032600	MBL-P4	47.5	1.504	0.587	0.061	0.984
121933032600	MBL-P4	55.2	0.637	0.736	0.111	1.043
121933032600	MBL-P4	69.8	0.499	0.950	0.080	1.022
121933032600	MBL-P4	74.5	0.652	0.598	0.006	0.932
121933032600	MBL-P4	89.9	0.919	1.448	0.279	2.752
121933032600	MBL-P4	96.4	0.750	0.610	-0.004	0.947
121933032700	MBL-P5	14.3	1.461	0.552	0.131	1.089
121933032700	MBL-P5	14.5	1.478	1.148	0.409	3.113
121933032700	MBL-P5	16.5	1.619	0.634	0.188	1.261
121933032700	MBL-P5	33.5	1.428	1.059	0.399	2.624
121933032700	MBL-P5	37	2.061	0.496	0.030	0.964
121933032700	MBL-P5	41.2	1.809	0.946	0.038	0.911
121933032700	MBL-P5	45.5	1.172	0.549	0.077	0.997
121933032800	MBL-P6	2.5	1.379	1.226	0.379	2.767
121933032800	MBL-P6	6	2.057	0.624	0.158	1.172
121933032800	MBL-P6	11	2.099	1.173	0.404	1.485
121933032800	MBL-P6	15.9	2.594	0.974	0.264	1.456
121933032800	MBL-P6	20	2.073	0.585	0.046	0.978
121933032800	MBL-P6	32	1.500	0.575	0.127	1.077
121933032800	MBL-P6	40	1.727	0.591	0.045	0.993
121933032800	MBL-P6	44.5	1.537	1.216	0.355	1.569
121933032900	MBL-P7	6	4.382	2.867	0.149	0.686
121933032900	MBL-P7	11	4.575	1.539	0.260	1.212
121933032900	MBL-P7	11.2	3.827	1.384	0.435	1.426

121933032900	MBL-P7	15	2.319	0.582	0.042	0.990
121933032900	MBL-P7	21.5	2.773	0.921	0.196	1.267
121933032900	MBL-P7	31.8	1.111	0.595	0.010	0.965
121933033000	MBL-P8	10.2	1.540	1.064	0.376	2.820
121933033000	MBL-P8	15.5	1.972	0.598	0.159	1.179
121933033000	MBL-P8	20.5	1.894	1.051	0.336	1.733

A4: X-Ray Diffraction micronized bulk sample results

API Number	Core Number	Depth	clay (%)	quartz (%)	Kspar (%)	Pspar (%)	Calcite (%)	Dolomite (%)
121933302300	MBL P1	0.4	2	73	3	21	0	0
121933302300	MBL P1	1	1	86	11	2	0	0
121933302300	MBL P1	12	1	83	1	2	3	9
121933302300	MBL P1	20	1	90	2	3	1	2
121933302300	MBL P1	29.5	1	83	2	3	2	8
121933302300	MBL P1	31	2	66	3	14	9	5
121933302300	MBL P1	55	0	30	1	66	1	1
121933302300	MBL P1	66	1	83	1	12	2	1
121933302400	MBL P2	2	2	87	5	5	0	1
121933302400	MBL P2	5	1	91	3	5	0	0
121933302400	MBL P2	27	2	81	1	1	6	8
121933302400	MBL P2	40	0	7	1	81	2	8
121933302400	MBL P2	53	1	86	2	2	4	4
121933302400	MBL P2	67	0	95	1	2	0	1
121933302500	MBL P3	1	2	78	6	14	0	0
121933302500	MBL P3	8	1	58	5	31	1	4
121933302500	MBL P3	30	1	55	3	29	3	9
121933302500	MBL P3	42	2	87	2	4	3	3
121933302500	MBL P3	56	3	76	4	7	4	6
121933302500	MBL P3	76	1	42	1	55	0	1
121933302600	MBL P4	0.7	1	75	11	9	0	3
121933302600	MBL P4	11	5	73	5	8	4	5
121933302600	MBL P4	31	1	68	2	27	1	2
121933302600	MBL P4	45	2	89	2	2	2	4
121933302600	MBL P4	61.5	6	66	4	7	4	13
121933302600	MBL P4	78.5	2	94	1	1	1	1

A5: Results of Chittick analysis

Core No	Sample Depth (ft)	Calcite (%)	Dolomite (%)	Total Carbonate (%)
MBL-P1	6.5	2.8	4.8	7.6
MBL-P1	6.6	4.9	2.8	7.7
MBL-P1	36.5	5.7	7.5	13.2
MBL-P1	56.5	8.6	9.2	17.8
MBL-P1	61.5	7.7	6.6	14.3
MBL-P2	11.8	6.6	4.2	10.7
MBL-P2	22	4.7	8.6	13.3
MBL-P2	32	4.5	5.9	10.4
MBL-P2	42	6.0	6.9	12.9
MBL-P2	52	8.3	6.1	14.4
MBL-P2	59	6.4	5.2	11.7
MBL-P2	60	5.9	6.0	12.0
MBL-P2	64.5	2.3	4.4	6.7
MBL-P2	74	2.1	3.5	5.6
MBL-P3	17.5	6.7	6.3	13.0
MBL-P3	37.5	7.9	7.3	15.3
MBL-P3	47	5.9	6.6	12.5
MBL-P3	57	7.6	6.4	14.0
MBL-P3	65.5	2.5	6.8	9.3
MBL-P3	70	2.3	5.1	7.4
MBL-P3	75	0.3	1.6	1.8
MBL-P4	26.5	5.3	6.0	11.3
MBL-P4	7.4	7.9	1.9	9.8

MBL-P4	17.5	6.9	3.7	10.7
MBL-P4	27.5	8.1	8.3	16.5
MBL-P4	28	11.4	7.7	19.1
MBL-P4	28	10.7	7.9	18.6
MBL-P4	39.5	6.0	4.9	10.9
MBL-P4	47.5	3.7	3.6	7.3
MBL-P4	55	4.9	4.9	9.8
MBL-P4	60	4.8	5.8	10.7
MBL-P4	63	2.0	2.7	4.7
MBL-P4	67.5	2.9	3.3	6.2
MBL-P4	78	0.8	2.5	3.3
MBL-P4	82.5	0.4	0.8	1.2
MBL-P4	88.3	0.7	1.2	1.9
MBL-P4	90	5.0	6.0	11.1
MBL-P4	96	7.4	4.7	12.1

A6: Magnetic Susceptibility

API number	Depth (ft)	Elevation (ft)	Elevation (m)	MS (SI)	MS_{avg} - 3pt (SI)	MS_{avg} - 5pt (SI)
121933302300	0.6	393.4	119.9	210	210	210
121933302300	1.0	393.0	119.8	218	195	218
121933302300	1.5	392.5	119.6	156	156	149
121933302300	2.0	392.0	119.5	94	106	134
121933302300	2.5	391.5	119.3	69	98	108
121933302300	4.0	390.0	118.9	131	96	117
121933302300	4.5	389.5	118.7	88	141	116
121933302300	4.6	389.4	118.7	204	126	120
121933302300	5.0	389.0	118.6	87	127	111
121933302300	5.5	388.5	118.4	92	88	109
121933302300	6.0	388.0	118.3	86	85	90
121933302300	6.3	387.7	118.2	79	91	87
121933302300	6.5	387.5	118.1	110	86	80
121933302300	7.0	387.0	118.0	71	79	78
121933302300	9.2	384.8	117.3	57	68	78
121933302300	9.5	384.5	117.2	75	71	73
121933302300	110.0	284.0	86.6	80	80	76
121933302300	11.0	383.0	116.7	85	83	71
121933302300	11.5	382.5	116.6	86	67	69
121933302300	12.0	382.0	116.4	31	61	64
121933302300	12.5	381.5	116.3	67	51	52
121933302300	14.0	380.0	115.8	55	48	40
121933302300	14.5	379.5	115.7	24	35	42
121933302300	15.0	379.0	115.5	26	30	33
121933302300	15.5	378.5	115.4	40	29	27
121933302300	16.0	378.0	115.2	21	28	30
121933302300	16.5	377.5	115.1	22	28	29
121933302300	17.0	377.0	114.9	42	29	27
121933302300	17.5	376.5	114.8	23	30	29
121933302300	18.0	376.0	114.6	27	27	29
121933302300	19.5	374.5	114.1	31	27	26
121933302300	20.0	374.0	114.0	22	27	27
121933302300	20.5	373.5	113.8	28	25	26
121933302300	21.0	373.0	113.7	26	25	27
121933302300	21.5	372.5	113.5	22	28	28
121933302300	22.0	372.0	113.4	35	29	32
121933302300	22.5	371.5	113.2	31	38	39
121933302300	24.0	370.0	112.8	49	46	45
121933302300	24.5	369.5	112.6	60	53	48

121933302300	25.0	369.0	112.5	50	53	53
121933302300	25.5	368.5	112.3	50	52	51
121933302300	26.0	368.0	112.2	56	49	48
121933302300	26.5	367.5	112.0	42	46	53
121933302300	27.0	367.0	111.9	41	53	53
121933302300	27.5	366.5	111.7	76	55	57
121933302300	28.0	366.0	111.6	50	67	62
121933302300	28.5	365.5	111.4	76	64	66
121933302300	31.0	363.0	110.6	66	68	62
121933302300	31.5	362.5	110.5	61	62	58
121933302300	32.0	362.0	110.3	58	50	49
121933302300	32.5	361.5	110.2	31	39	39
121933302300	33.0	361.0	110.0	29	25	37
121933302300	34.0	360.0	109.7	16	33	31
121933302300	34.5	359.5	109.6	54	31	33
121933302300	35.0	359.0	109.4	24	40	47
121933302300	35.5	358.5	109.3	43	55	57
121933302300	36.0	358.0	109.1	99	69	55
121933302300	36.5	357.5	109.0	66	69	57
121933302300	37.0	357.0	108.8	42	47	56
121933302300	39.5	354.5	108.1	34	39	46
121933302300	40.0	354.0	107.9	42	41	47
121933302300	40.5	353.5	107.7	48	53	49
121933302300	41.0	353.0	107.6	69	57	55
121933302300	41.5	352.5	107.4	56	61	54
121933302300	42.0	352.0	107.3	60	51	51
121933302300	42.5	351.5	107.1	37	43	44
121933302300	43.0	351.0	107.0	32	34	50
121933302300	43.5	350.5	106.8	34	52	64
121933302300	44.0	350.0	106.7	90	84	63
121933302300	46.0	348.0	106.1	128	83	71
121933302300	46.5	347.5	105.9	32	77	78
121933302300	47.0	347.0	105.8	73	57	63
121933302300	47.5	346.5	105.6	67	52	42
121933302300	49.0	345.0	105.2	17	34	39
121933302300	49.5	344.5	105.0	19	19	33
121933302300	50.0	344.0	104.9	21	28	27
121933302300	50.5	343.5	104.7	43	33	32
121933302300	51.0	343.0	104.5	34	41	41
121933302300	51.5	342.5	104.4	45	46	60
121933302300	52.0	342.0	104.2	60	74	58
121933302300	52.5	341.5	104.1	116	70	62
121933302300	53.0	341.0	103.9	33	69	61
121933302300	55.0	339.0	103.3	58	43	63
121933302300	55.5	338.5	103.2	38	55	53

121933302300	56.0	338.0	103.0	69	58	57
121933302300	56.5	337.5	102.9	68	64	58
121933302300	57.0	337.0	102.7	55	61	56
121933302300	57.5	336.5	102.6	61	48	47
121933302300	59.5	334.5	102.0	28	37	41
121933302300	60.0	334.0	101.8	23	29	39
121933302300	61.0	333.0	101.5	37	36	41
121933302300	61.5	332.5	101.3	49	51	46
121933302300	62.5	331.5	101.0	67	57	52
121933302300	63.0	331.0	100.9	55	58	51
121933302300	63.5	330.5	100.7	51	47	53
121933302300	64.0	330.0	100.6	34	48	50
121933302300	64.5	329.5	100.4	58	49	49
121933302300	65.0	329.0	100.3	54	53	57
121933302300	66.0	328.0	100.0	48	64	48
121933302300	75.0	319.0	97.2	92	92	92
121933302400	0.5	379.5	115.7	85	85	85
121933302400	1.0	379.0	115.5	94	91	94
121933302400	1.5	378.5	115.4	93	103	112
121933302400	2.0	378.0	115.2	123	128	124
121933302400	2.5	377.5	115.1	167	144	136
121933302400	3.0	377.0	114.9	144	154	125
121933302400	4.0	376.0	114.6	153	113	110
121933302400	4.5	375.5	114.5	41	80	81
121933302400	5.0	375.0	114.3	45	36	56
121933302400	5.5	374.5	114.1	23	29	28
121933302400	6.0	374.0	114.0	20	18	20
121933302400	6.5	373.5	113.8	10	11	13
121933302400	9.0	371.0	113.1	4	8	23
121933302400	9.5	370.5	112.9	10	28	38
121933302400	10.0	370.0	112.8	69	58	58
121933302400	10.5	369.5	112.6	95	91	60
121933302400	11.5	368.5	112.3	110	73	62
121933302400	14.0	366.0	111.6	14	48	57
121933302400	14.5	365.5	111.4	21	26	41
121933302400	15.0	365.0	111.3	45	26	27
121933302400	15.5	364.5	111.1	14	34	28
121933302400	16.0	364.0	110.9	42	24	27
121933302400	16.5	363.5	110.8	17	26	23
121933302400	17.0	363.0	110.6	18	19	26
121933302400	17.5	362.5	110.5	23	24	19
121933302400	19.0	361.0	110.0	31	20	33
121933302400	20.0	360.0	109.7	5	42	43
121933302400	21.5	358.5	109.3	90	53	54
121933302400	22.0	358.0	109.1	65	78	64

121933302400	24.0	356.0	108.5	80	76	107
121933302400	24.5	355.5	108.4	83	128	120
121933302400	25.0	355.0	108.2	221	151	110
121933302400	26.0	354.0	107.9	150	130	130
121933302400	27.0	353.0	107.6	19	115	117
121933302400	28.0	352.0	107.3	178	71	81
121933302400	28.5	351.5	107.1	17	79	66
121933302400	29.0	351.0	107.0	43	44	80
121933302400	29.5	350.5	106.8	73	69	57
121933302400	30.0	350.0	106.7	92	75	67
121933302400	31.0	349.0	106.4	62	73	72
121933302400	32.0	348.0	106.1	67	65	60
121933302400	32.5	347.5	105.9	67	49	54
121933302400	39.0	341.0	103.9	15	47	76
121933302400	39.5	340.5	103.8	59	82	99
121933302400	40.0	340.0	103.6	172	138	89
121933302400	40.5	339.5	103.5	183	124	95
121933302400	44.0	336.0	102.4	19	82	98
121933302400	44.5	335.5	102.3	45	45	89
121933302400	45.0	335.0	102.1	71	82	63
121933302400	46.0	334.0	101.8	130	83	63
121933302400	46.5	333.5	101.7	50	66	56
121933302400	47.0	333.0	101.5	19	26	46
121933302400	49.0	331.0	100.9	11	17	32
121933302400	50.0	330.0	100.6	21	31	32
121933302400	51.0	329.0	100.3	61	44	36
121933302400	51.5	328.5	100.1	51	49	45
121933302400	52.0	328.0	100.0	37	48	46
121933302400	54.0	326.0	99.4	56	40	42
121933302400	55.0	325.0	99.1	26	41	37
121933302400	56.0	324.0	98.8	41	31	38
121933302400	56.5	323.5	98.6	27	36	29
121933302400	57.0	323.0	98.5	39	27	28
121933302400	58.0	322.0	98.1	15	25	32
121933302400	59.0	321.0	97.8	21	32	38
121933302400	60.0	320.0	97.5	60	45	40
121933302400	60.7	319.3	97.3	56	54	43
121933302400	61.5	318.5	97.1	48	45	48
121933302400	62.0	318.0	96.9	33	42	45
121933302400	63.0	317.0	96.6	46	40	38
121933302400	64.0	316.0	96.3	42	37	34
121933302400	64.5	315.5	96.2	25	31	32
121933302400	65.0	315.0	96.0	28	24	28
121933302400	66.0	314.0	95.7	20	24	27
121933302400	67.5	312.5	95.3	25	28	37

121933302400	69.0	311.0	94.8	38	46	37
121933302400	69.5	310.5	94.6	76	47	35
121933302400	70.0	310.0	94.5	27	38	33
121933302400	71.0	309.0	94.2	11	18	31
121933302400	72.0	308.0	93.9	16	18	29
121933302400	74.5	305.5	93.1	29	36	39
121933302400	75.0	305.0	93.0	65	56	46
121933302400	75.5	304.5	92.8	74	62	62
121933302400	76.0	304.0	92.7	47	47	47
121933302500	0.5	368.5	112.3	90	90	90
121933302500	1.0	368.0	112.2	42	48	42
121933302500	1.5	367.5	112.0	12	21	33
121933302500	2.0	367.0	111.9	10	12	18
121933302500	3.5	365.5	111.4	14	12	12
121933302500	4.0	365.0	111.3	12	13	12
121933302500	4.5	364.5	111.1	12	12	12
121933302500	5.0	364.0	110.9	12	11	10
121933302500	5.5	363.5	110.8	10	10	9
121933302500	6.0	363.0	110.6	7	7	12
121933302500	6.5	362.5	110.5	5	12	14
121933302500	9.0	360.0	109.7	26	18	15
121933302500	9.5	359.5	109.6	22	22	20
121933302500	10.0	359.0	109.4	18	24	23
121933302500	10.5	358.5	109.3	32	22	31
121933302500	11.0	358.0	109.1	18	38	29
121933302500	11.5	357.5	109.0	65	33	43
121933302500	12.0	357.0	108.8	15	55	47
121933302500	12.5	356.5	108.7	84	51	49
121933302500	14.0	355.0	108.2	53	56	55
121933302500	14.5	354.5	108.1	30	59	78
121933302500	15.0	354.0	107.9	93	85	68
121933302500	15.5	353.5	107.7	132	86	72
121933302500	16.0	353.0	107.6	32	79	74
121933302500	16.5	352.5	107.4	74	49	59
121933302500	17.0	352.0	107.3	42	44	36
121933302500	20.0	349.0	106.4	16	25	35
121933302500	20.5	348.5	106.2	19	21	27
121933302500	21.0	348.0	106.1	28	27	25
121933302500	21.5	347.5	105.9	34	30	34
121933302500	22.0	347.0	105.8	29	42	39
121933302500	22.5	346.5	105.6	64	45	37
121933302500	23.0	346.0	105.5	44	42	39
121933302500	24.0	345.0	105.2	18	34	58
121933302500	24.5	344.5	105.0	40	60	58
121933302500	25.0	344.0	104.9	123	76	61

121933302500	25.5	343.5	104.7	66	83	68
121933302500	26.0	343.0	104.5	61	59	73
121933302500	26.5	342.5	104.4	50	58	62
121933302500	27.0	342.0	104.2	65	61	64
121933302500	27.5	341.5	104.1	67	70	85
121933302500	30.5	338.5	103.2	77	104	125
121933302500	31.5	337.5	102.9	169	165	120
121933302500	32.0	337.0	102.7	249	152	114
121933302500	32.5	336.5	102.6	40	108	107
121933302500	34.0	335.0	102.1	37	39	85
121933302500	34.5	334.5	102.0	42	46	48
121933302500	35.0	334.0	101.8	61	54	62
121933302500	35.5	333.5	101.7	59	77	75
121933302500	36.0	333.0	101.5	111	91	90
121933302500	36.5	332.5	101.3	104	110	81
121933302500	37.0	332.0	101.2	115	78	73
121933302500	39.0	330.0	100.6	16	51	56
121933302500	39.5	329.5	100.4	21	20	42
121933302500	40.0	329.0	100.3	23	26	24
121933302500	40.5	328.5	100.1	34	27	60
121933302500	41.0	328.0	100.0	25	85	100
121933302500	42.0	327.0	99.7	195	148	105
121933302500	42.5	326.5	99.5	225	155	112
121933302500	44.0	325.0	99.1	47	113	176
121933302500	44.5	324.5	98.9	69	153	143
121933302500	45.0	324.0	98.8	343	148	104
121933302500	45.5	323.5	98.6	31	134	101
121933302500	46.0	323.0	98.5	28	32	101
121933302500	46.5	322.5	98.3	36	43	43
121933302500	47.0	322.0	98.1	65	52	46
121933302500	48.0	321.0	97.8	56	55	55
121933302500	49.5	319.5	97.4	43	57	60
121933302500	50.0	319.0	97.2	73	59	55
121933302500	51.0	318.0	96.9	62	59	56
121933302500	51.5	317.5	96.8	42	55	56
121933302500	52.0	317.0	96.6	62	49	51
121933302500	52.5	316.5	96.5	44	50	45
121933302500	54.0	315.0	96.0	44	40	54
121933302500	54.5	314.5	95.9	32	56	133
121933302500	55.0	314.0	95.7	91	193	257
121933302500	55.5	313.5	95.6	456	403	254
121933302500	56.0	313.0	95.4	663	382	253
121933302500	59.0	310.0	94.5	28	240	241
121933302500	59.5	309.5	94.3	30	28	155
121933302500	60.0	309.0	94.2	28	28	26

121933302500	60.5	308.5	94.0	28	24	25
121933302500	61.0	308.0	93.9	18	23	25
121933302500	64.0	305.0	93.0	24	23	24
121933302500	64.5	304.5	92.8	28	25	22
121933302500	65.0	304.0	92.7	23	23	22
121933302500	65.5	303.5	92.5	19	20	25
121933302500	66.0	303.0	92.4	20	25	27
121933302500	66.5	302.5	92.2	37	31	27
121933302500	74.0	295.0	89.9	37	32	25
121933302500	74.5	294.5	89.8	22	23	26
121933302500	75.0	294.0	89.6	10	19	23
121933302500	75.5	293.5	89.5	25	18	22
121933302500	76.0	293.0	89.3	20	26	23
121933302500	76.5	292.5	89.2	33	28	24
121933302500	77.0	292.0	89.0	30	26	24
121933302500	77.5	291.5	88.8	15	22	22
121933302500	78.0	291.0	88.7	21	21	21
121933302600	0.3	372.7	113.6	65	65	65
121933302600	0.5	372.5	113.5	53	56	53
121933302600	1.0	372.0	113.4	49	45	43
121933302600	1.5	371.5	113.2	32	33	32
121933302600	2.0	371.0	113.1	18	19	23
121933302600	2.5	370.5	112.9	9	12	20
121933302600	3.0	370.0	112.8	8	16	17
121933302600	4.0	369.0	112.5	32	19	20
121933302600	4.5	368.5	112.3	17	28	21
121933302600	5.0	368.0	112.2	35	21	26
121933302600	5.5	367.5	112.0	13	28	39
121933302600	6.0	367.0	111.9	35	47	45
121933302600	6.5	366.5	111.7	94	59	46
121933302600	7.0	366.0	111.6	47	61	56
121933302600	7.5	365.5	111.4	44	51	58
121933302600	9.0	364.0	110.9	63	50	50
121933302600	9.5	363.5	110.8	43	53	47
121933302600	10.0	363.0	110.6	54	43	45
121933302600	11.0	362.0	110.3	32	40	36
121933302600	11.5	361.5	110.2	33	27	31
121933302600	12.0	361.0	110.0	18	24	29
121933302600	12.5	360.5	109.9	21	27	28
121933302600	14.0	359.0	109.4	44	30	26
121933302600	14.5	358.5	109.3	25	30	25
121933302600	15.0	358.0	109.1	22	21	36
121933302600	15.5	357.5	109.0	15	36	43
121933302600	16.0	357.0	108.8	72	55	52
121933302600	16.5	356.5	108.7	79	75	65

121933302600	17.0	356.0	108.5	74	80	76
121933302600	17.5	355.5	108.4	87	76	79
121933302600	19.0	354.0	107.9	67	80	83
121933302600	19.5	353.5	107.7	88	85	93
121933302600	20.0	353.0	107.6	102	103	85
121933302600	20.5	352.5	107.4	120	91	76
121933302600	21.0	352.0	107.3	51	63	66
121933302600	21.5	351.5	107.1	17	36	54
121933302600	22.0	351.0	107.0	41	33	44
121933302600	22.5	350.5	106.8	41	51	42
121933302600	23.0	350.0	106.7	72	51	47
121933302600	24.0	349.0	106.4	39	51	51
121933302600	24.5	348.5	106.2	43	48	55
121933302600	25.0	348.0	106.1	62	55	52
121933302600	25.5	347.5	105.9	61	59	60
121933302600	26.0	347.0	105.8	54	65	57
121933302600	26.5	346.5	105.6	81	55	52
121933302600	27.0	346.0	105.5	29	49	49
121933302600	27.5	345.5	105.3	38	36	49
121933302600	30.1	342.9	104.5	42	45	36
121933302600	31.5	341.5	104.1	57	37	33
121933302600	34.6	338.4	103.1	14	29	29
121933302600	35.0	338.0	103.0	17	16	26
121933302600	35.5	337.5	102.9	18	20	20
121933302600	36.0	337.0	102.7	26	23	22
121933302600	36.5	336.5	102.6	25	26	25
121933302600	37.0	336.0	102.4	26	27	30
121933302600	37.5	335.5	102.3	30	33	29
121933302600	38.0	335.0	102.1	43	32	30
121933302600	39.5	333.5	101.7	24	31	31
121933302600	40.0	333.0	101.5	27	28	31
121933302600	40.5	332.5	101.3	33	30	26
121933302600	41.0	332.0	101.2	30	27	25
121933302600	41.5	331.5	101.0	18	22	26
121933302600	42.0	331.0	100.9	19	23	26
121933302600	42.5	330.5	100.7	32	28	22
121933302600	43.0	330.0	100.6	32	25	21
121933302600	44.0	329.0	100.3	12	18	20
121933302600	44.5	328.5	100.1	11	13	20
121933302600	46.5	326.5	99.5	16	19	18
121933302600	47.0	326.0	99.4	29	23	23
121933302600	47.5	325.5	99.2	23	29	31
121933302600	48.0	325.0	99.1	36	36	37
121933302600	49.3	323.7	98.7	50	44	42
121933302600	49.5	323.5	98.6	46	51	56

121933302600	50.0	323.0	98.5	57	64	69
121933302600	50.5	322.5	98.3	90	83	80
121933302600	51.0	322.0	98.1	103	98	87
121933302600	51.5	321.5	98.0	103	95	90
121933302600	52.0	321.0	97.8	81	85	88
121933302600	52.5	320.5	97.7	72	79	73
121933302600	53.0	320.0	97.5	84	60	56
121933302600	55.0	318.0	96.9	26	43	45
121933302600	55.5	317.5	96.8	19	23	44
121933302600	56.0	317.0	96.6	24	37	32
121933302600	56.5	316.5	96.5	67	39	33
121933302600	57.0	316.0	96.3	26	42	35
121933302600	59.0	314.0	95.7	32	28	38
121933302600	59.5	313.5	95.6	28	32	33
121933302600	60.0	313.0	95.4	38	35	37
121933302600	60.5	312.5	95.3	40	43	43
121933302600	61.0	312.0	95.1	50	49	50
121933302600	61.5	311.5	94.9	58	58	54
121933302600	62.0	311.0	94.8	66	60	51
121933302600	62.5	310.5	94.6	56	49	46
121933302600	64.5	308.5	94.0	26	35	38
121933302600	65.0	308.0	93.9	25	23	147
121933302600	66.0	307.0	93.6	19	218	141
121933302600	66.5	306.5	93.4	610	218	148
121933302600	67.0	306.0	93.3	24	232	153
121933302600	69.0	304.0	92.7	62	46	164
121933302600	69.5	303.5	92.5	51	62	58
121933302600	70.0	303.0	92.4	72	68	69
121933302600	70.5	302.5	92.2	80	78	70
121933302600	71.0	302.0	92.0	81	76	72
121933302600	71.5	301.5	91.9	67	70	66
121933302600	72.0	301.0	91.7	62	56	53
121933302600	72.5	300.5	91.6	39	39	38
121933302600	74.0	299.0	91.1	15	21	31
121933302600	74.5	298.5	91.0	10	19	24
121933302600	75.0	298.0	90.8	32	22	20
121933302600	75.5	297.5	90.7	26	24	20
121933302600	76.5	296.5	90.4	16	20	21
121933302600	77.0	296.0	90.2	17	15	18
121933302600	77.5	295.5	90.1	13	16	16
121933302600	78.0	295.0	89.9	17	15	16
121933302600	79.0	294.0	89.6	15	17	17
121933302600	80.0	293.0	89.3	20	18	17
121933302600	81.0	292.0	89.0	19	18	17
121933302600	81.5	291.5	88.8	15	16	17

121933302600	82.0	291.0	88.7	15	15	16
121933302600	84.0	289.0	88.1	16	15	17
121933302600	84.0	289.0	88.1	16	18	18
121933302600	85.0	288.0	87.8	23	19	20
121933302600	86.0	287.0	87.5	20	23	19
121933302600	87.0	286.0	87.2	26	20	21
121933302600	88.0	285.0	86.9	13	20	21
121933302600	89.0	284.0	86.6	22	20	27
121933302600	89.5	283.5	86.4	27	32	30
121933302600	90.0	283.0	86.3	47	39	36
121933302600	90.5	282.5	86.1	43	43	34
121933302600	91.0	282.0	86.0	41	33	32
121933302600	95.0	278.0	84.7	16	24	30
121933302600	95.5	277.5	84.6	16	23	28
121933302600	96.0	277.0	84.4	36	28	26
121933302600	96.5	276.5	84.3	33	33	30
121933302600	97.0	276.0	84.1	32	32	30
121933302600	97.5	275.5	84.0	33	27	27
121933302600	98.0	275.0	83.8	16	16	16
121933302700	0.3	389.7	118.8	77	77	77
121933302700	1.0	389.0	118.6	71	67	71
121933302700	1.5	388.5	118.4	53	62	66
121933302700	2.0	388.0	118.3	64	60	61
121933302700	2.5	387.5	118.1	64	60	60
121933302700	3.0	387.0	118.0	54	62	63
121933302700	4.0	386.0	117.7	68	63	59
121933302700	4.5	385.5	117.5	68	60	62
121933302700	5.0	385.0	117.3	45	63	60
121933302700	5.0	385.0	117.3	77	56	56
121933302700	6.0	384.0	117.0	45	57	48
121933302700	6.5	383.5	116.9	48	40	42
121933302700	9.5	380.5	116.0	27	30	34
121933302700	10.0	380.0	115.8	16	25	31
121933302700	10.5	379.5	115.7	33	26	29
121933302700	11.5	378.5	115.4	30	34	28
121933302700	14.0	376.0	114.6	38	31	30
121933302700	15.0	375.0	114.3	25	30	31
121933302700	15.5	374.5	114.1	26	30	35
121933302700	16.0	374.0	114.0	39	38	37
121933302700	16.5	373.5	113.8	50	45	41
121933302700	19.0	371.0	113.1	47	47	45
121933302700	19.5	370.5	112.9	43	46	50
121933302700	20.0	370.0	112.8	47	51	53
121933302700	20.5	369.5	112.6	64	58	55
121933302700	21.0	369.0	112.5	63	61	59

121933302700	21.5	368.5	112.3	56	61	55
121933302700	22.0	368.0	112.2	65	50	48
121933302700	24.0	366.0	111.6	29	41	42
121933302700	24.5	365.5	111.4	29	30	36
121933302700	25.0	365.0	111.3	32	29	31
121933302700	25.5	364.5	111.1	26	33	28
121933302700	26.0	364.0	110.9	43	27	26
121933302700	29.0	361.0	110.0	14	25	24
121933302700	29.5	360.5	109.9	19	17	28
121933302700	30.0	360.0	109.7	18	27	28
121933302700	31.0	359.0	109.4	46	36	30
121933302700	31.5	358.5	109.3	43	38	31
121933302700	32.0	358.0	109.1	26	31	37
121933302700	32.5	357.5	109.0	24	32	39
121933302700	33.0	357.0	108.8	48	41	33
121933302700	34.0	356.0	108.5	53	39	32
121933302700	35.5	354.5	108.1	17	29	33
121933302700	36.0	354.0	107.9	18	21	34
121933302700	36.5	353.5	107.7	28	34	36
121933302700	37.0	353.0	107.6	56	49	46
121933302700	39.0	351.0	107.0	63	62	53
121933302700	39.5	350.5	106.8	68	61	60
121933302700	40.5	349.5	106.5	53	60	64
121933302700	41.0	349.0	106.4	59	63	58
121933302700	45.0	345.0	105.2	78	56	56
121933302700	46.0	344.0	104.9	32	32	32
121933302800	0.3	386.7	117.9	110	110	110
121933302800	1.0	386.0	117.7	100	88	100
121933302800	1.5	385.5	117.5	54	60	66
121933302800	2.0	385.0	117.3	27	41	51
121933302800	2.5	384.5	117.2	42	33	39
121933302800	3.0	384.0	117.0	31	37	32
121933302800	4.0	383.0	116.7	39	31	33
121933302800	4.2	382.8	116.7	22	31	45
121933302800	5.5	381.5	116.3	32	51	52
121933302800	6.0	381.0	116.1	100	67	49
121933302800	6.5	380.5	116.0	68	63	49
121933302800	7.0	380.0	115.8	22	38	47
121933302800	9.0	378.0	115.2	23	22	33
121933302800	9.5	377.5	115.1	23	26	28
121933302800	10.0	377.0	114.9	32	32	37
121933302800	10.5	376.5	114.8	41	47	35
121933302800	11.0	376.0	114.6	69	40	39
121933302800	11.5	375.5	114.5	11	41	45
121933302800	12.0	375.0	114.3	44	39	40

121933302800	14.0	373.0	113.7	61	40	30
121933302800	14.5	372.5	113.5	17	31	36
121933302800	15.0	372.0	113.4	16	25	32
121933302800	15.5	371.5	113.2	44	27	27
121933302800	16.0	371.0	113.1	22	35	27
121933302800	16.5	370.5	112.9	39	25	46
121933302800	17.0	370.0	112.8	14	54	41
121933302800	17.5	369.5	112.6	110	47	57
121933302800	19.0	368.0	112.2	19	78	61
121933302800	19.5	367.5	112.0	105	61	84
121933302800	20.0	367.0	111.9	59	97	67
121933302800	20.5	366.5	111.7	126	71	67
121933302800	21.0	366.0	111.6	27	56	48
121933302800	21.5	365.5	111.4	16	19	39
121933302800	22.0	365.0	111.3	14	13	19
121933302800	22.5	364.5	111.1	10	17	18
121933302800	24.5	362.5	110.5	27	20	24
121933302800	25.0	362.0	110.3	23	32	30
121933302800	26.5	360.5	109.9	46	38	36
121933302800	29.0	358.0	109.1	45	43	36
121933302800	29.5	357.5	109.0	37	37	38
121933302800	30.5	356.5	108.7	30	33	32
121933302800	31.0	356.0	108.5	31	26	28
121933302800	31.5	355.5	108.4	17	25	25
121933302800	32.0	355.0	108.2	27	22	27
121933302800	34.0	353.0	107.6	21	30	28
121933302800	34.5	352.5	107.4	41	32	32
121933302800	35.0	352.0	107.3	34	38	32
121933302800	35.5	351.5	107.1	38	33	38
121933302800	36.0	351.0	107.0	26	38	44
121933302800	36.5	350.5	106.8	49	50	54
121933302800	39.0	348.0	106.1	75	68	64
121933302800	39.5	347.5	105.9	81	82	77
121933302800	40.0	347.0	105.8	92	87	83
121933302800	41.0	346.0	105.5	88	87	86
121933302800	41.5	345.5	105.3	82	86	87
121933302800	42.0	345.0	105.2	88	85	88
121933302800	42.5	344.5	105.0	85	90	98
121933302800	44.0	343.0	104.5	99	107	106
121933302800	45.0	342.0	104.2	138	119	119
121933302800	16.5	370.5	112.9	121	121	121
121933302900	0.5	376.5	114.8	80	80	80
121933302900	1.0	376.0	114.6	103	106	103
121933302900	1.5	375.5	114.5	135	117	96
121933302900	2.0	375.0	114.3	113	100	100

121933302900	2.5	374.5	114.1	52	88	83
121933302900	4.0	373.0	113.7	100	55	65
121933302900	4.5	372.5	113.5	14	53	50
121933302900	5.0	372.0	113.4	46	32	42
121933302900	5.5	371.5	113.2	37	33	27
121933302900	6.0	371.0	113.1	15	25	46
121933302900	6.5	370.5	112.9	23	48	66
121933302900	7.0	370.0	112.8	108	93	93
121933302900	9.0	368.0	112.2	149	142	102
121933302900	9.5	367.5	112.0	169	126	106
121933302900	10.5	366.5	111.7	61	90	96
121933302900	11.0	366.0	111.6	42	53	117
121933302900	11.5	365.5	111.4	58	119	87
121933302900	12.0	365.0	111.3	259	110	77
121933302900	12.5	364.5	111.1	14	96	91
121933302900	13.0	364.0	110.9	15	47	97
121933302900	14.0	363.0	110.6	111	72	59
121933302900	14.5	362.5	110.5	89	89	113
121933302900	15.0	362.0	110.3	67	147	117
121933302900	15.5	361.5	110.2	286	129	101
121933302900	17.0	360.0	109.7	35	117	90
121933302900	17.5	359.5	109.6	30	32	84
121933302900	18.0	359.0	109.4	31	32	32
121933302900	19.0	358.0	109.1	36	32	36
121933302900	20.0	357.0	108.8	30	40	43
121933302900	20.5	356.5	108.7	55	49	56
121933302900	21.0	356.0	108.5	63	72	57
121933302900	21.5	355.5	108.4	99	68	57
121933302900	22.0	355.0	108.2	42	55	51
121933302900	22.5	354.5	108.1	26	31	53
121933302900	23.0	354.0	107.9	25	42	42
121933302900	24.0	353.0	107.6	74	48	46
121933302900	24.5	352.5	107.4	46	60	51
121933302900	25.0	352.0	107.3	59	52	60
121933302900	25.5	351.5	107.1	52	60	57
121933302900	26.0	351.0	107.0	70	61	58
121933302900	26.5	350.5	106.8	61	59	48
121933302900	27.0	350.0	106.7	48	40	44
121933302900	29.0	348.0	106.1	12	30	32
121933302900	29.5	347.5	105.9	31	18	23
121933302900	30.0	347.0	105.8	12	18	16
121933302900	30.5	346.5	105.6	12	12	16
121933302900	31.0	346.0	105.5	13	13	16
121933302900	31.5	345.5	105.3	15	19	22
121933302900	32.0	345.0	105.2	29	28	24

121933302900	32.5	344.5	105.0	40	31	31
121933302900	33.0	344.0	104.9	25	25	25
121933303000	0.5	389.5	118.7	135	135	135
121933303000	1.0	389.0	118.6	130	118	130
121933303000	1.5	388.5	118.4	90	90	100
121933303000	2.0	388.0	118.3	50	79	100
121933303000	2.5	387.5	118.1	96	93	100
121933303000	3.0	387.0	118.0	133	120	89
121933303000	3.5	386.5	117.8	130	101	97
121933303000	4.5	385.5	117.5	39	85	90
121933303000	5.0	385.0	117.3	87	62	72
121933303000	5.5	384.5	117.2	60	63	56
121933303000	6.0	384.0	117.0	43	52	59
121933303000	6.5	383.5	116.9	53	50	45
121933303000	7.0	383.0	116.7	53	41	35
121933303000	7.5	382.5	116.6	17	26	30
121933303000	10.0	380.0	115.8	10	14	21
121933303000	10.5	379.5	115.7	16	12	13
121933303000	11.0	379.0	115.5	10	13	12
121933303000	11.5	378.5	115.4	12	11	15
121933303000	14.0	376.0	114.6	11	17	18
121933303000	14.5	375.5	114.5	27	23	17
121933303000	15.0	375.0	114.3	32	21	16
121933303000	15.5	374.5	114.1	5	13	16
121933303000	16.0	374.0	114.0	4	8	31
121933303000	16.5	373.5	113.8	15	40	61
121933303000	17.0	373.0	113.7	102	99	71
121933303000	19.0	371.0	113.1	180	112	80
121933303000	19.5	370.5	112.9	53	95	80
121933303000	20.0	370.0	112.8	52	39	61
121933303000	20.5	369.5	112.6	13	24	28
121933303000	21.0	369.0	112.5	9	12	32
121933303000	21.5	368.5	112.3	15	32	38
121933303000	22.0	368.0	112.2	74	56	56
121933303000	22.5	367.5	112.0	79	79	79

A7: Summary of OSL age dating

ISGS Number	Sample Number	Depth (m)	Water Content (%)	Equivalent Dose (Gy)	No. Aliquots	Dose Rate (Gy/ka)				Age
						Beta	Gamma	Cosmic	Total	(ka)
ISGS 213	MBL-P1-67	20.5	9	39.85 ± 1.64	24	0.672 ± 0.056	0.337 ± 0.020	0.031 ± 0.002	0.040 ± 0.060	38.32 ± 3.26
ISGS 214	MBL-P1-55	17	12	33.55 ± 1.71	21	0.646 ± 0.055	0.316 ± 0.020	0.040 ± 0.002	1.002 ± 0.059	39.49 ±3.02
ISGS 215	MBL-P1-31	9.5	19	32.77 ± 0.98	21	0.717 ± 0.063	0.333 ± 0.022	0.072 ± 0.004	1.122 ± 0.067	29.22 ± 2.31
ISGS 216	MBL-P1-10	3	3	24.95 ± 1.21	19	0.679 ± 0.058	0.326 ± 0.021	0.142 ± 0.007	1.147 ± 0.062	21.75 ± 1.87
ISGS 232	MBL-P2-41	12.5	12	40.14 ± 1.77	20	0.592 ± 0.050	0.295 ± 0.018	0.056 ± 0.003	0.943 ± 0.054	42.59 ± 3.60
ISGS 233	MBL-P2-67	20.5	9	33.37 ± 2.12	24	0.655 ± 0.055	0.332 ± 0.020	0.031 ± 0.002	1.018 ± 0.058	32.76 ± 3.19
ISGS 234	MBL-P2-53	16	14	45.91 ± 3.65	11	0.648 ± 0.053	0.329 ± 0.019	0.042 ± 0.002	1.019 ± 0.057	45.07 ± 4.81
ISGS 235	MBL-P2-27	8	9	41.11 ± 1.17	21	0.582 ± 0.049	0.285 ± 0.017	0.082 ± 0.004	0.949 ± 0.052	43.31 ± 3.30
ISGS 243	MBL-P4-45	14	9	42.06 ± 2.46	24	0.891 ± 0.074	0.428 ± 0.026	0.050 ± 0.003	1.369 ± 0.079	30.72 ± 2.90
ISGS 244	MBL-P4-32	10	15	47.25 ± 0.83	19	0.667 ± 0.057	0.323 ± 0.020	0.070 ± 0.003	1.059 ± 0.060	44.60 ± 3.29

ISGS 245	MBL-P4-10	3	5.5	24.38 ± 1.15	23	0.743 ± 0.062	0.366 ± 0.022	0.140 ± 0.007	1.248 ± 0.066	19.53 ± 1.64
ISGS 246	MBL-P5-46	14	13.5	36.6 ± 2.29	21	0.596 ± 0.052	0.280 ± 0.018	0.049 ± 0.002	0.049 ± 0.002	39.53 ± 3.89
ISGS 247	MBL-P3-29	9	19.6	26.5 ± 1.19	22	0.734 ± 0.062	0.349 ± 0.022	0.077 ± 0.004	1.16 ± 0.066	22.85 ± 1.92
ISGS 248	MBL-P3-60	18	2.5	32.62 ± 1.59	23	0.629 ± 0.054	0.308 ± 0.019	0.036 ± 0.002	0.973 ± 0.58	33.52 ± 3.06
ISGS 249	MBL-P3-7	7	22	30.72 ± 1.01	20	1.231 ± 0.097	0.688 ± 0.036	0.158 ± 0.008	2.077 ± 0.103	14.79 ± 1.07
ISGS 250	MBL-P5-27	8	18.6	35.13 ± 1.77	20	0.618 ± 0.052	0.304 ± 0.019	0.081 ± 0.004	1.002 ± 0.056	35.05 ± 2.99

A8: ^{14}C Age date summary

ISGS #	Sample #	Material	$d^{13}C$	Fraction of MC[1]	±	$D^{14}C$	±	^{14}C yr BP[2]	±	Calibration[3]	ca yr range[4]
A2843	MBL-P37	Soil	-13	0.3076	0.001	-692	1	9470	#	intcal13.14c	10670-10751
A2846	MBL-P38.3	seeds	-27	0.1701	9E-04	-830	1	14230	#	intcal13.14c	17231-17436

[1]MC = modern carbon

[2]A half-life of 5568 is used for the age calculation. BP = before 1950.

[3]Stuiver et al. (2014)

[4]Calendar years before present

Publications and presentations

PHILLIPS, Andrew, LARSON, Timothy, CARON, Olivier, and ALBERTS, R.A.,, 2014. Fluvial history of the lower Wabash Valley: slackwater, torrents, lazy rivers. Geological Society of America *Abstracts with Programs.* Vol. 46, No. 4, p.11 (Phillips)

Phillips, Andrew, Olivier Caron, Hong Wang, Tim Larson, and Scott Elrick, 2014. Proglacial alluviation in the Wabash Valley, Illinois-Indiana, USA: Challenges in OSL chronology, to be presented at LED2014, Montreal, Canada, 7 to 11 July, 2014.

Phillips, Andrew, 2014. The Meadow Bank: Tectonics or torrents? University of Illinois Department of Geology Colloquium Series April 14, 2014.